



Spring 2018

Structural Characterization of a Human/Porcine Chimeric FVIII Construct and an Improved Human Factor VIII Model and Progress Towards Determination of the FVIII C1 Domain In Complex With Inhibitory Antibodies

Ian Smith

Western Washington University, smithi.wa@gmail.com

Follow this and additional works at: <https://cedar.wwu.edu/wwuet>

 Part of the [Chemistry Commons](#)

Recommended Citation

Smith, Ian, "Structural Characterization of a Human/Porcine Chimeric FVIII Construct and an Improved Human Factor VIII Model and Progress Towards Determination of the FVIII C1 Domain In Complex With Inhibitory Antibodies" (2018). *WWU Graduate School Collection*. 710.
<https://cedar.wwu.edu/wwuet/710>

This Masters Thesis is brought to you for free and open access by the WWU Graduate and Undergraduate Scholarship at Western CEDAR. It has been accepted for inclusion in WWU Graduate School Collection by an authorized administrator of Western CEDAR. For more information, please contact westerncedar@wwu.edu.

**Structural Characterization of a Human/Porcine Chimeric FVIII Construct and an
Improved Human Factor VIII Model**

and

Progress Towards Determination of the FVIII C1 Domain

In Complex With Inhibitory Antibodies

By

Ian Wesley Smith

Accepted in Partial Completion
of the Requirements for the Degree
Master of Science

ADVISORY COMMITTEE

Dr. Clint Spiegel, Chair

Dr. Gerry Prody

Dr. John Antos

GRADUATE SCHOOL

Dr. Gautam Pillay, Dean

Master's Thesis

In presenting this thesis in partial fulfillment of the requirements for a master's degree at Western Washington University, I grant to Western Washington University the non-exclusive royalty-free right to archive, reproduce, distribute, and display the thesis in any and all forms, including electronic format, via any digital library mechanisms maintained by WWU.

I represent and warrant this is my original work, and does not infringe or violate any rights of others. I warrant that I have obtained written permissions from the owner of any third party copyrighted material included in these files.

I acknowledge that I retain ownership rights to the copyright of this work, including but not limited to the right to use all or part of this work in future works, such as articles or books.

Library users are granted permission for individual, research and non-commercial reproduction of this work for educational purposes only. Any further digital posting of this document requires specific permission from the author.

Any copying or publication of this thesis for commercial purposes, or for financial gain, is not allowed without my written permission.

Signature: Ian Wesley Smith

Date: Monday, June 4th, 2018

**Structural Characterization of a Human/Porcine Chimeric FVIII Construct and an
Improved Human Factor VIII Model
and
Progress Towards Determination of the FVIII C1 Domain
In Complex With Inhibitory Antibodies**

A Thesis
Presented to
The Faculty of
Western Washington University

In Partial Fulfillment
Of the Requirements for the Degree
Master of Science

by
Ian Wesley Smith
June 2018

Abstract

Blood coagulation factor VIII (FVIII) is a non-enzymatic protein cofactor, which plays a crucial role in the formation of a stable blood clot. Absence or deficiency of FVIII results in the blood disorder hemophilia A, with symptoms including internal hemorrhaging and the inability to stop bleeding from open wounds. Treatment of hemophilia A relies on replacement of FVIII with blood, plasma, or protein concentrate infusions. Unfortunately, approximately 30% of patients receiving replacement FVIII generate pathologic anti-FVIII inhibitory antibodies, which both reduce the effectiveness of the FVIII therapeutic and increase the severity of hemophilia A symptoms.

This thesis reports the determination of the molecular structure for “Et3i”, a next-generation human/porcine chimeric FVIII protein for hemophilia A therapy. At 3.2 Å resolution with a R_{work} of 0.2146 and R_{free} of 0.2879, this will be the highest resolution structure of FVIII to date and will be of substantial interest to the hematological community. Furthermore, an improved model of human FVIII with more robust geometry and amino acid register assignment, and a R_{work} of 0.2655, and R_{free} of 0.2895 based on previous 3.7 Å data has been constructed. Lastly, progress has been made towards the structural determination of the inhibitory antibodies M6143, 2A9, and B136 in complex with the C1 domain of human FVIII. Details of these interactions could inform the development of future hemophilia A protein therapeutics with reduced immunogenicity.

Acknowledgments

The work described here was undertaken in the Spiegel lab at Western Washington University from the Fall of 2016 to the Spring of 2018. I wish to thank Dr. Spiegel and offer my sincerest gratitude for the opportunity to join his research group, as well as his time, research acumen, and guidance of his mentorship. I also wish to recognize the previous graduate students Serena Wo and Amanda Weis. Their assistance and training were instrumental to my successful reintegration to the laboratory. The cumulative past and present members of the Spiegel lab are to thank as well, for their dedication, ingenuity, and comradery.

The murine anti-C1 hybridomas were provided by Dr. Pete Lollar's lab at Emory University. Dr. Pete Lollar, John Healey, Ernest Parker, and Hunter Baldwin were exceptional in their hospitality and accommodation while training both Dr. Spiegel and myself in mammalian cell culturing. The Et3i construct was provided by Expression Therapeutics, LLC and I sincerely thank Dr. Christopher Doering and Dr. Gabriela Denning for providing ample protein for our research.

The ability to perform this work is a result of generous financial support from the Arlan Norman Award for Excellence in Student Mentoring, Western Washington University Department of Chemistry's Teaching Assistantship, and Dr. Spiegel's Research Assistantship position supported by the NIH/NHLBI. I am especially appreciative of my thesis committee members, Dr. Spiegel, Dr. Gerry Prody and Dr. John Antos, for their thoughtful advice and substantial efforts to provide edits in preparation of this thesis.

Lastly, utmost thanks are owed to Katie Woolsey for her sacrifice and support during my graduate studies.

Table of Contents

Abstract.....	iv
Acknowledgments.....	v
List of Figures.....	vii
List of Abbreviations	x
Introduction.....	1
Chapter 1: Blood Coagulation and FVIII.....	2
Chapter 2: Protein X-Ray Crystallography and Molecular Modeling	19
Chapter 3: Isolated C1 Domain of FVIII in Complex wit Inhibitory Antibodies	27
Chapter 4: Structural Modeling of Human Porcine Chimeric Et3i.....	50
Conclusion	65
Bibliography / Reference Works Cited.....	67
Appendix A.....	73
Appendix B.....	76

List of Figures

Figure 1 Schematic of syringe used in first blood transfusion to treat hemophilia.	3
Figure 2 The thermolabile discovery of FVIII.	4
Figure 3 Enzyme Cascade Model of Blood Coagulation.	5
Figure 4 The Waterfall Model of Blood Coagulation.	5
Figure 5 The Blood Coagulation Cascade.	6
Figure 6 The Cell Based Model of Hemostasis.	6
Figure 7 "Low-responder" Patient Antibody Titer.	7
Figure 8 Sulfur Mustard Mechanism of Action.	8
Figure 9 Cyclophosphamide Pathway of Activation.	8
Figure 10 Immune Tolerance Induction (ITI) Campaign in a "High-responder" Patient.	9
Figure 11 Map of the F8 Gene.	10
Figure 12 Comparison between cubic (A) and rhomboid (B) packing of spheres.	19
Figure 13 First communicated X-ray image.	19
Figure 14 Structural Model of Hemoglobin.	20
Figure 15 Protein Crystallization Solubility Curve.	21
Figure 16 Hanging Vapor Drop Diffusion.	21
Figure 17 The Unit Cell and the reflecting planes.	22
Figure 18 Scattering against a crystal lattice plane.	23
Figure 19 X-ray scattering by system of two electrons.	24
Figure 20 Comparing two waves offset by phase.	24
Figure 21 The Argand Diagram.	24
Figure 22 WinCoot Model Building.	25
Figure 23 Automated model refinement with Phenix.	26
Figure 24 The pET-32a-c(+) plasmid expression region sequence.	34

Figure 25 Diagram of gravity chromatography with siphon-safety loop.	39
Figure 26 C1 IMAC Purification.	42
Figure 27 Sequential IMAC Purifications of C1 fusion protein.	43
Figure 28 C1 Fusion Enterokinase Cleavage.	43
Figure 29 Hybridoma cells (2A9) viewed at 400x magnification (95% confluence).	44
Figure 30 Hybridoma purification by ion-exchange chromatography (IEC).	44
Figure 31 IgG 2A9 Fab Protein A Purification.	45
Figure 32 Anti-C1 2A9 Fab Bradford Assay.	45
Figure 33 Non-diffracting crystals of complexed C1 and 2A9 Fab.	46
Figure 34 Fungal contamination of B136 hybridoma cells.	48
Figure 35 Stereotypical crystals of Et3i.	52
Figure 36 Structure of Et3i Molecule A.	55
Figure 37 Two molecules in the Et3i asymmetric unit.	56
Figure 38 Spatial Comparison of Non-Crystallographic Symmetry (NCS) between Et3i Molecule A and B.	56
Figure 39 C2 Domain Comparison in Overlay of the Molecule A and B in Profile.	57
Figure 40 Deglycosylation of Et3i by PNGase F.	58
Figure 41 Morphologies of Deglycosylated Et3i Crystals.	58
Figure 42 Comparison of Et3i and Improved hFVIII to Previous Model.	59
Figure 43 Comparison of Surface Electrostatics between Et3i and hFVIII Models.	60
Figure 44 A2 Domain Amino Acid Register Improvement.	60
Figure 45 Cu binding site in ET3i.	61
Figure 46 Previously Published C2 Domain Conformation Shifts.	61
Figure 47 Molecular Depiction of hFVIII C2 Domain in Complex with 3E6 and G99 antibody Fabs.	62
Figure 48 Brison et al. 3E6 Antibody Abrogates PS Binding and New PS Binding Model. ..	62

Figure 49 C2 Domain Conformation Shift in Context with 3E6.	63
Figure 50 C1 fusion Co(II) IMAC purification.....	73
Figure 51 C1 fusion Cu(II) IMAC purification.....	73
Figure 52 C1 fusion Fe (III) IMAC purification.	74
Figure 53 C1 fusion Ni(II) IMAC purification.....	74
Figure 54 C1 fusion Zn(II) IMAC purification.....	75
Figure 55 Biolayer Interferometry (BLI) C1 Titration & "Group A" Mab M6143.	76
Figure 56 BLI Titration of C1 & "Group A" Mab 2A9 [300 nM].	76
Figure 57 BLI Titration of C1 & "Group B" Mab B136 [300 nM].....	77

List of Abbreviations

AAV	Adeno-Associated Virus
AHF	Anti-hemophilic Factor
AIDS	Acquired Immune Deficiency Syndrome
AMR	Ashwell Morell Receptor
APC	Activated Protein C
APCs	Antigen Presenting Cells
ASGPR	Asialoglycoprotein Receptor
BDD	B-Domain Deleted FVIII
BLI	Biolayer Interferometry
BMA	β -D-Mannose
Cat.#	Catalog Number (3 rd Party Vendor)
CDC	Center for Disease Control
CLEC4M	C-Type Lectin Domain Family 4 Member
CV	Column Volume (mL of resin)
DMSO	Dimethyl Sulfoxide
EACA	Epsilon-aminocaproic Acid
ELISA	Enzyme-Linked Immunosorbent Assay
Et3i	Human/Porcine Chimeric FVIII
FI	Blood Coagulation Factor I / Fibrinogen
FII	Blood Coagulation Factor II / Prothrombin
FV	Blood Coagulation Factor V
FVII	Blood Coagulation Factor VII
FVIII	Blood Coagulation Factor VIII
FIX	Blood Coagulation Factor IX
FX	Blood Coagulation Factor X
FXI	Blood Coagulation Factor XI

FXII	Blood Coagulation Factor XII
F(S)	Crystallographic Structure Factor
Fab	Antigen-binding IgG Fragment
F _c Factor	Crystallographic Calculated Structure
Fc	Crystallizable IgG Fragment
FcRn	Neonatal IgG Fc Receptor
FDA	Food and Drug Administration
FEIBA	Factor Eight Inhibitor Bypassing Activity
F _o	Crystallographic Observed Structure Factor
FUC	α -L-Fucose
FVIII-KB013bv	Anti-vWF Nanobody – FVIII Fusion Protein
Gal	Galactose
GalNAc	N-Acetylgalactosamine
HDX-MS	Hydrogen-Deuterium Exchange Mass Spectroscopy
hFVIII	Human FVIII
HIV	Human Immunodeficiency Virus
HSC	Hematopoietic Stem Cells
I22I	<i>F8</i> gene Intron 22 Inversion
IEC	Ion Exchange Chromatography
IITR	International Immune Tolerance Registry
IMAC	Immobilized Metal Affinity Chromatography
ITI	Immune Tolerance Induction
LDLR	Low-Density Lipoprotein Receptor
LLR	Lectin-like Receptor
LRP1	LDLR -Related Protein
Mab	Monoclonal IgG Antibody

MAN	α -D-Mannose
MMR/CD206	Macrophage Mannose Receptor Type 1
MMWR	Morbidity and Mortality Weekly Report
MR	Molecular Replacement
NAG	N-Acetyl-D-Glucosamine
NCS	Non-Crystallographic Symmetry
NHS	N-Hydroxysuccinimide
PCP	<i>Pneumocystis carinii</i> Pneumonia
PDB	Protein Data Bank
PEG	Polyethylene Glycol
pFVIII	Porcine FVIII
PS	Phosphatidylserine
Ref.#	Reference Number (Manufacturer)
rFVIII	Recombinant FVIII
rhFVIII	Recombinant Human FVIII
rpFVIII	Recombinant Porcine FVIII
SCARA5	Scavenger Receptor Class A Member 5
Siglec5	Sialic Acid Binding IgG-like Lectin 5
STAB2	Stabilin-2
TF	Tissue Factor Protein
TFPI	Tissue Factor Pathway Inhibitor Protein
vWF	von Willebrand's Factor
w/v	weight per volume

Introduction

Chapter 1 presents the physiological context of the research. First is presented a brief overview of blood coagulation and the role of blood coagulation factor VIII (FVIII) in the disease state of hemophilia A. Next, a brief history of blood coagulation research and a review of the biochemical process is described. Lastly, details of contemporary hemophilia A therapeutics are provided. This background information will be pertinent to the details discussed in Chapters 2, 3, and 4.

Chapter 2 provides a brief introduction to the history and technique of X-ray crystallography and the subsequent computation of a three-dimensional molecular model. While the technical derivations of the molecular electron density map are omitted, this chapter undertakes a broad appreciation of the protein crystallographic method and how X-ray diffraction can be used to determine a molecular structure.

Chapter 3 details the progress toward the recombinant isolated C1 domain of FVIII in complex with inhibitory antibodies. Work performed in the lab includes expression of the protein of interest from a bacterial expression system and chromatographic purification methods. Additionally, anti-C1 antibodies were expressed and purified, and preliminary binding studies between the isolated C1 domain and anti-C1 antibodies were performed.

Chapter 4 describes the solution of the molecular model of a novel human/porcine chimeric FVIII replacement protein “Et3i”, developed by collaborators at Emory University and Expression Therapeutics. This chapter encompasses the preparation of the crystal by previous researchers, treatment of the X-ray diffraction data set to generate an electron density map, and solution of the Et3i molecular model. Additionally, this has led to an improved model of human FVIII, refined against previously published 3.7 Å data.

Citations of primary literature are denoted with numeral superscript. References to physical lab notebook entries are denoted by Roman numeral superscript and appended as footnotes to each respective page with the format (Researcher Initials(Notebook Number)Page Number).

Chapter 1: Blood Coagulation and FVIII

1.1 Introduction to Blood Coagulation and Hemophilia

In vertebrates, the circulatory system is a closed-system that plays a crucial role in the delivery of nutrients and removal of waste. In the event of vascular injury, a two-phase process termed “hemostasis” is initiated to preserve the vital blood supply. Immediately following damage, primary hemostasis initiates smooth muscle cell constriction to reduce blood flow to the wounded vessel. Next, platelets aggregate on the vessel walls near the site of injury to form a “soft-plug”. Secondary hemostasis involves activated thrombin’s proteolytic attack on fibrinogen to form fibrin, and the cross-linking of fibrin to form a clot across the vessel wound. This stable fibrin clot accompanies the transition of blood from a liquid to a firm gel state. Secondary hemostasis relies on a network of proteins, known as blood coagulation factors, which control unwanted clotting and localize coagulation to the site of injury.

Hemophilia is an X-linked bleeding disorder in which hemostasis is interrupted because the gene for blood coagulation factor VIII (hemophilia A) or blood coagulation factor IX (hemophilia B) is inactive or damaged. The inability to stop bleeding from open wounds and crippling internal hemorrhaging are a few of the detrimental symptoms of hemophilia. The research of the Spiegel lab, and this document, will focus on blood coagulation factor VIII (FVIII) and hemophilia A. In hemophilia A, FVIII is either absent or non-functional, and the stable fibrin clot does not form effectively. There are degrees of severity for hemophilia A, depending on the amount of FVIII present. Severe hemophiliacs have <1% normal FVIII levels, moderate hemophiliacs have 1%-5%, and mild hemophiliacs have >5% - <40% FVIII levels.

1.2 Historical Overview of Blood Coagulation Research and Treatment

The biochemical mechanisms underpinning blood coagulation were only recently understood, yet the phenomenon of uncontrolled bleeding that would come to be known as

hemophilia has a long history of investigation. In the second century A.D., Rabbi Judah in the *Mishnah* of Jewish law wrote that if a woman “circumcised her first child and he died [as a result of bleeding from the operation], and a second one also died [similarly], she must not circumcise her third child”.¹ The medieval Islamic surgeon Albucasis wrote about bleeding disorders in his encyclopedic *Al Tasrif*, circa 1000 A.D.^{1,2} Queen Victoria of the United Kingdom was a hemophilia carrier, and many of her progeny bore the infamous “Royal Disease”. Her descendants included Prince Leopold who suffered an untimely death after a mild accident, and the severe hemophiliac Tsarevich Alexei Nikolaevich, whose compromising disease contributed to the downfall of the ruling house of Romanov in 1918 Imperial Russia.³

One of the earliest clinical descriptions of hemophilia was by Dr. John Conrad Otto in 1803, who described “bleeders” and prescribed sodium sulfate to encourage hemostasis.⁴ Nasse first described a formula for the transmission of hemophilia in 1820^{1,5}, and it was in the *Handbuch der Physiologie des Menschen* (1833) that the German microscopist Johannes Müller described the protein “fibrin” as the constituent material of a blood clot.⁶ In 1840, Lane communicated the remarkable first therapeutic human blood transfusion to treat hemophilia (Figure 1).⁷

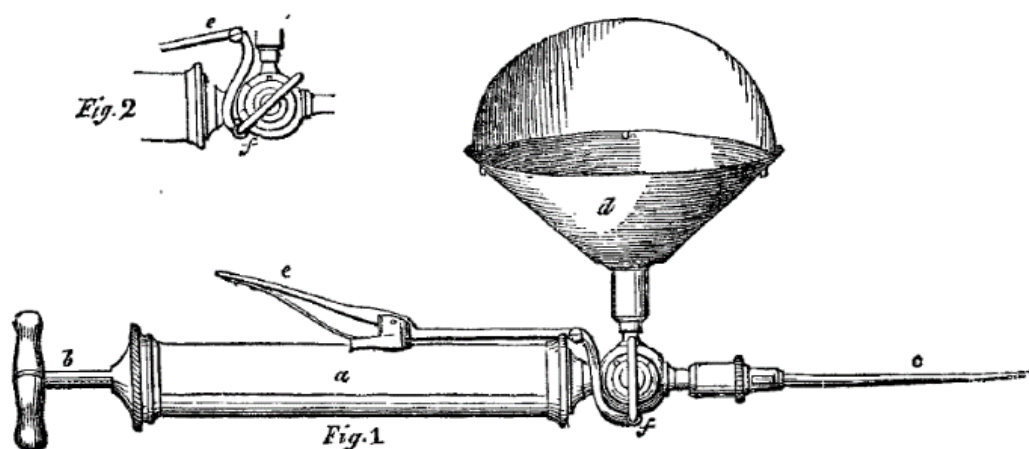


Figure 1 Schematic of syringe used in first blood transfusion to treat hemophilia. The hemophiliac boy described by Lane suffered from a nearly mortal six-day bleed following an eye surgery. Prior to this, treatments for hemophiliac bleeding episodes were largely non-existent. (Lane, 1840)

In 1872, Schmidt noted that blood in contact with an open wound coagulated more readily than that collected by venipuncture. He theorized that fibrin must have a precursor, fibrinogen, in the blood and that a “zymoplastic” agent present in injured tissue must control the activation of prothrombin to thrombin and generation of stabilized clots.⁸ In the 1890s it was demonstrated that the addition of cation chelation agents such as citrate or oxalate could delay blood coagulation; indicating calcium ions were important for clotting.⁹⁻¹¹ The first quantitative test for hemophilia was developed in 1893 by Wright, who placed blood into capillary glass tubes and inverted them at set time intervals until the blood had solidified.¹² Following Hammarsten’s successful purification of fibrin in 1899,^{11,13} Morawitz’s 1905 “blood coagulation model” posited a tissue-based “thrombokinase” protein (now known as Tissue Factor or “TF”) as the agent of prothrombin activation in the presence of calcium ions.¹⁴

The twentieth century heralded the discovery of the blood coagulation factors, intermediary proteins that regulate blood coagulation from the initial exposure of extrinsic TF to the final formation of fibrin clots. In 1937, Patek and Taylor measured the effect of temperature on the coagulation time of citrated blood plasma, noting that at 48 °C an unknown clotting agent was completely inactivated. When this plasma was dialyzed against distilled water, they collected a protein precipitate which was separated from the plasma by centrifugation and re-suspended in a 0.85% (w/v) sodium chloride solution. This precipitate resuspension retained the thermolabile clotting characteristic of whole plasma, and furthermore, could be used to clot samples of hemophiliac blood. This unknown “globulin substance” later became known as Anti-hemophilic Factor (AHF), or Factor VIII (FVIII) (Figure 2).¹⁵

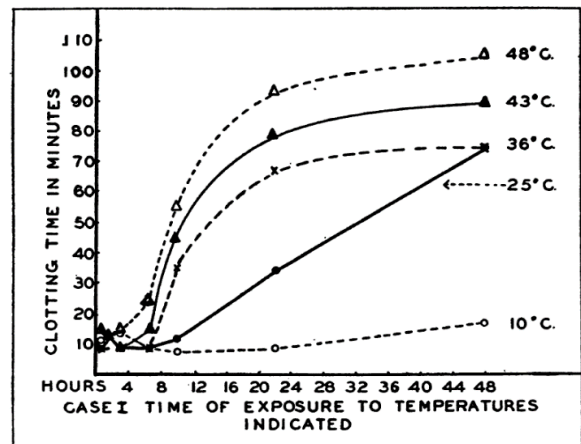


Figure 2 The thermolabile discovery of FVIII. Blood plasma held at 36 °C for 10 hours displayed decreased clotting capability. (Patek and Taylor, 1937)

The remaining blood coagulation factor discoveries came shortly, and include: Factor V (FV, a.k.a. Proaccelerin) by Owren in 1947^{11,16}; Factor XIII (FXIII, a.k.a. Laki Lorand Factor) by Laki and Lorand in 1948¹⁷; Factor VII (FVII, a.k.a. Proconvertin) by Koller et al. in 1951¹⁸; Factor IX (FIX, a.k.a. Christmas Factor) by Biggs and MacFarlane in 1952¹⁹; Factor XI (FXI, a.k.a. Plasma Thromboplastin Antecedent) by Rosenthal in 1953²⁰; Factor XII (FXII, a.k.a. Hageman factor) by Ratnoff and Colopy in 1955²¹; and Factor X (FX, a.k.a. Stuart-Prower Factor) separately by Telfer and Graham in 1956 and 1957, respectively.^{22,23} The story of the discoveries of these blood factors is a fascinating one that unfortunately is outside of the scope of this document.

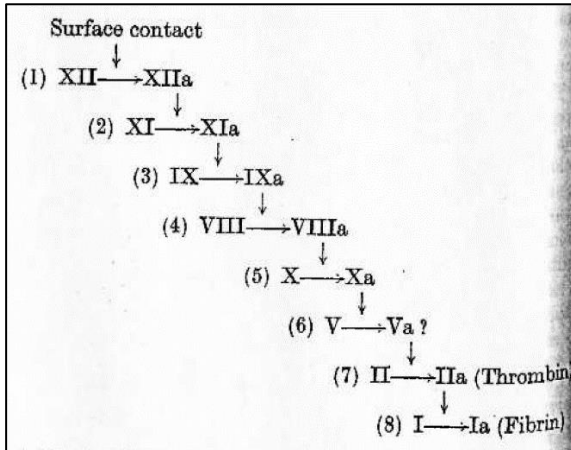


Figure 3 Enzyme Cascade Model of Blood Coagulation. (MacFarlane, 1964)

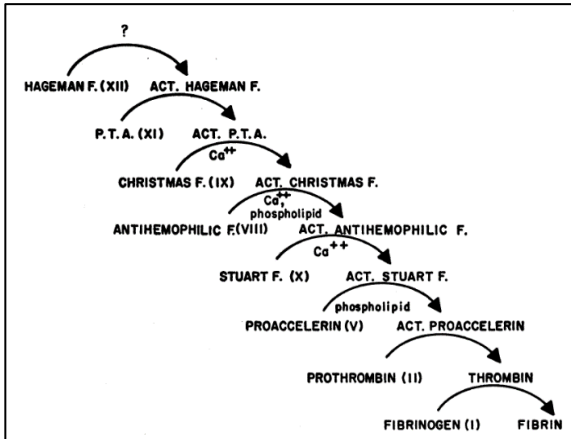


Figure 4 The Waterfall Model of Blood Coagulation. (Davie and Ratnoff, 1964)

The first descriptions of blood coagulation as a sequential cascade of protein interactions were independently published in 1964, first by R. G. MacFarlane (Figure 3) and then shortly after by Davie and Ratnoff (Figure 4).^{24,25} Initially conceived as a single “waterfall” route, the “blood coagulation cascade” came to describe the two “extrinsic” and “intrinsic” pathways, which both feed into the “common” pathway of thrombin-generated fibrin clot formation (Figure 5).²⁶ The extrinsic pathway originates from exposed Tissue Factor (TF) protein on subendothelial cells external to the lumen of the vascular endothelium. The TF activates FVII (FVIIa), and TF:FVIIa in the presence of calcium activates FX (FXa). The

intrinsic pathway relies on activated FXII (FXIIa) generating activated FXI (FXIa), which in turn activates FIX (FIXa). Separately, thrombin cleaves FVIII in complex with the carrier protein von

Willebrand's Factor (vWF) to activate FVIII (FVIIIa) and dissociate it from vWF. The coordination of FVIIIa and FIXa is known as the intrinsic FX-ase (or "Ten-ase") complex. The common pathway is composed of the FXa:FVa complex that cleaves prothrombin (FII) to thrombin (FIIa). Thrombin in turn cleaves fibrinogen (FI) into a mesh of fibrin (FIa), which is cross-linked by FXIIIa to form stable fibrin clots.

In 2001, Hoffman proposed a novel cell-based model for hemostasis. In contrast to the blood coagulation cascade's focus on protein factors, the cell-based model describes three-phases (initiation, propagation, and amplification) wherein hemostasis is controlled by the presence and activation of specific cellular features (Figure 6). In the Initiation phase, extravascular TF-presenting cells (e.g., fibroblast cells) serve as the origin of activation for FVIIa, FXa, thrombin, and FIXa. However, FXa is quickly degraded by anti-coagulation proteases if it leaves the extravascular cell surface. The Amplification phase consists of the trace thrombin generated during initiation traveling to nearby platelet surfaces and activating platelet surfaces, FV, FVIII, and FXI.

Once the platelets and factors have been primed, the Propagation phase produces a concentrated burst of activated thrombin to produce fibrin clots. This model addresses issues raised by the

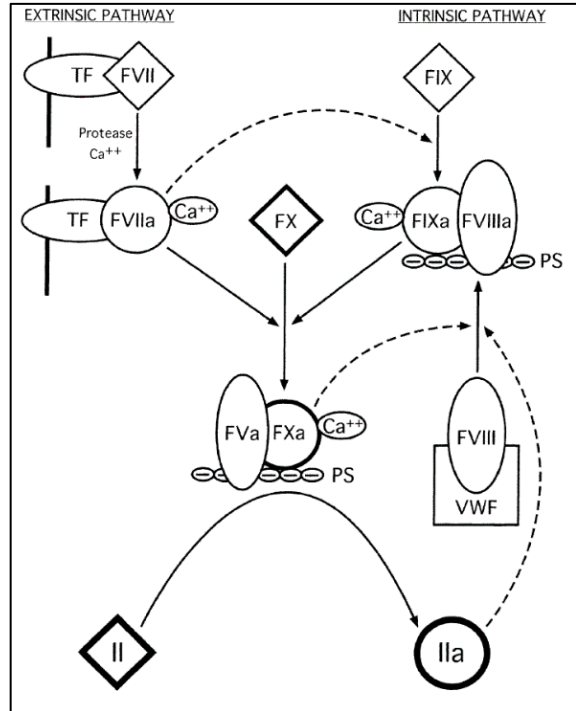


Figure 5 The Blood Coagulation Cascade. The extrinsic and intrinsic routes funnel into the "common" pathway of thrombin activation by FXa:FVa in the presence of Ca²⁺. Factor I (FI) is omitted from this diagram. (Spiegel and Stoddard, 2002)

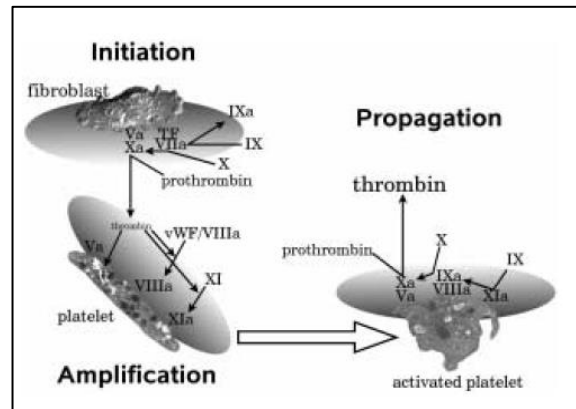


Figure 6 The Cell Based Model of Hemostasis. The presence of anti-coagulation proteases localizes FXa to cellular surfaces. Thrombin generated at TF-presenting extravascular cells during "Initiation" travel to platelet surfaces to "Amplify" platelet and factor activation and allow high-output "Propagation" of thrombin activation. (Hoffman, 2001)

historical cascade model in explaining hemostasis *in vivo*, such as why extrinsic FVIIa/TF-initiated FXa cannot compensate for missing FVIII or FIX activity in hemophiliacs.²⁷

While whole blood transfusions represented the first form of treatment for hemophilia, the standard of care until the 1960s was frozen or lyophilized plasma in response to a bleeding episode. One complication of plasma therapy was that whole plasma delivered the entire protein profile and ~50% of the volume of blood instead of only the necessary clotting factors. Hypervolemia (excessive blood fluid) and organ failure were often the limiting factors for the rate and efficacy of plasma infusion used to treat bleeding episodes. In 1964, Dr. Judith Graham Pool communicated a procedure of quickly thawing frozen plasma and collecting the precipitation of blood coagulation factors which formed.²⁸⁻³⁰ This concentrated “cryoprecipitate” ushered in a marked improvement in patient care, as it granted the ability to deliver small therapeutic dosages and prophylactic treatment of hemophilia with regular infusions.³¹ Unfortunately, approximately 30% of patients receiving FVIII-containing whole blood, plasma, or concentrates develop anti-FVIII inhibitory antibodies (Figure 7). These “inhibitors” reduce the efficacy of replacement factor treatment and increase the severity of hemophilia symptoms. Hemophiliacs with absent or significant deletions of FVIII have 20-80% risk of developing an inhibitor, whereas those with minor missense

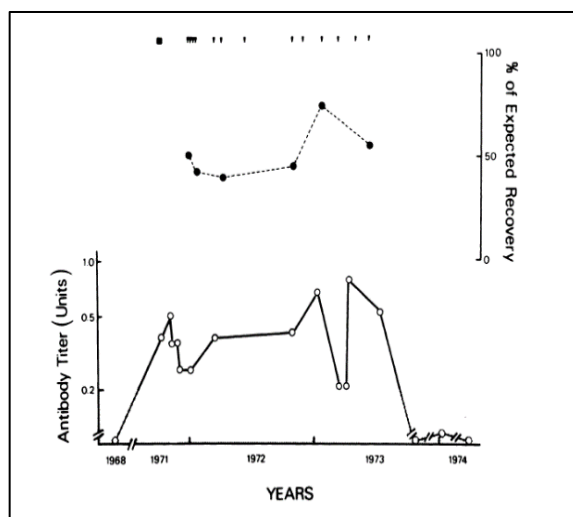


Figure 7 "Low-responder" Patient Antibody Titer. This patient displayed sustained titer level with normal FVIII dosages. (Allain and Frommel, 1976)

mutations demonstrate an inhibitor prevalence of 5%.³² Furthermore, researchers have identified stereotypes of patient immune response to FVIII, including “high-responders” and “low-responders”. High-responder patients maintain elevated immunogenic memory, increase the affinity of antibodies to FVIII with exposure, and have high-titer antibodies. Low-responder patients, on the other hand, do not exhibit these immunity changes (Figure 7).³³

In the early 1900s, the main treatment for inhibitory antibodies was general immunosuppression therapy with cytotoxic nitrogen mustard compounds. First discovered by WWI physicians who noted decreased white blood cells in soldiers exposed to mustard gas, therapeutic alkylating agents such as cyclophosphamide relied upon the formation of cyclic ammonium to covalently bind to DNA guanine nucleobases and induce cell apoptosis (Figure 8, Figure 9). While devastating to cell populations engaged in the immune response, the many off-targets affected by this therapy were not ideal.³⁴

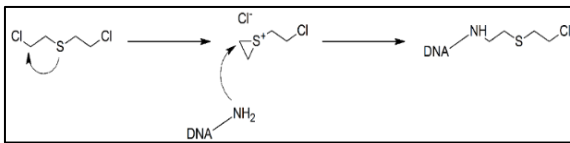


Figure 8 Sulfur Mustard Mechanism of Action. The highly reactive cyclic intermediate disrupts DNA and many off-targets. (Hall and Tilby, 1992)

In 1977, Brackmann and Gormsen reported immune tolerance induction (ITI) as an alternative to general immunosuppression in the treatment of inhibitory antibodies. The patient was delivered large doses (>1000 U/day) of FVIII for several months; after an initial strong immune

response, their FVIII inhibitor titer reduced (Figure 10).³⁵ The mechanism by which ITI proceeds is not fully understood, but proposals include clonal deletion of anti-FVIII B cells, receptor editing of antibodies, regulatory T cell induction, and anti-idiotypic antibodies.³⁶ The success of ITI campaigns has been shown to depend on the patient age, the FVIII inhibitor titer, and the dose of replacement FVIII.³⁶ Data from the International Immune Tolerance Registry (IITR) indicated that higher dosages of FVIII (>200 IU/kg/day) in ITI protocols correlate to increased success rates.³⁶

These advances in treatment were soon the fulcrum for an epidemic that particularly devastated the hemophilia community, as the 1980's marked the outbreak of the human immunodeficiency virus (HIV). On June 5th, 1981, the Centers for Disease Control (CDC)

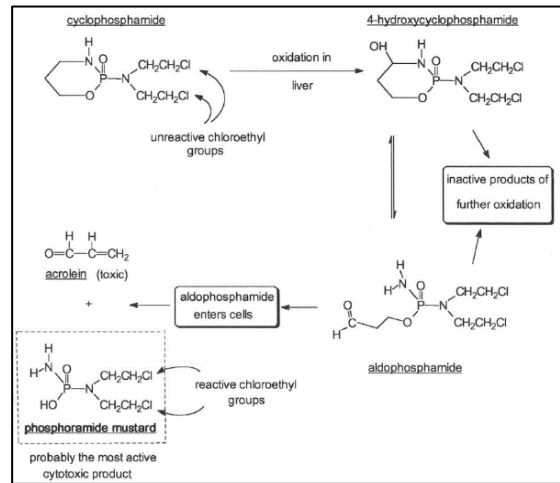


Figure 9 Cyclophosphamide Pathway of Activation. Modification of the mustard nitrogen's nucleophilicity allows for therapeutic pro-drug administration that requires activation in the liver. (Hall and Tilby, 1992)

Morbidity and Mortality Weekly Report (MMWR) communicated that five immune-compromised men in Los Angeles were diagnosed with *Pneumocystis carinii* pneumonia (PCP). This peculiar infection by an opportunistic fungus would come to be recognized as a symptom of Acquired Immune Deficiency Syndrome (AIDS). Not long after this, on July 16th, 1982 the CDC communicated hemophiliacs who had received blood factor concentrates had developed AIDS.^{37,38} While

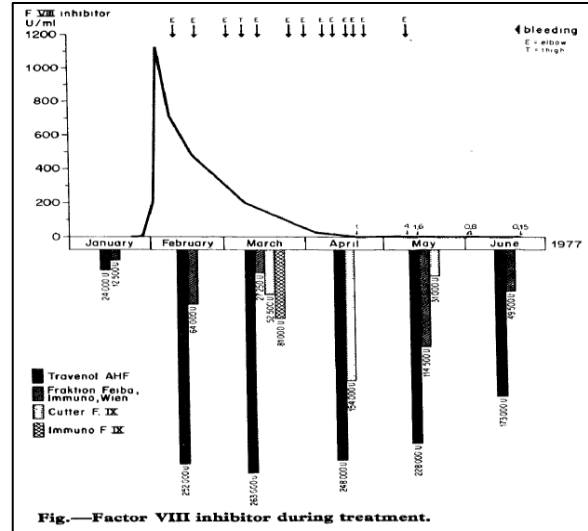


Figure 10 Immune Tolerance Induction (ITI) Campaign in a "High-responder" Patient. The FVIII inhibitor U/mL is reported in Bethesda dilution factor of antibodies present. At 1200U/mL the patient's blood could be diluted 1200 X and still clear 50% of the FVIII present in a normal blood sample. (Brackmann and Gormsen, 1977)

HIV was suspected in the blood supply as early as 1982, due to lack of knowledge about HIV and resistance from the Food and Drug Administration (FDA) it was not until late 1984 that steps were taken to deactivate the virus in the blood supply through heat-treatment.³⁹ By 1993, a class action lawsuit against the National Hemophilia Foundation and blood-derived therapeutic companies claimed approximately 10,000 hemophiliacs had contracted HIV from the contaminated blood supply.⁴⁰

1.3 FVIII Molecular Details

The FVIII protein is expressed from the 187 kilobase *F8* gene, comprised of 26 exons and ~9 kilobase pairs of coding sequence. First described by Gitschier in 1984, at the time of communication, *F8* was the largest gene yet characterized, encompassing ~0.1% of the human X chromosome (Figure 11).⁴¹ The gene contains three sequential "A" domains, a unique "B" domain, and two sequential "C" domains.

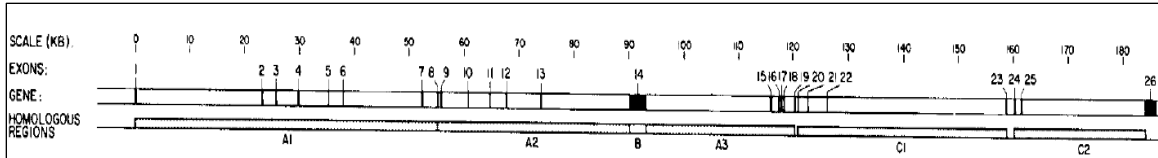


Figure 11 **Map of the F8 Gene.** The gene contains 26 exons and contains the protein domain sequence A1-A2-B-A3-C1-C2. The B domain is subsequently excised in wildtype FVIII maturation, and is often omitted from recombinant FVIII constructs (denoted as B-Domain Deleted a.k.a. BDD). (Gitschier et al., 1984)

The A domains have a 30% homology pairwise (20% conserved among all three) and are related to the copper-binding protein ceruloplasmin, while the C domains share a 37% homology and are related to the membrane-binding discoidin protein family.⁴¹ The 2332 amino acid residue FVIII protein is expressed with the domain sequence of A1-A2-B-A3-C1-C2. Consideration of the non-overlapping C1 and C2 domain intron boundaries in the gene led researchers to postulate that the domains are the results of a DNA segmental replication event. Conversely, the B domain may stem from a processed gene insertion into the established A2-A3 boundary area.⁴¹

A second transcript of the *F8* gene has been identified, a reverse direction ~1700 base copy originating in a CpG island within intron 22. This transcript was demonstrated to express in a wide variety of cell types.⁴² Additionally, a third transcript of the *F8* intron 22 region has been identified; an in-frame, eight amino acid sequence which is spliced to exons 23-26 containing the C2 domain of FVIII.⁴³ Approximately 40% of the genetic mutations resulting in severe hemophilia A are the intron 22 inversion (I22I) of the *F8* gene. This mutation interrupts the secretion of FVIII, and patients with this mutation have no endogenously synthesized FVIII circulating in their blood.⁴³⁻⁴⁵

The synthesis of FVIII occurs in hematopoietic Kupffer cells, somatic liver sinusoidal endothelial cells, and extrahepatic endothelial cells.⁴⁶ FVIII does not express at high levels endogenously, with average serum concentrations of 0.5 nM.⁴⁷ To be secreted from the cell, FVIII must be proteolytically cleaved intracellularly at residue R740 and R1689 by Furin (a.k.a paired basic amino acid cleaving enzyme (PACE)), which partially removes the FVIII B domain. This processed heterodimeric FVIII contains a domain sequence of A1-A2/A3-C1-C2. In the absence of a hemostatic event, the carrier glycoprotein von Willebrand's Factor (vWF) complexes to inactive

FVIII and shields it from proteolysis and some clearance receptors in the blood. The binding interaction between FVIII and vWF is not fully understood, but interactions have been demonstrated between FVIII and the D' domain of vWF.⁴⁸⁻⁵⁰ Intracellular complexes of vWF:FVIII have been shown to be secreted from cells in Weibel-Palade bodies.⁵¹

In the event of vascular injury, vWF binds to activated platelet surfaces expressing the glycoprotein Ib-IX (GpIb/IX) receptor, bringing the vWF:FVIII complex in proximity to the site of coagulation. Inactive, heterodimeric FVIII is then cleaved by thrombin (FIIa) at residue R372 to dissociate from vWF and become an activated FVIII heterotrimer (FVIIIa) with the domain structure A1/A2/A3-C1-C2. The C1 and C2 domains of FVIIIa bind to phosphatidylserine (PS) rich activated-platelet surfaces, where FVIIIa and FIXa associate to form the intrinsic “Ten-ase” Complex, and enzymatically cleave FX to form FXa.^{27,50,52} FVIIIa is inherently unstable in the heterotrimeric form, and the A2 domain spontaneously dissociates from the core protein. Once the A2 domain has detached, the half-life of FVIIIa is significantly decreased.⁵³

Both free FVIIIa and FVIII:vWF are regularly recycled from the blood. While clearance receptors for FVIIIa, vWF, and for vWF:FVIII are not fully understood, the identified receptors include: low-density lipoprotein receptor (LDLR); low-density lipoprotein receptor-related protein-1 (LRP1); asialoglycoprotein receptor (ASGPR); macrophage mannose receptor type 1 (MMR/CD206); heparan sulfate proteoglycans; sialic acid binding IgG-like lectin 5 (Siglec5); scavenger receptor class A member 5 (SCARA5); stabilin-2 (STAB2); and C-type lectin domain family 4 member M (CLEC4M).^{46,54}

The presence of terminal sialic acids on vWF glycan sites positively contribute to the levels of serum vWF present. In 2015, Yang presented a model of protein degradation based upon exposure to glycosidases and asialylated protein recognition by lectin-like-receptors (LLR).⁵⁵ Knockout of an LLR “MGL”, which presents the receptor for hyposialylated vWF, significantly extends the serum half-life of vWF. Future research is investigating the role of FVIII sialylation and clearance.⁵⁵⁻⁵⁷

Recent work has highlighted the Ashwell Morell receptor (AMR) in vWF clearance. Predominantly expressed on the surface of hepatocyte cells, AMR is an (ASGPR), and the first recognized C-type (requiring calcium) lectin (glycan-binding protein), originally demonstrated in binding asialylated ceruloplasmin. Human ASGPR proteins also capture and signal the destruction of glycan proteins with terminal galactose (Gal) or N-acetylgalactosamine (GalNAc) residues not produced endogenously in humans. Glycan mediated immunogenicity represents an considerable challenge for replacement FVIII:vWF products produced in non-human mammalian cells.⁵⁴

1.4 Modern Hemophilia A Therapies

Recombinant FVIII was first produced by Wood et al. at Genentech in 1984, approved under the brand name Recombinate™ in 1992. Today, a number of recombinant products form the gold standard for hemophilia A therapy.⁵⁸ In addition to unmodified FVIII, classes of therapeutics include but are not limited to small molecule therapies, modified FVIII constructs, bypassing agents for use in the presence of an inhibitor, and developments towards gene therapy. Highlights of current or communicated future therapeutics include:

SMALL MOLECULE THERAPIES

These low molecular weight pharmaceutical compounds are used to effect a physiological change in a hemophilia patient, without directly providing replacement blood coagulation factor.

Desmopressin acetate (1-deamino-8-D-arginine vasopressin, DDAVP // Ferring Pharmaceuticals)
(FDA approved, patent expired)

A synthetic analog of the hormone vasopressin, Desmopressin stimulates the secretion of vWF release from endothelial cells. The increased concentration of vWF favors formation of the protective vWF:FVIII complex and reduces proteolytic degradation of free FVIII. This treatment is only for those with mild FVIII deficiency.⁵⁹

Epsilon-aminocaproic Acid (Amicar // Akorn, Inc.)

(FDA approved)

Epsilon-aminocaproic Acid (EACA) is an inhibitor of the plasminogen-mediated “fibrinolytic” pathway for degradation of formed fibrin clots. While EACA administered alone will not compensate for a severe hemophiliac’s complete inability to form fibrin clots, it has found use as an adjunct therapy to support clotting during dental procedures and minor surgery.⁶⁰

MODIFIED REPLACEMENT FVIII

These therapeutics augment the architecture and functionality of FVIII to increase half-life, stability, and efficacy of replacement therapy.

Anti-vWF-Nanobody FVIII Fusion Protein (FVIII-KB013bv // Novo Nordisk A/S)

(Under Development)

Heterodimeric FVIII dissociation from vWF is strongly correlated with increased FVIII clearance from the blood by proteolysis and the immune system. Generating a FVIII therapeutic with an increased affinity for vWF would strengthen the vWF:FVIII complex and reduce the immunogenicity of the replacement FVIII therapy. Lenting et al. communicated a recombinant FVIII construct with the B domain replaced by an anti-vWF camelid single domain antibody (nanobody). This FVIII-nanobody fusion protein, “FVIII-KB013bv”, demonstrated a 100-fold reduction in K_D from vWF, and a two-fold half-life increase *in vivo* compared to recombinant FVIII (rFVIII).⁶¹

Human/Porcine Chimeric FVIII (Et3i // Expression Therapeutics)

(Under Development)

Due to the large quantity of FVIII required for ITI campaigns, development of a high-yield recombinant human FVIII (rhFVIII) is of high interest to the hematological community. Recombinant B-domain-deleted (BDD) porcine FVIII (rpFVIII) expresses at 10-14 fold higher levels than rhFVIII.⁶² A novel human/porcine chimeric construct (“Et3i”) containing the porcine A1 and A3 domains expresses 5.3 ± 0.75 fold higher than rhFVIII from transiently transfected COS-7 cells and stably transfected BHK cells, while maintaining comparable clotting activity.⁶³ Et3i has recently received positive feedback from an FDA Pre-Investigational New Drug (IND) program. Additionally, Et3i is being evaluated as a potential gene therapy candidate, as transgenic Et3i transfected BHK-M cells demonstrated ~13 fold greater expression than BDDhFVIII.⁶³⁻⁶⁵

Site-directed PEGylated rhFVIII (BAY 94-9027 // Bayer)

(FDA Investigational Agent Biologics License Application (BLA) accepted)

Commonly, polyethylene glycol (PEG)-FVIII products rely on N-hydroxy succinimide (NHS) ester chemistry for PEGylation, an effective though inaccurate conjugation targeting lysine or N-terminal amine residues. BAY 94-9027 is a site-directed PEGylated FVIII using engineered cysteine and maleimide chemistry. Several sites were screened for cysteine insertion, and optimization of PEGylation increased BAY 94-9027 half-life sufficiently to allow prophylaxis once every seven days.^{66,67}

B-Domain Selectively PEGylated rhFVIII (Adynovate, BAX855 // Shire Pharmaceuticals)

(FDA Approved)

Adynovate is a modified recombinant human FVIII (rhFVIII) construct with ~60% of the PEGylation selectively targeted to the B domain. This reduces unwanted PEGylation at sites that would cause steric hindrance of FVIII binding to vWF, phosphatidylserine (PS) platelet membrane

surfaces, or coordinating FIXa and FX. Additionally, the majority of the B domain is enzymatically removed from FVIII during thrombin activation to the heterotrimeric form. Adynovate demonstrated 1.4-1.5 fold increased half-life ($T_{1/2}$) and residence time compared to unmodified recombinant human FVIII.⁶⁸

Antibody Crystallizable Fragment (Fc) rhFVIII Fusion Protein (Eloctate // Bioverativ Inc.)

(FDA approved)

The neonatal Fc receptor (FcRn) is an MHC class I-like protein which recognizes the Fc region of IgG1 antibodies. In vascular endothelial cells, endosome-expressed FcRn rescues and recycles pinocytosed antibodies from the lysosomal degradation pathway.⁶⁹ A B-domain deleted (BDD) FVIII-(IgG1 Fc domain) fusion protein has been created (rFVIII-Fc) to take advantage of this FcRn functionality. The rFVIII-Fc construct does not reduce clearance of vWF:FVIII complexes by liver hematopoietic Kupffer cells, but has demonstrated recycling of uncomplexed, free-rFVIII-Fc by somatic liver sinusoidal cells. In clinical phase 1/2a and 3 (A-LONG) trials, the rFVIII-Fc construct demonstrated ~1.5 fold increased half-life compared to rFVIII.^{46,70}

A2-A3 Disulfide Anchored FVIII (Bayer)

(Under development)

The spontaneous dissociation of the heterotrimeric FVIIIa A2 domain hinders the potential half-life of replacement therapies. Gale et al. communicated a rFVIII that contains an engineered cysteine pair (C664-C1826) disulfide bridge between the A2 (heavy chain) and A3 (light chain) domains of heterotrimeric FVIII. This construct has demonstrated increased half-life *in vivo* while maintaining binding affinity for vWF and normal proteolytic degradation by activated protein C (APC).^{53,71}

Porcine FVIII (Obizur, OBI-1// Shire Pharmaceuticals)

(FDA approved)

Following the communication of the cDNA for the porcine FVIII gene,⁷² the use of porcine FVIII has been demonstrated as an effective alternative therapy in hemophilia A patients with anti-FVIII inhibitors.⁷³ Obizur is a B-domain deleted (BDD) porcine FVIII therapeutic that has low immunogenicity in patients with established anti-hFVIII titers.⁷⁴

BYPASSING AGENTS

For patients with potent inhibitors, even radically modified rFVIII at high dosages can be ineffective. Bypassing agent therapeutics do not rely on modifications to FVIII. Instead, they circumvent the function of FVIIIa by enhancing alternate routes through the coagulation cascade to augment clotting capability. These therapies are most likely used in conjunction with ITI campaigns.

Anti-FIX-FX Bispecific Antibody (Hemlibra, Emicizumab, ACE910 // Roche)

(FDA approved with black box warning)

Hemlibra is a prophylactic bispecific humanized antibody that binds FIXa and FX, replacing FVIIIa's coordinating role in the Ten-ase complex. Due to neonatal Fc receptor (FcRn) recycling, Hemlibra demonstrates significantly improved half-life of 4-5 weeks compared to traditional prophylaxis treatment. In clinical trials, minimal anti-Hemlibra antibodies were detected, although recent thrombosis (clot-formation) complications have caused the FDA to issue a warning.^{75,76}

Activated FVII bypassing agent (NovoSeven, rFVIIa // Novo Nordisk A/S)

(FDA approved)

Recombinant activated FVII (rFVIIa) has been shown effective as a backup regimen for hemophilia A patients with inhibitors. Termed “secondary prophylaxis”, rFVIIa generates increased amounts of extrinsic pathway TF:rFVIIa activated FX to maintain clotting capability and avoid bleeding induced arthropathy during high inhibitor loads.⁷⁷

Activated prothrombin complex concentrate (FEIBA NF - Shire)

(FDA approved, patent expired)

To overcome inhibitors, the therapeutic Factor Eight Inhibitor Bypassing Activity (FEIBA) provides a cocktail of factors II, IX, X and VIIa to overcome the deficient FVIIIa.⁷⁸

Anti-Tissue Factor Pathway Inhibitor Antibody (Concizumab // Novo Nordisk A/S)

(Phase I Clinical Trials)

The Tissue Factor Pathway Inhibitor (TFPI) protein reversibly inhibits the formation of FVIIa/TF-initiated FXa. Concizumab is a humanized monoclonal anti-TFPI antibody which allows increased levels of extrinsic FVIIa/TF-generated FXa to accumulate and compensate for the lack of intrinsic FVIIIa/FIXa functionality.⁷⁹

GENE THERAPY

Gene therapy is an attempt to correct defective or absent genetic information in the cells of a diseased organism. While still in the developmental stages for humans, animal models of Hemophilia A with retroviral/lentiviral, adenoviral, and adeno-associated viral (AAV) have been successful.

The challenges presented by viral transduction of a therapeutic gene are numerous. For example, first-generation retroviruses cannot penetrate the nuclear membrane, and can only

transduce dividing cells. Lentiviral vectors can infect non-dividing cells, but expression of a foreign protein on infected antigen presenting cells (APCs) can trigger immune deletion of the altered cells. Additionally, the risk for oncogenesis when using viral therapies is a dire concern. Despite these complications, gene therapy has the potential to cure hemophilia and is the subject of intense research.⁸⁰

Platelet-localized FVIII (Blood Research Institute, Blood Center of Wisconsin)

(Under Development)

Lentiviral transduction of FVIII into hematopoietic stem cells (HSC's) generated platelets containing FVIII protein and mRNA. Due to activated platelets localization to the site of vascular injury, therapeutic recovery of hemostasis can be achieved using this method with levels of FVIII much lower than in replacement therapy.⁸¹

Chapter 2: Protein X-Ray Crystallography and Molecular Modeling

2.1 A Brief History of Protein X-ray Crystallography

During the winter of 1611 in Prague, Johannes Kepler published the booklet *A New Year's Gift, or on the six-cornered Snowflake* for his patron Counselor John Matthew Wacker. In it, Kepler pondered the six-sided snowflakes falling outside, and surmised that their hexagonal shape “could not be a property of the water vapor, which lacks form, or of the cold air; but must have been a particularly suitable or favorable orientation for the water to arrange in”.⁸² This was the first published work attempting to establish a connection between the outer appearance of a material and the internal organization of its regular-packing components (Figure 12). Kepler drew comparisons between snowflakes and the hexagonal arrangement of honeycombs or the rhombohedral surfaces of a pomegranate seed, but he was unable to answer his inquiry, stating “...I have knocked at the door of chemistry and see how much remains to be said before we can get hold of our cause...”.⁸²

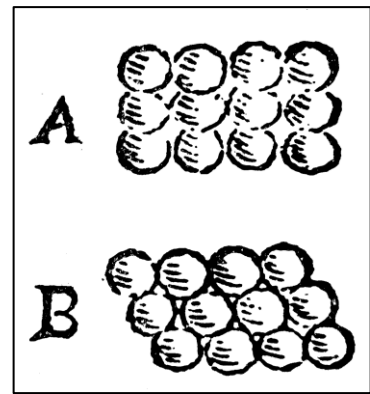


Figure 12 Comparison between cubic (A) and rhomboid (B) packing of spheres. (Kepler, 1611)



Figure 13 First communicated X-ray image. (Röntgen 1896. Rosenow 1995)

This question would go unanswered for nearly three centuries, until 1895 when the German physicist Wilhelm Röntgen demonstrated the existence of X-rays and the capability to probe the interior of a solid (Figure 13). He received the first Nobel prize in Physics in 1901 for his discovery; although he never fully revealed the details of his experimentation, and due to his reclusive nature even avoided giving his Nobel lecture.⁸³ In 1912, Max von Laue reported using crystals of copper sulfate as a “diffraction grating” for X-rays, demonstrating both the wave-like nature of X-rays and the

regularity of crystal lattices, earning him the 1914 Nobel Prize in Physics.^{84,85} Sirs William and Lawrence Bragg related the production of X-ray reflections to the distance between crystal lattice planes, formalized in Bragg's law, earning Lawrence the 1915 Nobel Prize in Physics.⁸⁶

Later, as the Cavendish Professor of Physics at Cambridge, Sir Lawrence Bragg encouraged his protégés Max Perutz and John Kendrew towards the structural determination of hemoglobin and myoglobin. Beginning in 1937, Perutz spent twenty-two years attempting to solve the molecular structure of hemoglobin. He made little headway until 1953 when he soaked protein crystals of hemoglobin in mercury to bind to cysteine residues. This isomorphous replacement with heavy metal atoms allowed Perutz to calculate the phase angles of the X-rays diffracted from protein crystals, the aptly named "phase problem" of crystallography. Kendrew published the three-dimensional structure of myoglobin in 1958⁸⁷, shortly followed by Perutz with the structure of hemoglobin in 1960⁸⁸; feats for which they jointly received the 1962 Nobel Prize in Chemistry.

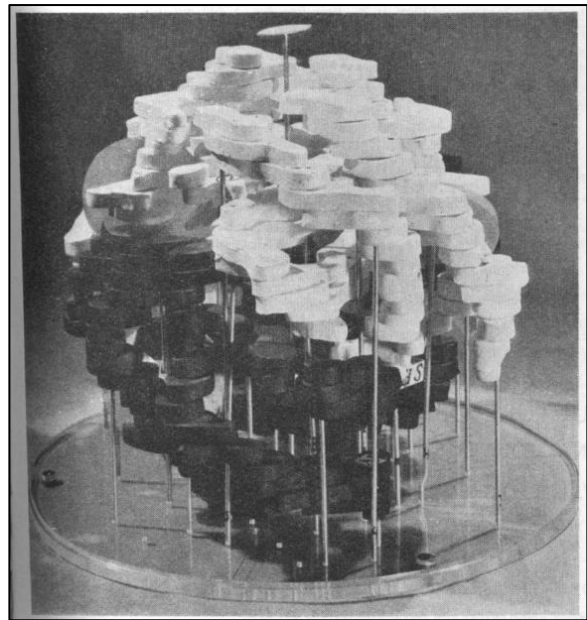


Figure 14 Structural Model of Hemoglobin. At the time of publication, the structural basis for hemoglobin's dynamic oxygen affinity remained a mystery. This structure revealed a distant placement of heme groups between protein subunits, implicating a quaternary protein structure basis for allostery. (Perutz, 1960)

There are two principal modern light sources used to generate X-rays for protein crystal diffraction, the X-ray diffractometer, and the synchrotron particle accelerator. In an X-ray diffractometer, a vacuum-sealed cathode filament emits electrons to an anode (typically copper (Cu) for protein crystallography). Excitation and relaxation of the anode Cu electrons generate a broad spectrum of X-rays, but predictable peaks of radiation are emitted when incoming cathode-generated electrons eject resident Cu electrons from the innermost (K) shell. Cu electrons from

outer (L or M) shells then relax into these vacant (K) positions and emit peaks of X-rays at specific wavelengths, producing the $K\alpha$ (K-L) or $K\beta$ (K-M) emission wavelengths.⁸⁵

Synchrotron X-ray radiation, by comparison, takes advantage of the fact that electrons or positrons experiencing acceleration emit X-rays. Furthermore, there is a correlation between the intensity of particle acceleration, and the wavelength of X-rays emitted. Unlike a diffractometer, where the peak wavelength distribution of X-rays generated is dependent on the anode element (Cu), synchrotron particle accelerators employ complicated “wiggler” or “undulator” paths which particles must pass through. Synchrotrons generate high-brilliance and tunable wavelength X-ray radiation for use in crystallographic experiments.⁸⁵

2.2 Protein Crystallography

A simplified model of protein crystallization occurs in two phases, nucleation, and growth. A saturated solution of protein is perturbed, either through chemical additives, osmosis, or evaporation to become supersaturated (Figure 15). The highly

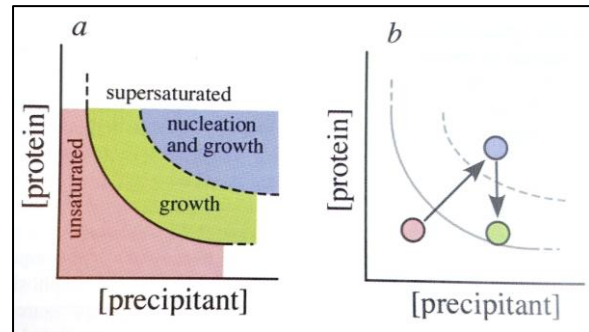


Figure 15 Protein Crystallization Solubility Curve. The supersaturated protein solution initiates the nucleation of the crystal followed by slow growth. (Rhodes, 2006)

concentrated solution seeks to regain equilibrium and will precipitate proteins from the solution to a solid phase. If this transition is approached correctly, the precipitated protein forms an ordered aggregate nucleus and then recruits free-solution molecules. A common method for achieving supersaturation and protein crystallization is hanging drop vapor diffusion; wherein a droplet of protein solution is placed in a hermetically sealed vapor equilibrium with a “mother liquor” of higher osmotic strength.⁸⁹ (Figure 16)

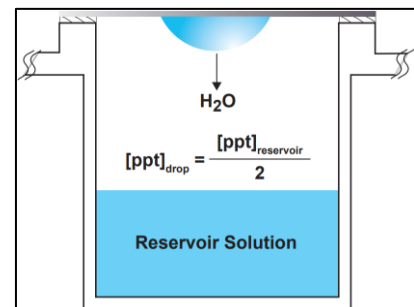


Figure 16 Hanging Vapor Drop Diffusion. (Hampton Research)

Before exposure to X-rays, protein crystals are commonly “cryo-protected” (for example with dimethyl

sulfoxide (DMSO) or glycerol) and then flash-frozen in liquid nitrogen. This treatment allows water in the crystal and droplet to vitrify, forming non-crystalline amorphous ice, and lower temperatures reduce diffusion of oxygen radicals formed from X-ray radiation within the protein crystal.^{85,89}

Protein crystals can be modeled as a lattice of repeating blocks, the smallest of which contains all the structural information of the crystal. These blocks, known as the asymmetric units, are related to their neighbors by crystallographic symmetry and are therefore identical. However, each asymmetric unit can contain multiple molecules which do not have crystallographic symmetry and can adopt different conformations.⁸⁵

The asymmetric unit combined with symmetry operators creates the next largest component within the crystal, the unit cell. The unit cells of a crystal can be defined as having vectors a , b , and c , and angles α , β , and γ (Figure 17). The crystallographic symmetry operators (n -fold symmetry, screw axis, mirror plane, glide plane, inversion center) can be combined into 230 configurations, or space groups. However, the chiral nature of L-amino acids limits the possible space groups for proteins to 65.⁹⁰ These unit cells are the smallest volume of space that contains all the structural and symmetry information of the crystal, and that repeated by translation will create the entire crystal in three dimensions.

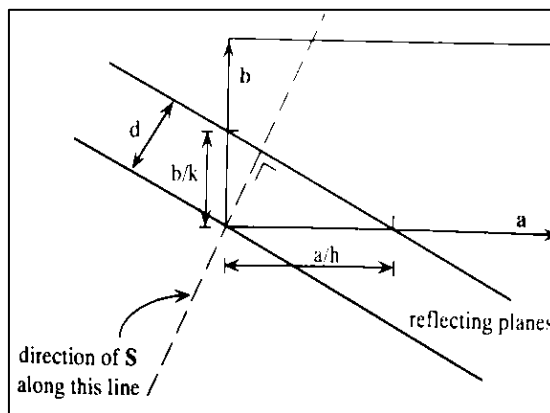


Figure 17 The Unit Cell and the reflecting planes. Incident X-rays along S reflect against imaginary planes within the crystal lattice. (Drenth, 1999)

2.3 X-ray Diffraction

X-rays are electromagnetic waves which travel as a cosine function, with energy $E(t = 0; z) = A \cos 2\pi \left(\frac{z}{\lambda} \right)$, where A is equal to amplitude, z is equal to distance traveled, and λ stands for wave period. X-ray waves incident on a molecular electron system are absorbed by the electrons, which then emit X-ray waves of the same frequency.

X-rays are scattered almost exclusively by the electrons in a crystal. The angles in which X-rays are diffracted by a protein crystal hold information about the dimensions of the unit cell. Additionally, the intensities of the diffracted X-rays reveal details about the distribution and identity of the electron density of the crystal structure.

Diffraction of X-rays can be modeled as reflections against imaginary “reflecting planes” within the crystal lattice; planes that are parallel, equidistant with perpendicular distance = d , and with plane boundaries defined as integer indices (h,k,l) dividing the unit cell a,b,c axes (a/h, b/k, c/l) (Figure 17).^{85,91} When the distance between these reflecting planes results in complete constructive interference, X-ray diffraction is measurable and described by Bragg's Law: $2d\sin\theta = \lambda$. Where d equal to the reflecting plane distance, and θ is equal to the angle between the incident X-ray and the lattice plane. The crystal resolution is described by this Bragg distance (d); with a crystal of 5 Å being poor quality, 2.0-2.5 Å normal quality, and 1.0-1.5 Å high quality (Figure 18).^{85,90,91}

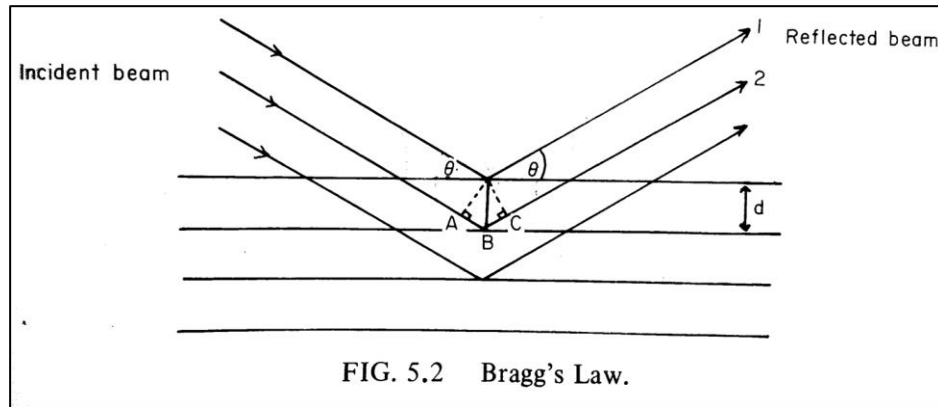


Figure 18 Scattering against a crystal lattice plane. X-rays (arrows) incident from angle θ to a crystal lattice plane will appear to reflect away at angle 2θ . (Blundell and Johnson, 1976)

Consider beams striking electrons (e_1 and e_2) in a lattice, spaced by distance r (Figure 19). The diffracted beam from e_2 travels a path that is $p + q$ longer than the diffracted wave by e_1 , resulting in a phase difference (“Z”) between the waves unless $p + q$ is equal to an integer of $2\pi\lambda$.

Waves of the same wavelength and amplitude but separated by a phase shift of Z , $\left(\frac{Z}{\lambda}\right) \times 2\pi = \alpha$, can be summed together (Figure 20). The waves can be directly compared by breaking both waves into real and imaginary parts, at phase shifts of 0 and 90° respectively. Where wave 1 is the real wave components, and wave 2 is the imaginary wave components. These can be graphically related with an Argand diagram (Figure 21).

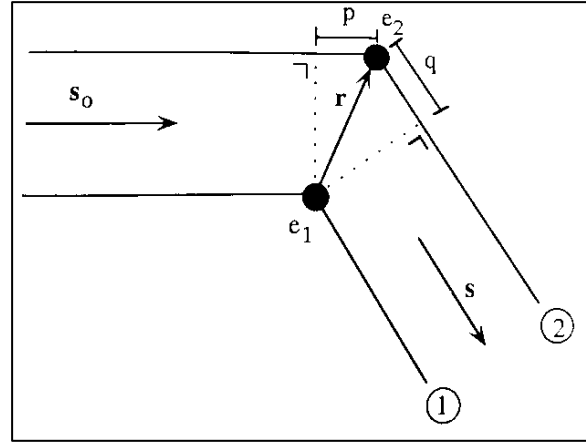


Figure 19 X-ray scattering by system of two electrons. Incident X-rays along S_0 that diffract off e_2 towards S will travel a distance of $p+q$ farther than X-rays diffracting off e_1 . (Drenth, 1999)

The summation of waves allows the scattering of an entire atom can be summed, and results in the atomic scattering factor “ f ”. Furthermore, the scattering of all the atoms in the unit cell can be summed and produces the structure factor “ $F(S)$ ”. Finally, the scattering from all unit cells in the crystal can be aggregated into the crystal scattering factor $K(S)$.⁸⁵

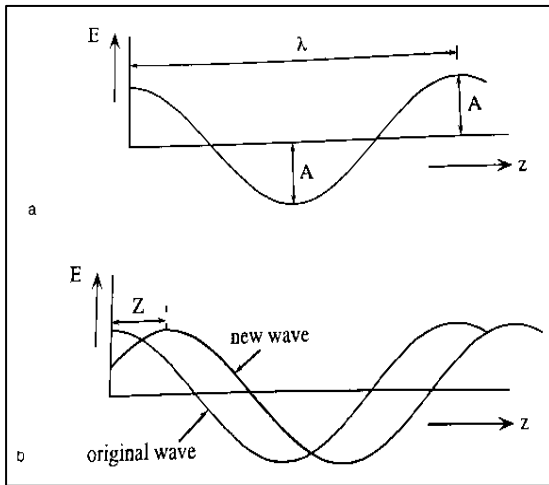


Figure 20 Comparing two waves offset by phase. An original wave can be summed with a new wave, offset by phase angle Z . The resulting wave sum will exhibit either constructive or destructive interference. (Drenth, 1999)

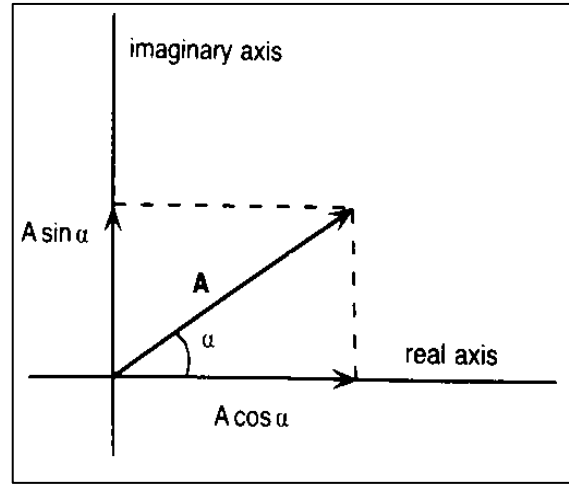


Figure 21 The Argand Diagram. The real and imaginary components of a wave can be graphed along orthogonal axes. The total wave A is depicted as a dot product vector with real ($A \cos \alpha$) and imaginary ($A \sin \alpha$) components, with angle α equal to the phase angle. (Drenth, 1999)

2.4 Phase Determination, Model Building, and Refinement

For the structure building discussed in this document, phase angles for the X-ray diffractions were solved by molecular replacement (MR).

The MR computational method for calculating the phase angles utilizes previously published molecular structures as templates and maximizes “model fit” solutions to the calculated electron density map. First, a published molecular structure is superimposed into electron density and then rotated and translated through the unit cell until an approximate electron density fit and estimated phase angle calculation is found.

Once a model is generated, a molecular graphics program for model building and refinement, such as WinCoot can be used to manually manipulate the model’s atomic coordinates (Figure 22).^{92,93} In tandem to manual adjustments of the model, automated refinement of the molecular structure and electron density map can be accomplished through software suites such as Phenix (Figure 23).⁹⁴

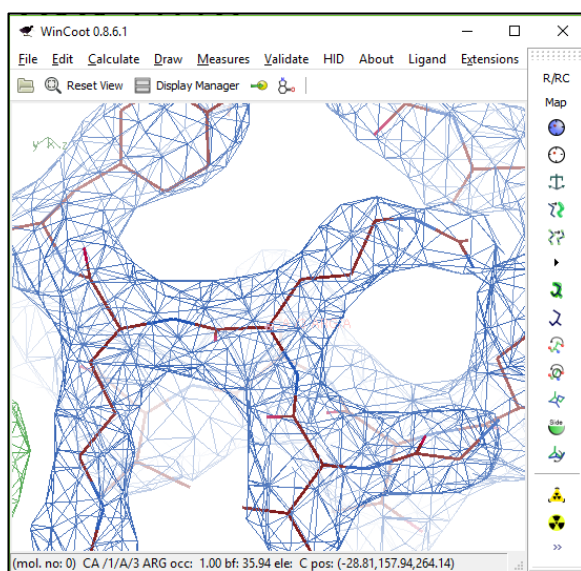


Figure 22 WinCoot Model Building. Individual amino acids (red) are manipulated to optimize placement within the calculated electron density map (blue wire mesh).

Several metrics monitor how well a molecular model fits into the crystal electron density. The constructed model is used to generate a calculated electron density map, and the agreement between the observed and calculated structure factors (F_o and F_c) is described by the R factors, R_{work} and R_{free} , where

$$R = \frac{\sum_{all\ reflections} |F_o - F_c|}{\sum_{all\ reflections} |F_o|}$$

The R_{work} term describes the total agreement between the molecular structure and the electron density. Additionally, the R_{free} term describes the correlation of the model against ~10% of the reflections that are reserved from any refinement and is a measure of how biased the electron density has become as a result of refinement. Additional structural information such as bond lengths, angles, and Ramachandran outliers are used to determine the geometric feasibility of the molecular structure.⁹⁵

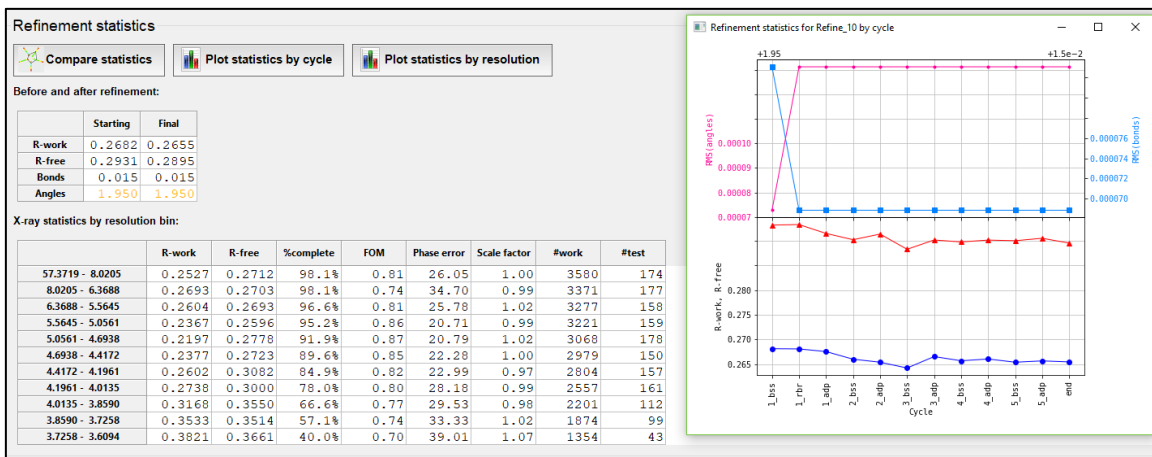


Figure 23 Automated model refinement with Phenix. Standard metrics of model accuracy (R_{work} , R_{free}) provide quantitative, real-time tracking of changes made during computational refinement cycles.

Chapter 3: Isolated C1 Domain of FVIII in Complex with Inhibitory Antibodies

3.1 Introduction

A major complication of hemophilia A treatment with replacement FVIII is the development of inhibitory antibodies. Previous work in the Spiegel lab identified the atomic binding interactions between the C2 domain of FVIII and the anti-C2 inhibitory antibodies 3E6 and G99. The epitope bound by 3E6 included the C2 Arg²²⁰⁹-Ser²²¹⁶ sequence, while G99's epitope on the opposing face of C2 comprised the Pro²²²¹-Trp²²²⁹ sequence.^{96,97} This investigation not only illuminated the interaction between C2 and inhibitory antibodies, but it also augmented the understanding of how C2 binds to phosphatidylserine (PS) rich activated-platelet surfaces.⁹⁸

While the C2 and A2 domains of FVIII have long been considered the most immunogenic domains, a substantial number of anti-C1 domain antibodies have been identified.⁹⁹ The C1 domain of FVIII has been shown to play a pivotal role in PS platelet membrane binding, vWF binding, and uptake by dendritic cells.⁹⁹ Two distinct anti-C1 epitopes recognized by anti-C1 antibodies were determined by competitive enzyme-linked immunosorbent assay (ELISA) and hydrogen deuterium exchange mass spectroscopy (HDX-MS).^{96,100} Seven "Group A" epitope antibodies displayed high affinity for FVIII but weakly interrupted FVIII binding to PS surfaces, vWF or procoagulant activity. A singular "Group B" antibody, strongly inhibited FVIII's binding to vWF, procoagulant activity, and binding to phospholipid membranes.^{99,101} This research describes investigations of a subset of the Group A antibodies, M6143 and 2A9, and the singular Group B antibody B136.

3.2 Research Aims

Structural characterization of the isolated C1 domain of hFVIII in complex with inhibitory antibodies could reveal antibody epitopes in atomic detail, and enhance the knowledge of the C1 domain's function in hemostasis. Complexes were formed between recombinant C1 and the antigen-binding fragments (Fab) of the anti-C1 monoclonal antibodies (Mab) M6143, 2A9, and

B136. Hanging drop vapor diffusion was attempted to coax solution protein complexes to form sufficient quality crystals capable of X-ray diffraction.

3.3 Materials and Methods

3.3.1 Materials

3.3.1.1 Expression Vector

The pET-32a-c(+) plasmid was purchased from Novagen. Restriction enzymes *Bam*HI and *Xho*I were purchased from New England Biolabs (NEB). SHuffle K12 cells were purchased from NEB (Cat.# C3026J). Plasmid DNA preps and overnight aliquots of Lysogeny Broth (LB) (1% tryptone (w/v), 1% NaCl (w/v), 0.5% yeast extract (w/v)) were shaken in a ThermoScientific MaxQ 4000 (Cat.# SHKE4000). The bacterial 1 L growth solutions were shaken in a New Brunswick Scientific Excella E25. Plasmid preps were completed with QIAGEN Qiaprep Spin Miniprep Kit (Cat.#: 27106). Super Optimal Broth with Catabolite repression (SOC) media (2% tryptone (w/v), 0.5% yeast extract (w/v), 10 mM NaCl, 2.5 mM KCl, 10 mM MgCl₂, 20 mM glucose) was prepared on site. The transformation selection ampicillin / LB-agar plates (1% tryptone (w/v), 1% NaCl, 0.5% yeast extract, 1.5% agar, 50 μM ampicillin sodium salt) were prepared in lab.

3.3.1.2 Growth and Expression

The LB media and the Terrific Broth (TB) media (2.4% yeast extract (w/v), 1.2% tryptone (w/v), 0.4% glycerol (w/v), 0.23% KH₂PO₄, 1.64% K₂HPO₄) were prepared in-house. Ampicillin sodium salt (BioReagent grade) was purchased from Sigma Aldrich (Cat.# A0166-25G). Non-filter, non-sterile SureOne™ 2 μL, 200 μL, 1000 μL pipette tips were purchased from Fisherbrand™ (Cat.# (0.1-10 μL) 02-707-137, (0.5-200 μL) 02-707-415, (100-1250 μL) 02-707-407). Bacterial growth optical density was assessed on a VWR Spectrophotometer V-122, with samples in plastic

disposable cuvettes purchased from BRAND GMBH (Cat.# 759075D). Isopropyl β -D-1-thiogalactopyranoside (IPTG) was purchased from Sigma-Aldrich (Cat.# I6758-10G).

3.3.1.3 Cell Lysis

Cells were pelleted from TB media by centrifugation on a ThermoFisher F12x6-500Y rotor and Sorvall Lynx 4000 preparatory centrifuge. Lysis buffer (300 mM NaCl, 20 mM tris(hydroxymethyl)aminomethane (Tris) (pH 7.5), 10% glycerol (w/v), 10 mM imidazole (pH 8.0), 0.1% Triton X100 (w/v), 0.45 μ m cellulose acetate membrane filtered) was prepared in house. Pelleted cells were resuspended by vertical mixing in a Benchtop Lab Systems Vertical Rotating Mixer, model VM-80. Cells were sonicated with a Branson Ultrasonics - Sonifier 450 (Power Setting 5 and Duty Cycle 50%). Insoluble cell debris was separated from soluble proteins by centrifugation with a Sorvall Lynx 4000 centrifuge and ThermoFisher F20-12x50 LEX 096-124375 rotor. Buffer solutions and cellular lysate were filtered through Whatman cellulose acetate membranes (Cat.# 10404112).

3.3.1.4 Protein Purification

The gravity columns used were Kontes Flex-Columns of various height. The Wash I buffer (150 mM NaCl, 20 mM Tris (pH 7.5), 10% glycerol (w/v), 10 mM imidazole (pH 8.0), 0.45 μ m cellulose acetate membrane filtered), Wash II buffer (150 mM NaCl, 20 mM Tris (pH 7.5), 10% glycerol (w/v), 50 mM imidazole (pH 8.0), 0.45 μ m cellulose acetate membrane filtered), Wash III buffer (150 mM NaCl, 20 mM Tris (pH 7.5), 10% glycerol (w/v), 100 mM imidazole (pH 8.0), 0.45 μ m cellulose acetate membrane filtered), Elution buffer (150 mM NaCl, 20 mM Tris (pH 7.5), 10% glycerol (w/v), 150mM imidazole (pH 8.0)), and Dialysis/Storage buffer (150 mM NaCl, 25 mM Tris (pH 7.5), 10% glycerol (w/v)) were prepared in-house. The TALON Co²⁺ resin, Ni-IDA resin, and Ni-NTA resin were purchased respectively from Takara Bio USA (formerly Clontech) (Cat.#

635503); UBP Bio (Cat.# P3010-25); and Qiagen (Cat.# 30210). Concentrations of protein were calculated with a BioTek Epoch Microplate Spectrophotometer.

3.3.1.5 Chromatography Metal Charging Procedure

HiTrap Chelating HP columns were purchased from GE Healthcare Lifesciences (Cat.#17040801). Candidate cation solutions were filtered with Whatman nylon membranes (Cat.# 7402-004).

3.3.1.6 Enterokinase Cleavage of Thioredoxin-Hexahistidine Tag

Recombinant Enterokinase (rEK), Enterokinase affinity resin (rEKapture agarose), and rEK cleavage buffer were purchased from Millipore Sigma (Cat.# 69067-3). Tabletop centrifugation was performed on a Sorvall Legend X1R. Eppendorf reactions were centrifuged using an Eppendorf® 5415D centrifuge and F45-24-11 rotor. The affinity resin was separated with a Costar Spin-X® 0.22µm cellulose acetate centrifuge tube filter (Cat.# 8161). Concentration and non-dialysis buffer-swapping of protein was accomplished with Amicon Ultra spin concentrators.

3.3.1.7 Anti-C1 Hybridoma Growth

All mammalian cell research was performed in a Holten LaminAir HH72 tissue culture hood. Hybridoma cells were grown in Clonacell-HY hybridoma growth Medium E (MedE) from STEMCELL Technologies Incorporated. Dimethyl sulfoxide (DMSO) for mammalian cell cryoprotection was purchased from Sigma Aldrich (DMSO Hybri-Max, (Product #D26250-100mL). The conical centrifuge tubes employed were Corning propylene, plug-seal 15 mL (Ref.# 430052) and 50 mL (Ref.# 430290) units. Mammalian cell growth proceeded in Corning 75 cm² (“T-75”) C/N vent-cap flask (Ref# 3290). Large-scale mammalian cell growth occurred in triple-layer ThermoScientific Nunclo Delta Surface flasks (Cat.# 132867). Mammalian cell growth occurred in Tabai ESPEC Corporation (Model BNA210) and Forma Scientific (Model 3546) CO₂ incubators, with USP Medical Grade CO₂ gas from Airgas® Corporation (Cat.# UN1013). Solution

volumes were pipetted with a Falcon® Pipet Controller (Cat.# 10028-602). Cell culture volumes were transferred with Falcon 2 mL (Cat.# 357507), 10 mL (Cat.# 357551), 25 mL (Cat.# 357525), and 50 mL (Cat.# 357550) serological pipettes.

3.3.1.8 Mammalian Cell Assessment

Mammalian cell density was assessed with iNCyto C-Chip Neubauer Improved (DHC-N01-5) hemacytometer slides. Microscopy was performed on an Olympus IM cell tissue culture microscope.

3.3.1.9 Anti-C1 Hybridoma Expression

Versene (Gibco™) dissociation media was purchased from Fisher Scientific (Cat.# 15-040-066). Hybridoma expression occurred in CD Hybridoma Media (Gibco™) purchased from Fisher Scientific (Cat.# 11-279-023).

3.3.1.10 Anti-C1 Hybridoma Mab Purification

Sulfopropyl (SP) Fastflow™ ion exchange (IEC) resin was purchased from GE Healthcare Life Sciences (Prod.# 17-0729-01). The IEC “Buffer B” recipe (10 mM 2-ethanesulfonic acid (MES), 20 mM NaCl, 0.05% NaN₃ (w/v), pH 6.0) and IEC “Buffer C” recipe (20 mM 4-(2-hydroxyethyl)-1-piperazineethanesulfonic acid (HEPES), 150 mM NaCl, 0.05% NaN₃ (w/v), pH 7.4) were prepared in-house. The IEC “Buffer A” recipe (100 mM MES, 200 mM NaCl, 0.05% NaN₃ (w/v)) was used as a 10x stock for “Buffer B”. Cell centrifugation was accomplished with a ThermoScientific Sorvall Legend X1R.

3.3.1.11 Anti-C1 Fab Generation by Immobilized Papain

Fab cleavage from Mabs was accomplished with ThermoFisher Scientific Immobilized Papain agarose resin (Prod.# 20341). Papain Sample Buffer (20 mM NaPO₄, 10 mM

ethylenediaminetetraacetic acid (EDTA), pH 7.0) and Papain Digestion Buffer (20 mM NaPO₄, 20 mM cysteine • HCl, pH 7.0) were prepared on site.

3.3.1.12 Fab Protein A Purification

The papain-cleaved Fabs were isolated by Protein A affinity chromatography with ThermoScientific Nab Protein A plus Spin kits (Prod.# 89948). Protein A Binding Buffer (100 mM K₂PO₄, 150 mM NaCl, pH 7.2, 0.05% NaN₃ (w/v), 0.45µm cellulose acetate membrane filtered), Protein A Neutralization buffer (1 M Tris·HCl), and Protein A Resin PBS Storage Buffer (137 mM NaCl, 2.7 mM KCl, 10 mM Na₂HPO₄, 1.8mM KH₂PO₄, 0.02% NaN₃ (w/v), 0.45 µm cellulose acetate membrane filtered) were prepared in-house. The Protein A IgG Elution buffer (pH 2.8) was supplied in the manufacturer kit.

3.3.1.13 Biolayer Interferometry of C1 and Anti-C1 Mabs

Biolayer interferometry (BLI) assays were completed on a Pall FortéBio® BLItz instrument. The BLI tips used to bind anti-C1 antibodies were Anti-Mouse IgG Fc Capture (AMC) (Cat.# 18-0025). Kinetics were measured using BLItz Pro software, version 1.1.0.31. Concentrations of protein were calculated with a BioTek Epoch Microplate Spectrophotometer.

3.3.1.14 C1:Fab Crystal Trials

The 24 well crystal trays were purchased from Hampton Research. The conditions used for protein crystallography included Hampton Research's Index 1-96 kit (HR2-144), as well as the "Et3i trial B2"ⁱ and "B2(D2)35,45,47"ⁱⁱ tray conditions. Al's Oil (50% paraffin oil, 50% silicone oil) was purchased from Hampton Research. Crystals were exposed to X-rays on a Rigaku Micromax-007HF rotating anode generator and diffraction measured with a Saturn 994+ CCD area detector

ⁱ (Ian Wesley Smith (IWS)(II)p.100)

ⁱⁱ (IWS(II)p.122)

in conjunction with the Stoddard lab at the Fred Hutchinson Cancer Research Center. Protein crystals were cryoprotected with BioReagent grade Hybri-Max™ dimethyl sulfoxide (DMSO) from Sigma Aldrich (Ref.# D2650-100ML).

3.3.2 Methods

3.3.2.1 Expression vectorⁱⁱⁱ

Expression from the pET-32a-c(+) plasmid is under control of the lac operon and produces the FVIII C1 domain protein of interest with an N-terminal thioredoxin (“Trx•Tag”) fusion partner (Figure 24). To prepare the vector transformation, competent ShuffleK12 strain (NEB) E. coli were thawed on ice for 10 minutes. Then, 5 µL of 10.5 ng/mL pET-32a-c(+) plasmid DNA were added to the ShuffleK12 cells and allowed to incubate on ice for 30 minutes. The sealed mixture was submerged in a 42 °C water bath for precisely 30 seconds, and then returned to ice for 5 minutes. Subsequently, 950 µL of SOC media were added to the mixture and shaken at 250 rotations per minute (RPM) at 30 °C for 60 minutes. Several 10 fold serial dilutions were made of the cells and were plated on LB-ampicillin agar plates and grown overnight at 30 °C.

Additional stock of C1 pET-32a-c(+) plasmid was produced by inoculating 10 mL of LB with C1 pET-32a-c(+) SHuffle K12 cells, and shaking at 150 RPM at 37 °C overnight. The plasmid was isolated using QiaPrep Spin MiniPrep (QIAGEN) kit instructions.

ⁱⁱⁱ (IWS(I)p.81)

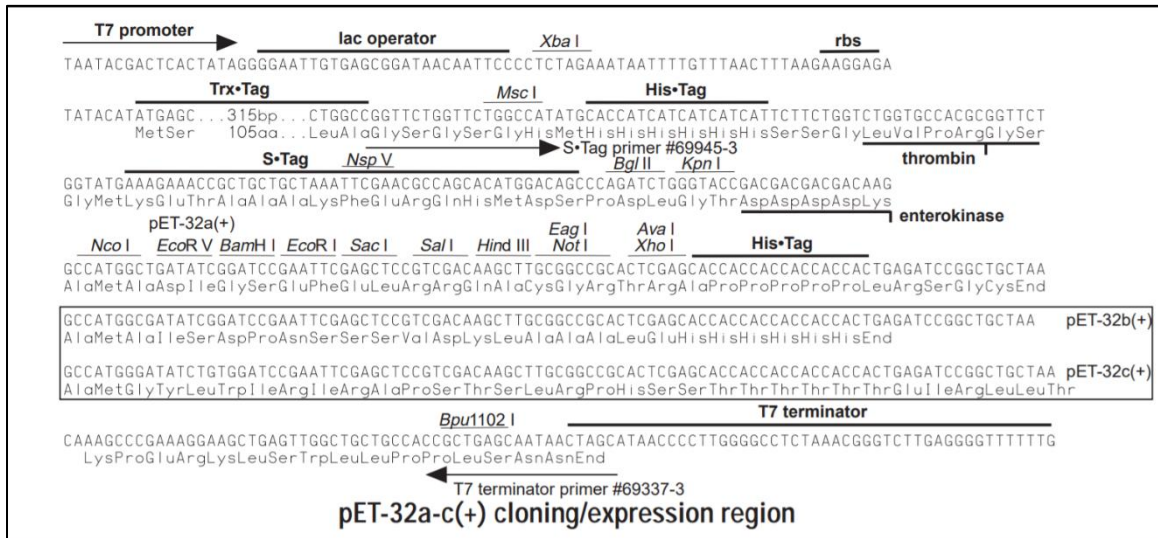


Figure 24 The pET-32a-c(+) plasmid expression region sequence. The FVIII C1 domain protein of interest was inserted into the plasmid with BamH I and Xho I restriction enzymes. (Novagen)

3.3.2.2 Growth/Expression^{iv}

The day before a standard 6 L growth, six 10 mL aliquots of LB and six 1 L solutions of TB were prepared and autoclaved at 124 °C for 70 minutes. Once the autoclaved solutions had cooled to approximately 25 °C, the bacterial resistance selection agent ampicillin sodium salt was added to the LB and TB solutions to a final concentration of 50 µg/mL (Amp₅₀). Aliquots of LB were inoculated with C1/ShuffleK12 cells by submerging a sterile p200 pipette tip into partially thawed cell stock and dispensing the tip into the LB solution. The inoculated aliquots were shaken at 37 °C for at least 18 hours, until visibly turbid. On the day of the growth, a 1 mL sample of TB was taken as an optical density blank, and each liter of TB was inoculated with 10 mL of the LB containing C1/SHuffle K12 cells. Inoculated TB flasks were shaken at 150 RPM at 30 °C, and beginning four hours after inoculation the optical density of bacterial growth was assessed hourly at 600 nm wavelength light (OD₆₀₀). Once an OD₆₀₀ value of 0.4 - 0.8 was recorded, the shaking temperature was reduced to 15 °C. Then, 1 mL of 1 M isopropyl β-D-1 thiogalactopyranoside (IPTG) was added to induce protein expression, which occurred overnight for approximately 16 hours.

^{iv}(IWS(I) p.126)

3.3.2.3 Cell Lysis^v

Following expression, cells were separated from the supernatant by centrifugation for 10 minutes at 4 °C at a Relative Centrifugal Force (rcf) of 6371 x G using a ThermoFisher F12x6-500Y rotor. Exhausted TB media was decanted from the cell pellet and discarded. Cells were divided into 50 mL conical centrifuge tubes, with ~15 mL of pelleted cells per tube. To each pellet, 20 mL of Lysis buffer were added. Cell pellets were resuspended in this mixture by vertical rotation at 4 °C for 30 minutes. Lysis of bacterial cells occurred through ultrasonication on ice in three sets of 30 seconds, with 30 second rests in between. The cell lysate was transferred to a small centrifuge tube, and centrifuged for 1.5 hours at 4 °C and 17500 RPM. Centrifuged lysate supernatant was decanted from the insoluble cell pellet and filtered sequentially through 5 µm, 0.45 µm, and 0.22 µm cellulose acetate membranes.

3.3.2.4 Protein Purification^{vi}

The hexahistidine (“His-Tag”) containing C1 protein was purified from the bacterial lysate supernatant by immobilized metal affinity chromatography (IMAC) batch purification. In a gravity column, 2 mL of 50% slurry TALON immobilized Co²⁺ resin was equilibrated in at least 10 mL of Lysis buffer. The equilibrated TALON resin was collected and combined with the filtered bacterial lysate in a separate 125 mL Erlenmeyer and mixed slowly at 4 °C for 30 minutes. The lysate-resin mixture was returned to the gravity column. The flow-through lysate was collected, followed sequentially by twenty column-volumes (20 CV, or 40 mL) of Wash I buffer; 4 CV of Wash II buffer; and 2 CV of Wash III buffer. Next, 2 CV of Elution buffer was added to the column and allowed to equilibrate for 15 minutes prior to collection. Finally, an additional 10 CV of Elution buffer was added to the resin bed and allowed to elute at ~1 mL/minute to ensure complete elution of immobilized protein. Imidazole was removed from the solution of purified protein by dialysis

^v (IWS(I)p.126)

^{vi} (IWS(I)p.108)

with Dialysis/Storage Buffer. If purity of protein sample was not sufficient after one round of IMAC purification, the IMAC purification scheme could be repeated until desired purity was achieved.

3.3.2.5 Chromatography Metal Charging Procedure^{vii}

To troubleshoot poor IMAC affinity of C1, HP Hitrap Columns were charged with several candidate cations to determine optimum C1 fusion protein interaction. The following metal ion salts were charged onto 1 mL HP Hitrap Columns according to manufacturer instructions: $(\text{NiCl}_2) \cdot 6\text{H}_2\text{O}$, $(\text{CoCl}_2) \cdot 6\text{H}_2\text{O}$, ZnCl_2 , $\text{CuSO}_4 \cdot 5\text{H}_2\text{O}$, $\text{FeCl}_3 \cdot 6\text{H}_2\text{O}$. Metal ion-salts were dissolved in deionized distilled water (ddH_2O) to a final concentration of 0.1 M, and solutions were 0.22 μm syringe filtered. To immobilize cations in the resin matrix, each HiTrap column was washed with 10 mL of ddH_2O using a sterile syringe and Luer lock attachment, followed by 10 mL of the respective metal solutions. The FeCl_3 solution was immobilized at pH 3.0 to avoid precipitation of insoluble ferric (Fe^{3+}) iron. After metal binding, the 1 mL HP Hitrap columns were washed with 5 mL ddH_2O . Next, 5 CV of Elution buffer was flowed over the column, followed by 5 CV of Dialysis/Storage Buffer. These prepared columns were employed in IMAC purifications as previously described.

3.3.2.6 Enterokinase Cleavage of Thioredoxin and His-Tag^{viii}

Recombinant Enterokinase (rEK) was utilized to separate the C1 protein of interest from the thioredoxin fusion partner and intermediary His-Tag. The amino acid sequence Asp-Asp-Asp-Asp-Lys is recognized by rEK and cleaved, leaving a seven amino acid “tail” in front of the C1 domain sequence (Figure 24). To accomplish this, 50 U (3.25 μL) of rEK was added to a sample tube containing 22.5 mL (0.5 mg/mL) of expressed fusion C1 sample at 4 °C. To this, 1 mL of

^{vii} (IWS(I) p.138)

^{viii} (IWS(I) p.144)

concentrated 10x rEK cleavage buffer was added to a final concentration of 0.5x. The rEK and protein were incubated overnight at 4 °C for a total of ~14 hours.

To remove rEK after the cleavage reaction, 2 mL of enterokinase affinity (rEKcapture) agarose resin 50% slurry was added to a SpinX-Costar filter Eppendorf tube and equilibrated in 1 mL 1x Cleavage Capture Buffer and centrifuged for 5 minutes at 500 x G. The resin flow-through was discarded, and the resin was washed with 2 x 1 mL of C1 Dialysis/Storage buffer; centrifuged for 5 minutes at 500 x G each time. Equilibrated rEKcapture agarose resin was pipetted from the SpinX CoStar filter Eppendorf and added to the rEK + C1 protein solution and incubated for 15 minutes at 25 °C with gentle mixing. The protein + EK + resin mixture was pipetted back to a Co-Star SpinX centrifuge tube and centrifuged for 5 minutes at 500 x G and the flow-through collected. The resin was washed with 1 mL of Dialysis/Storage buffer, centrifuged for 5 minutes at 500 x G, and the flow-through volumes were pooled.

To separate the cleaved Thioredoxin-His Tag from isolated C1, a secondary IMAC procedure was performed as described (page 35) with 2 mL of TALON immobilized Co²⁺ resin 50% slurry. The cleaved C1 protein of interest was collected in the IMAC flow-through. Isolated C1 protein was concentrated to ~0.8 mg/mL with an Amicon 3000 kD MWCO spin filter.

3.3.2.7 Anti-C1 Hybridoma Growth^{ix}

In a sterile cell culture hood, 9 mL of Hybridoma Medium E (MedE) was placed into a 15 mL conical centrifuge tube. Hybridoma cells (1 mL aliquots, ~1 million cells/mL) stored at -80 °C in MedE and 10% dimethylsulfoxide (DMSO) were warmed in a 37 °C water bath for approximately 60 seconds until just thawed. Cells were pipetted into the 9 mL MedE aliquot, and the centrifuge tube was capped and inverted several times gently. The cells were pelleted by centrifugation for 5 minutes at 1000 RPM. The DMSO-containing supernatant was discarded, and the hybridoma cell

^{ix} (IWS(I) p.148)

pellet was resuspended in 2 mL MedE and transferred to a separate T-75 flask containing 15 mL of MedE. This tissue flask was sealed with a vented cap and transferred to a sterile water bath incubator at 5% CO₂ and 37 °C. An additional 25 mL of MedE was added to the T-75 flask after 48 hours to a total volume of 42 mL.

3.3.2.8 Mammalian Cell Assessment^x

Observations of mammalian cell cultures were made daily. Cells were assessed for spherical shape, adherence to the T-75 surface, percentage of confluence, and presence of foreign organisms. A hemacytometer slide was used to assess the cell density at the time of cryopreservation or passaging. Cells to be counted were pelleted and resuspended in 10 mL of MedE. Then, 1 mL serial dilutions (1:1, 1:100, 1:1000) were made from this stock solution, and 200 µL dilution samples were loaded onto the hemacytometer. Cells were counted across 5 large hemacytometer squares, and the average cell per area was multiplied by the dilution factor to calculate the cell density.

3.3.2.9 Anti-C1 Hybridoma Expression

When cells reached ~80% confluence, the exhausted MedE (brown-red and turbid in appearance) was decanted from the adhered cells and discarded. To gently dissociate the cells from the T-75 surface, 1 mL of Versene was washed over the cells and discarded, followed by 2 mL of Versene added to the flask and the flask placed in the 37 °C incubator for 2 minutes. Dissociated with light tapping, the cells were pipetted into a 50 mL conical centrifuge tube and centrifuged at 1100 RPM for 10 minutes. The Versene supernatant was removed from the cell pellet and discarded. The cell pellets were resuspended in a 25 mL wash of CD Hybridoma Medium, centrifuged at 1100 RPM for 10 minutes, and the CD Hybridoma wash was decanted and discarded. The cells were then resuspended in 5 mL CD Hybridoma Medium and transferred to a new T-75 cell culture flask

^x (IWS(II)p.6,8,10,26,28,30,32)

containing 45 mL of CD Hybridoma Medium. Cell expression occurred for seven days, with daily observation to assess surface adherence and aliquots taken to validate expression by SDS-PAGE.

3.3.2.10 Anti-C1 Hybridoma Mab Purification^{xi}

In a gravity column, 16 mL of 50% slurry (8 mL packed resin) of Sepharose Sulfopropyl FastFlow strong cation ion exchange chromatography (IEC) resin were equilibrated with 50 mL of “Buffer B”. The 50 mL aliquot of CD Hybridoma expression media containing anti-C1 Mab’s was diluted 4x with ddH₂O (e.g. 50 mL Mab + 200 mL ddH₂O) and adjusted to pH 5.5 - 6.0 with 8 mL of 0.5 M MES (pH unadjusted). The diluted Mab’s were loaded onto the IEC column overnight using a “siphon safety-loop” at 4 °C, and the flow-through was collected (Figure 25). The column was washed with 50 mL of Buffer B with the wash collected separately. It was opted not to observe OD₂₈₀ baseline reading during the wash step, due to lack of a UV spectrophotometer in the 4 °C cold room. To elute the bound anti-C1 Mab’s, 30 mL of “Buffer C” were added to the column. The first 3 mL of eluent from the column and the next 27 mL of eluent were collected as separate fractions. Eluted antibody fractions were concentrated with 15 mL Amicon Ultra 10 kD MWCO spin concentrators, and the presence of Mabs determined by SDS-PAGE.

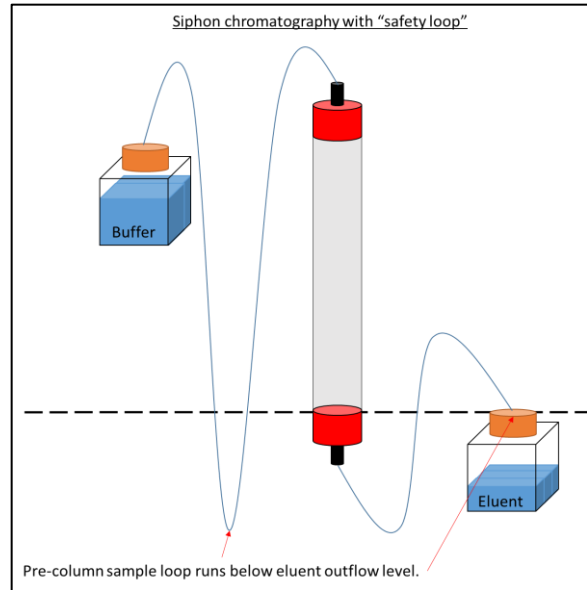


Figure 25 **Diagram of gravity chromatography with siphon-safety loop.** A siphon draws the buffer through the column. A section of the pre-column loop remains below the level of eluent outflow. When the buffer volume runs out the siphon will stop and the column will not run dry. This allows for unattended loading of the chromatography column.

^{xi} (IWS(II)p.24, 36)

3.3.2.11 Anti-C1 Fab Generation by Immobilized Papain^{xii}

To generate anti-C1 Fab fragments, the purified Mab samples were dialyzed into “Papain Sample Buffer” by dialysis tubing membrane overnight at 4 °C. Several times, EDTA was erroneously omitted from the Papain Sample Buffer preparation. The Mab sample was concentrated to approximately 20 mg/mL. Just before use, the “Papain Digestion Buffer” was prepared. Then, 0.5 mL of Digestion Buffer was combined with 0.5 mL of antibody sample, and the 1.0 mL reaction volume was then added to 0.5 mL of 50% slurry Immobilized Papain resin equilibrated in Papain Sample Buffer. Once the reaction was completed from 5-24 hours, the agarose resin was removed by a Co-Star Spin X filter Eppendorf and the supernatant mixture of Fc and Fab’s collected. Cleavage by immobilized papain was verified by SDS-PAGE.

3.3.2.12 Fab Protein A Purification^{xiii}

Bacterial Protein A binds tightly to IgG antibody Fc regions, and can be used to purify antibody Fabs. The 500 µL Immobilized Protein A columns were equilibrated in Protein A Binding Buffer according to manufacturer instructions. Next, 500 µL of papain-cleaved antibody sample was added to the column and gently shaken for 10 minutes at 25 °C. The unbound supernatant was removed by centrifugation at 5000 x G for 2 minutes. The column was washed in triplicate with 400 µL aliquots of Protein A Binding Buffer and centrifugation at 5000 X G for 1 minute. Then, the Fab of interest was eluted in from the column with triplicate 400 µL aliquots of Protein A Elution Buffer added to the resin, mixed gently for 1 minute, and removed by centrifugation at 5000 X G. Each elution was collected into separate Eppendorf tubes, containing 40 µL of Protein A Neutralization Buffer. Protein A purification was validated by SDS-PAGE.

^{xii} (IWS(II)p.60)

^{xiii} (IWS(II)p.62)

3.3.2.13 Biolayer Interferometry of C1 and Anti-C1 Mabs^{xiv}

Affinities of the murine-derived anti-C1 monoclonal antibodies were determined by biolayer interferometry. To complex C1 and Mab's in stoichiometric amounts, each was diluted to 300 nM and combined in equal volumes. FortéBio goat-derived anti-mouse IgG Fc Capture (AMC) Biosensor sample tips were hydrated in Dialysis/Storage buffer for 15 minutes. BLItzPro software "Advanced Kinetics" experiment template, five-phase trials (Baseline 30 seconds, Mab Association 300 seconds, Baseline 30 seconds, C1 Association 300 seconds, C1 Dissociation 300 seconds) were undertaken for each anti-C1 Mab. Negative controls for C1 and Mab's were performed for each C1:Mab pair. Kinetics for Mab binding were automatically calculated by the BLItzPro software.

3.3.2.14 C1:Fab Crystal Trials^{xv}

To pursue a molecular model of the FVIII C1 domain in complex with inhibitory antibodies, crystallization of isolated C1 domain and antibody Fab fragments was attempted. The concentration and extinction coefficient of pure C1 and 2A9 Fab was determined by Bradford assay and confirmed via light absorbance at 280 nm (A_{280}). Enterokinase cleaved C1 was complexed with 2A9 anti-C1 Fab fragments in stoichiometric amounts in an Eppendorf tube and allowed to sit on ice for 10 minutes. The mixture was pipetted into a 4 mL Amicon spin concentrator and centrifuged at 3000 rpm for 10 minutes. The mixture was transferred to a 15 mL conical tube and centrifuged at 3000 rpm for 5 minutes to pellet any aggregate.

The 24-well crystal trays were greased in-house. Each well was ringed with petroleum jelly using a 10 mL syringe fitted with a Leuer-lock needle tip, leaving a small gap (~1 mm) in the grease ring to allow air to escape when pressing down the coverslip for proper sealing. Following this, 400 μ L of mother liquor was added to each well. On a 18 mm siliconized glass cover slide, 2 μ L of mother liquor was pipetted into a 2 μ L droplet of protein complex sample.

^{xiv} (IWS(I)p.15,19,23)

^{xv} (IWS(III)p.4)

Next, 400 μ L of Al's Oil (50% paraffin oil and 50% silicone oil) was added to the mother liquor in the well to reduce the rate of vapor diffusion. The cover slide was then inverted (with the droplet hanging down) and pressed into the ring of grease to form a hermetic seal. Once all 24 wells were completed, the trays were gently relocated to a quiet location and placed on a 2" layer of insulation foam for up to 4 weeks before inspection. Crystals that formed were cryoprotected sequentially in solutions containing 10%, 20%, and 30% DMSO.

3.4 Results

3.4.1 Plasmid Prep^{xvi}

Previous researchers inserted the cDNA for the isolated C1 domain of hFVIII, consisting of 148 residues, into a pET-32a-c(+) plasmid using the *Bam*H1 and *Xho*I restriction enzyme cleavage sites. The C1-fusion-containing pET-32a-c(+) plasmid was transformed into competent SHuffle K12 cells.

3.4.2 Growth, expression, and purification of recombinant FVIII C1 domain.

Expression of recombinant FVIII C1 domain from pET-32a-c(+) plasmid in bacterial SHuffle K12 cells was visualized by SDS-PAGE, identifying a Thioredoxin-C1 fusion protein band at approximately ~34 kD migration. Approximately 6 mg of IMAC purified thioredoxin-C1 fusion protein was yielded for a typical 6 L growth prep in TB media (Figure 26).

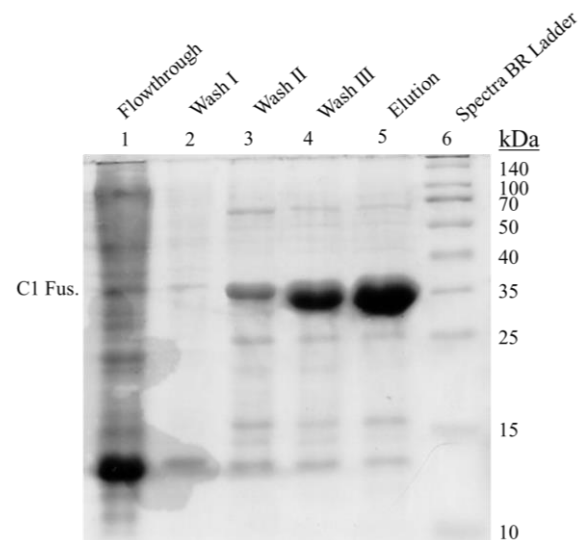


Figure 26 C1 IMAC Purification. (3.24.2017) The 15% acrylamide SDS-PAGE gel visualization of the ~36 kDa Thioredoxin-C1 fusion protein expressed from pET32-a-c(+) plasmid in SHuffle K12 cells. The imidazole content of Washes I-III and Elution buffer were 10 mM, 50 mM, 100 mM, and 150 mM, respectively.

^{xvi} (Laurel Sugden (LAS)(Dp.3)

To avoid interference with antibody binding experiments, the N-terminal thioredoxin fusion protein and hexahistidine tag were removed from C1 by enzymatic cleavage with recombinant enterokinase (rEK). Cleavage and separation of the Thioredoxin-C1 fusion protein by enterokinase was generally successful. However, the IMAC separation of the ~11 kD Thioredoxin-His-Tag and ~16 kD C1 components was often ineffective, requiring extensive dialysis for successful IMAC separation (Figure 27). The approximate purity of C1 after the secondary IMAC was ~70%. Purity increased to ~80% following secondary IMAC preparatory steps (Figure 28).

Optimization of the C1 IMAC affinity with candidate cations was attempted, with no improvement observed and some cations failing to bind His-tagged protein (See Appendix: Figure 50, Figure 51, Figure 52, Figure 53, Figure 54).

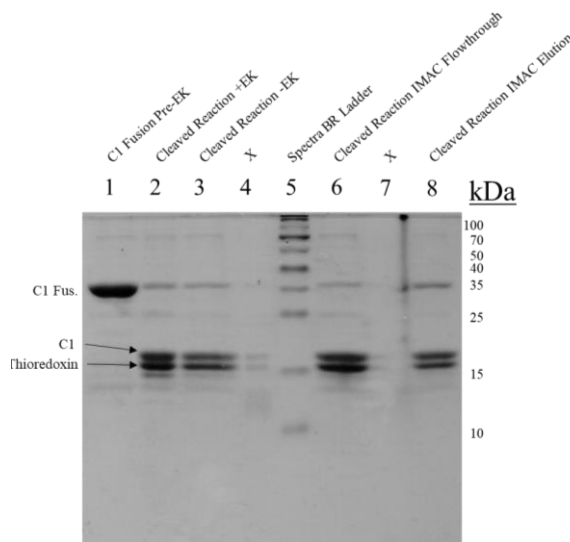


Figure 27 *C1 Fusion Enterokinase Cleavage*. The C1 fusion construct was cleaved by recombinant enterokinase (rEK) to remove the ~11 kDa thioredoxin and hexahistidine tag. Post rEK cleavage, the rEK was removed with rEKcapture affinity agarose. (4.12.2017)

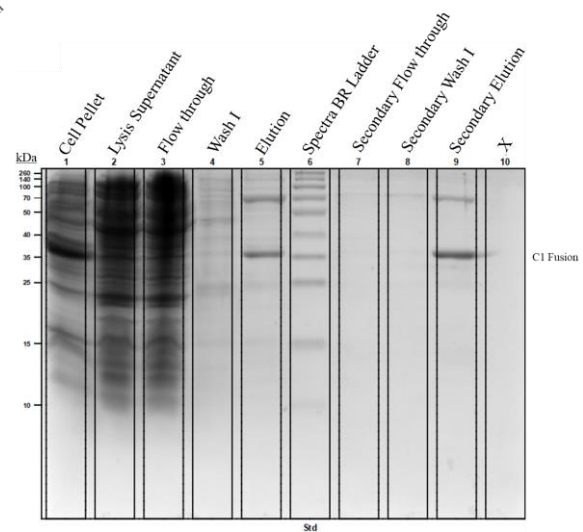


Figure 28 *Sequential IMAC Purifications of C1 fusion protein*. The second IMAC round was performed to achieve desired purity of recombinant protein. (9.18.2017)

3.4.3 Growth, expression, and purification of anti-C1 Mabs and generation of anti-C1 Fabs

Murine hybridomas expressing “Group A” (M6143 and 2A9) and “Group B” (B136) anti-C1 antibodies were successfully cultured (Figure 29). The hybridomas were passaged into larger flask

growths, and the expressed monoclonal antibodies were separated from the cells and expression media by cation-exchange chromatography (IEC) (Figure 30).

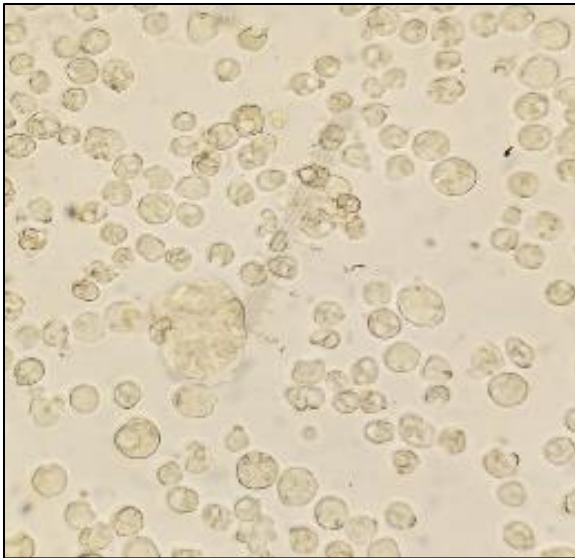


Figure 29 Hybridoma cells (2A9) viewed at 400x magnification (95% confluence). Confluence was assessed at 100x magnification. (7.28.2017 IWS(II)p.64)

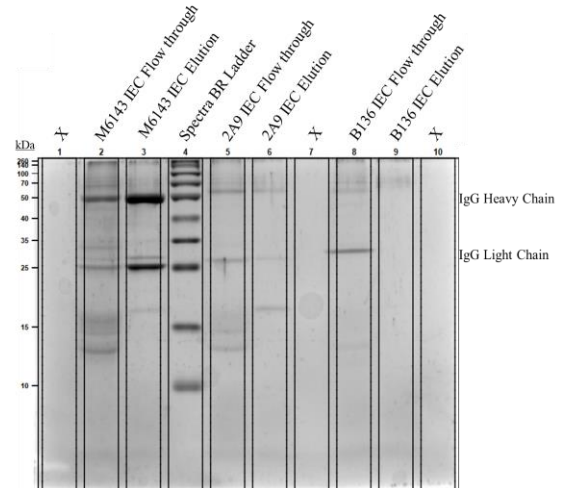


Figure 30 Hybridoma purification by ion-exchange chromatography (IEC). The Group A antibodies M6143 (lanes 2,3), 2A9 (lanes 5,6), and Group B antibody B136 (lanes 8,9) demonstrated differing expression levels.

3.4.4 Production of Fabs from Mabs^{xvii}

Anti-C1 Mabs were enzymatically cleaved by immobilized papain resin to generate respective Fab fragments for protein crystallography trials. Incomplete cleavage of Mabs was observed. Following cleavage by papain, the Fab fragments were successfully separated from the undesired crystallizable fragment (Fc) by Protein A affinity chromatography (Figure 31). The concentration of the Fab sample was determined by Bradford assay (Figure 32). The extinction coefficient of 2A9 Fab was calculated to be $21400 \text{ Lmol}^{-1}\text{cm}^{-1}$ (1% solution).

^{xvii} (IWS(III)p.7)

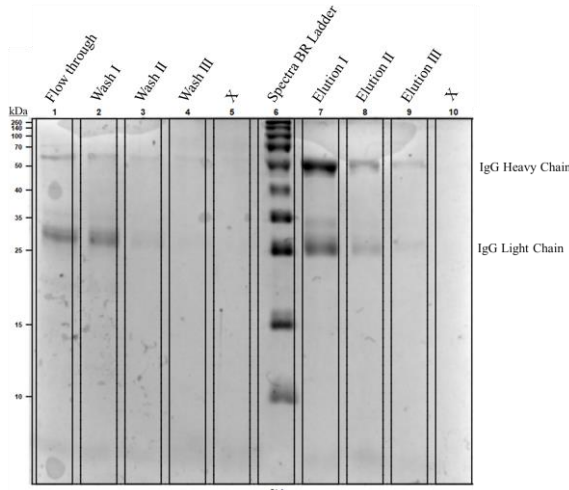


Figure 31 IgG 2A9 Fab Protein A Purification. The presence of 25 kD protein in the flow through and wash (lanes 1 and 2) were assumed to be IgG Fab. The 50 kD elution bands (lanes 7-9) indicate incomplete cleavage of Mabs by the immobilized papain resin. (11.13.2017 IWS(II)p.118)

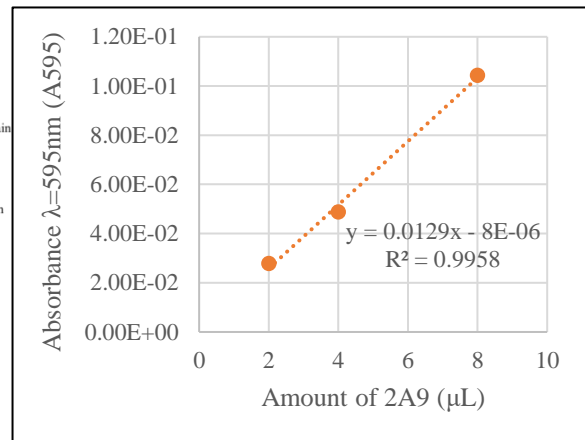


Figure 32 Anti-C1 2A9 Fab Bradford Assay. Gamma globulin (IgG) (2ug/uL) was used as a control standard. (11.21.2017 IWS(III)p.7)

3.4.5 Biolayer Interferometry of C1 and Anti-C1 Mabs

Binding affinities of Group A (2A9, M6143, I41, I84, I88, B153) and the Group B (B136) antibodies were measured via BLI. The antibodies which demonstrated reproducible kinetics, Group A antibodies (M6143 and 2A9) and Group B (B136) underwent additional titrations of C1 to establish a dose-dependent binding curve (Table 1, Appendix B: Figure 55, Figure 56, Figure 57).

Table 1 BLI Determined Anti-C1 Antibody Affinities. Data calculated by ForteBio BLItzPro.

Mab	Group	ka (1/Ms)	kd (1/s)	KD (M)	Rmax
M6143	A	1.43E+07	1.00E-07	1.00E-12	0.00E+00
2A9	A	7.82E+06	1.64E+06	2.10E-01	-1.43E+03
B136	B	1.79E+01	1.96E-02	1.10E-03	7.16E+02

3.4.6 C1:Fab Crystal Trials

2A9 Fab fragments were complexed with isolated C1 protein. The concentrated mixture (~0.37 mg/mL) was screened in hanging drop vapor diffusion crystal trials. Initial crystal hits in the #82 Index well (0.2 M MgCl₂·6H₂O, 0.1 M Bis-Tris pH 5.5, 25% w/v polyethylene glycol (PEG) 3350) and #83 Index well (0.2 M MgCl₂·6H₂O, 0.1 M Bis-Tris pH 6.5, 25% w/v PEG 3350) were negative for diffraction (Figure 33)^{xviii}.



Figure 33 Non-diffracting crystals of complexed C1 and 2A9 Fab. These crystals did not diffract X-rays in a manner indicative of a biological molecule, and were likely salt complexes. (12.18.2017 IWS(III)p.4)

3.5 Discussion

3.5.1 Bacterial Expression and Purification of Isolated C1 domain.

Several obstacles were encountered during the expression of isolated C1 domain of blood coagulation Factor VIII that should be noted in future work. The expression of C1 was lower yield and less well-behaved than the isolated domain of C2. One complication during purification was the early elution of the C1 fusion protein from IMAC resin upon introduction of the 50 mM imidazole Wash II buffer (Figure 26 (Lane 3), page 42). In practice, the Wash II and Wash III buffers were commonly omitted to maximize the retention of the C1 fusion in the eluent, at the price of reduced purity of the protein of interest. This reduced IMAC affinity was noted on all IMAC resins attempted. Poor cation affinity may be caused by the internal placement of the hexahistidine tag between the thioredoxin and recombinant C1 domain (Figure 24, page 34).

^{xviii} IWS(II)p.151

Post-enterokinase cleavage, the separation of the C1 domain from the thioredoxin-hexahistidine tag was difficult. The issue could stem from the use of diafiltration instead of dialysis to remove imidazole after the primary IMAC purification. Reduced efficacy in imidazole removal could explain the thioredoxin-hexahistidine band in the post-EK cleavage flow-through. (IWS (I) 145) (Figure 27 (Lanes 6 and 8))

Compared to recombinant FVIII C2 domain, the C1 domain exhibited decreased solubility above 1.0 mg/mL, especially once cleaved from its thioredoxin fusion partner. This behavior could result from differences in the increased hydrophobic face of isolated C1, which normally packs against the A3 domain of FVIII. The solubility of isolated C1 may be optimized with addition of zwitterionic or neutral detergents, but requires further investigation.

3.5.2 Mammalian Cell Growth and Expression of Antibodies

Mammalian cell culturing of anti-C1 antibodies were successful, however, several troubleshooting points and opportunities for improvement exist for the expression and purification procedures. It was observed that the three hybridoma strains (M6143, 2A9, and B136) exhibited significantly different character in the rate of proliferation, strength of adherence to the flask surface, expression of antibody, and vulnerability to stress and apoptosis. Of the three, 2A9 grew appreciably faster, reaching confluence in little over 48 hours. B136 was much slower in proliferation and susceptible to displaying cell stress morphologies, but highly adherent. M6143 was well behaved and seemed to express antibody at much higher levels than either 2A9 or B136.

Higher standards of cleanliness and sterility should be observed in the future when culturing mammalian cells. Several instances of contamination with fungus occurred. While not directly detrimental to the mammalian cells, the foreign organisms compete for media nutrients and likely complicate purification. The risk of contamination can be minimized through the addition of a fungicide to the mammalian medium, regular preventive maintenance and cleaning of equipment,

and increased observance of gloves and lab coats while working in the tissue culture room (Figure 34).

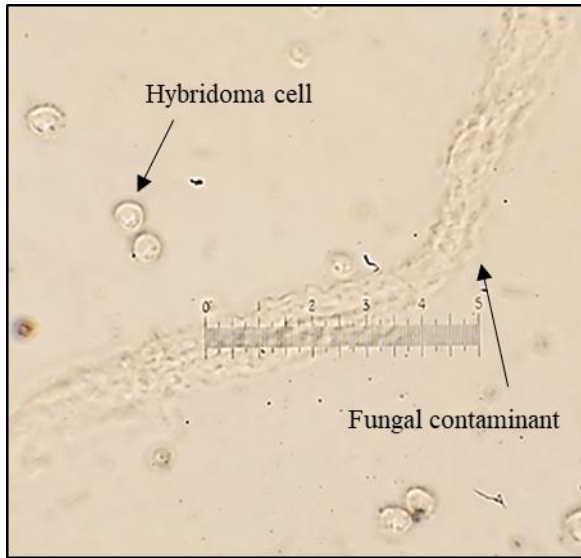


Figure 34 Fungal contamination of B136 hybridoma cells. The foreign organisms appeared after several passages of hybridoma cells were completed.

It was observed that papain cleavage of Mabs to produce Fabs consistently displayed incomplete reaction with Mabs. This could have stemmed from the erroneous omission of EDTA in several preparations. Alternatively, the reaction took place in an upright Eppendorf tube on a shaker table. The immobilized papain resin settled to the bottom of the reaction vessel, despite attempts to resuspend it or shake the Eppendorf tube at an

angle. As a result, insufficient resin-bound papain exposure with the Mab solution may have occurred. In the future, use of a specialized reaction vessel or attempting an immobilized papain cleavage in an Erlenmeyer flask with gentle stirring is recommended. Additionally, due to limited Mab material these reactions were performed below the manufacturer recommended concentration of 10 mg/mL. This could detrimentally affect reaction efficiency and require additional time for papain cleavage to occur.

3.5.3 Biolayer Interferometry of C1 and Anti-C1 Mabs

The BLI studies showed that recombinant C1 interacted with expressed Mabs in a dose-dependent manner, with increased binding detected for increasing stoichiometric ratios of C1, including 0.5 : 1 (150 nM C1: 300 nM Mab), 1 : 1 (300 nM C1: 300 nM), 1.33 : 1 (400 nM C1 : 300 nM Mab), and 2 : 1 (600 nM C1 : 300 nM Mab)(Table 1, Appendix B: Figure 55, Figure 56, Figure 57). However, in comparison to previous surface plasmon resonance (SPR) data,⁹⁹ discrepancies are apparent (Table 2). Differences in the calculated association rate (k_a), dissociation rate (k_d), and the

equilibrium dissociation constant (K_D) kinetics could stem from the sensitivity of the instrumentation, or the purity of the recombinant C1 protein preparation. Additionally, the use of 10% glycerol Dialysis/Storage buffer in BLI studies could cause a mass-transport effect, detrimentally affecting binding data. In the future, higher purity of recombinant C1, and a 0.5% glycerol buffer stabilized with detergents should be attempted.

Table 2 Comparing SPR (Batsuli et al.) and BLI Determined Anti-C1 Antibody Affinities

M6143 and C1	ka (1/Ms)	kd (1/s)	KD (M)	Rmax
SPR Data (Batsuli)	(0.5 ± 0.2)e6	(0.9 ± 0.1)e-4	2.00E-10	132.8 ± 25.3
BLI Data (Spiegel)	1.43E+07	1.00E-07	1.00E-12	0.00E+00
2A9 and C1	ka (1/Ms)	kd (1/s)	KD (M)	Rmax
SPR Data (Batsuli)	(0.3 ± 0.1)e6	(2.2 ± 0.2)e-4	9.00E-10	97.8 ± 1.1
BLI Data (Spiegel)	7.82E+06	1.64E+06	2.10E-01	-1.43E+03
B136 and C1	ka (1/Ms)	kd (1/s)	KD (M)	Rmax
SPR Data (Batsuli)	(3.1 ± 1.2)e6	(3.2 ± 0.4)e-4	1.00E-10	301.9 ± 26.5
BLI Data (Spiegel)	1.79E+01	1.96E-02	1.10E-03	7.16E+02

3.5.4 C1:Fab Crystal trials

The enterokinase cleaved recombinant C1 protein and 2A9 anti-C1 Fab complex were screened against the Hampton Research Index (HR2-144) conditions. Several initial crystal hits of C1:Fabs collected did not display diffraction properties akin to biological macromolecular crystals, and were likely small molecular salts. The crystal conditions for the C1:2A9 complex requires additional development.

Chapter 4: Structural Modeling of Human Porcine Chimeric Et3i

4.1 Introduction

The development of anti-FVIII inhibitory alloantibodies, known as “inhibitors”, represents a major complication of hemophilia A treatment. The standard remedy to negate inhibitors is immune tolerance induction (ITI), whereby large infusions of FVIII overwhelm the immune response. The significant cost of ITI¹⁰² is elevated by the fact that FVIII has a low endogenous serum concentration of ~0.5 nM,⁴⁷ and has proven refractory to recombinant production. Due to the large quantity of FVIII required for ITI campaigns, development of a high-yield recombinant human FVIII (rhFVIII) is of significant interest to the hematological community. It has been demonstrated that recombinant B-domain-deleted (BDD) porcine FVIII (rpFVIII) expresses at 10-14 fold higher levels than rhFVIII.⁶² A novel human/porcine chimeric construct (“Et3i”) containing the porcine A1 and A3 domains expresses 5.3 ± 0.75 fold higher than rhFVIII from transiently transfected COS-7 and stably transfected BHK cells, while maintaining comparable clotting activity.⁶³ Et3i has received positive feedback from an FDA Pre-Investigational New Drug (IND) program and is additionally being evaluated as a potential gene therapy candidate.⁶³⁻⁶⁵

Structural modeling of Et3i could aid in the development of less-immunogenic protein therapies and would improve upon the already published, intrinsically low-resolution FVIII structures (PDB: 2R7E¹⁰³, 3CDZ¹⁰⁴). In addition to clinical applications, characterizing the atomic structure of Et3i could supplement fundamental understanding of the architecture and activity of human and porcine FVIII. In particular, when FVIII is cleaved to the activated heterotrimeric state (A1/A2/A3-C1-C2), the rate at which the A2 domain dissociates from its A1/A3 interface is strongly correlated to the lifespan of the protein in serum.^{53,71} It has been demonstrated that pFVIII has increased stability of the A2 domain in the heterotrimeric state. Structural modeling of the interactions between the porcine A1 & A3 and human A2 domains could lead to knowledge of additional stabilizing mutations to and development of future therapeutics.

4.2 Research Aims

Structural characterization of the human/porcine chimeric FVIII construct “Et3i” could further understanding of the development of inhibitory antibodies and FVIII domain-domain interactions. To accomplish this, protein crystals of purified Et3i formed by hanging drop vapor diffusion were exposed to X-rays and their diffraction pattern measured. A data set describing the electron density map of the crystallographic asymmetric unit was generated, and a molecular model was refined by tools included in the WinCoot and Phenix software suites. Additionally, improved crystals were attempted with both unmodified and deglycosylated Et3i alone or in complex with the anti-C2 antibody G99 Fab.

4.3 Materials and Methods

4.3.1 Materials

4.3.1.1 Generation of 2014 Crystal and Data Set

Protein crystals were exposed to X-rays from the synchrotron Advanced Light Source (ALS) at the Lawrence Berkeley National Laboratory.

4.3.1.2 Et3i Model Refinement

The Phenix (Version 1.12-2829) software suite was employed to solve the phase problem by Phaser molecular replacement (MR), and automatically refine the molecular structure and electron density map. Manual adjustment of the protein model into the refined electron density map was performed with WinCoot (Version 0.8.6.1).

4.3.1.3 Attempted Improvement of Et3i Crystals

Crystal tray condition calculations were completed with Hampton Research's Make Tray (https://www.hamptonresearch.com/make_tray.aspx). The 24 well crystal trays were purchased from Hampton Research. Crystal screen conditions used included Hampton Research PEG/Ion2 (HR2-098) and Index (HR2-144). The rate of vapor diffusion to the mother liquor was reduced with Al's Oil (50% silicone oil, 50% paraffin oil, Hampton Research). Deglycosylation of Et3i was performed by Remove-iT PNGaseF, New England Biolabs (Prod.# P07065). Remove iT PNGaseF was sequestered with Chitin Magnetic Beads, New England Biolabs (Prod.# E80365) and Clontech magnetic stand for Eppendorf tubes (Cat.# 631964). Attempted improved crystals were exposed to X-rays on a Rigaku Micromax-007HF rotating anode generator and diffraction measured with a Saturn 994+ CCD area detector in conjunction with the Stoddard lab at the Fred Hutchinson Cancer Research Center.

4.3.2 Methods

4.3.2.1 Generation of 2014 Crystal and Data Set

Previous researchers employed hanging drop vapor diffusion to crystallize aliquots of Et3i in conditions (16% polyethylene glycol (PEG) 3350, 0 M MgCl₂, 0.025 M 4-(2-hydroxyethyl)-1-piperazineethanesulfonic acid) HEPES) with increasing PEG3350 across the tray X-axis (+2% / column), and increasing MgCl₂ down the tray Y-axis (+0.025 M / row) (Figure 35).

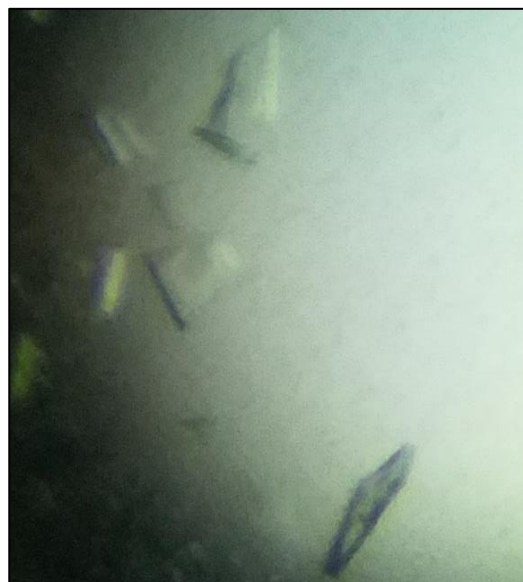


Figure 35 Stereotypical crystals of Et3i. Thin, trapezoidal crystals which layers of sheets were repeatedly obtained via hanging drop vapor diffusion.

4.3.2.2 Et3i Model Refinement

X-ray diffraction data were indexed, integrated and scaled with the program XDS to 3.2 Å resolution. Molecular Replacement with Phaser MR (template model: 2R7E¹⁰³) allowed for determination of the phase angles of X-ray diffraction data and generation of an electron density map. Manual adjustment of the protein model into the refined electron density map was performed with WinCoot. The Phenix software suite was employed to automatically refine the molecular structure and electron density map. The primary tool of refinement was the “phenix.refine” tool suite.⁹⁴ Refinement configurations relied on rigid-body, XYZ coordinates, real-space, and Individual B Factor parameters. Rigid-body refinement locks the geometry of the molecule and optimizes the models fit into the electron density through translation and rotation functions. XYZ coordinate refinement allows for Cartesian manipulation of model geometry to match the X-ray data. Real-space refinement achieves a similar effect, but optimizes model geometry against the calculated electron density map, instead of X-ray diffraction data. The individual B factor refinement tool adjusts the calculated atomic vibrational equilibrium position, or “temperature factor” for each atom in the model. For this model, B factors were calculated as isotropic. Once glycans were appended to the model with the WinCoot Carbohydrate module, the Phenix ReadySet tool generated ligand restraints and LINK entries in the .pdb file before each phenix.refine cycle. ReadySet employs the program suite eLBOW and PhenixRefine to generate and optimize ligand structural parameters.¹⁰⁵

To address a structural shift observed in the Molecule B’s C2 domain, the Phenix suite tool “Morph Model” was employed; which restrained local relative positions between amino acid residues while allowing the domain as a whole to perform translation and rotation optimization functions.^{106,107} The Phenix suite Omit Map tool was employed to remove and generate a more indicative difference map for difficult external loops and the Molecule B C2 domain.¹⁰⁸ The metrics of Rfree, Rwork validated the agreement between the molecular model and the crystallographic

electron density. The MolProbity suite tracked geometry of the model, tracking Ramachandran outliers, rotamer outliers, and steric clashes.

4.3.2.3 Attempted Improvement of Et3i Crystals^{xix}

To improve crystal quality, another Et3i prep (Expression Therapeutics, 6/5/2017, 0.84 mg/mL) was screened through crystallization trials. The starting 24-well tray crystal condition was reused from previous researchers^{xx} ((16% polyethylene glycol (PEG) 3350, 0M MgCl₂, 0.025 M 4-(2-hydroxyethyl)-1-piperazineethanesulfonic acid) HEPES) with increasing PEG3350 across the tray X-axis (+2%) / column), and increasing MgCl₂ down the tray Y-axis (+0.025 M) / row). Further optimizations included additions of Hampton Research (HR) Index Screen to HR PEG/ION2 Screen conditions.^{xxi} The percent (%) of PEG, and molarity (M) of MgCl₂ and HEPES were controlled, so that the final concentration was held constant upon addition of the PEG/ION2 conditions. This was accomplished with a functionalized Microsoft Excel spreadsheet of the following format:

Table 3 Crystal Condition Control for PEG content. Assume a 5 mL crystal condition solution.

Addtl. Vol. of PEG/Ion screen to add to PEG containing condition (μL)		X
Original PEG-Containing-Condition Chemical	Original Volume (μL)	New Vol.
50 % PEG 3350	1800	=1800-(((X)*(PEG % of X))/50)
0.96 M HEPES (8.26)	260.4	260.4
1.0 M MgCl ₂	312.5	312.5
100 % PEG 400	462.5	462.5
New PEG/Ion Screen	X	X
ddH ₂ O	2164.6	=(2164.6-X)+(((PEG% of X)*X)/50))
SUM=	5000	=SUM()
Obsv:		

^{xix} (IWS(II)p.89)

^{xx} (Anne d'Aquino (AD)(I) p.151)

^{xxi} (IWS(II)p.98,110,122)

Deglycosylation of Et3i with PNGase F was attempted to improve crystal quality.^{xxii} The reaction was first optimized under native and denaturing conditions with dithiothreitol (DTT). The refolding of Et3i after denaturation was not assessed.

Additionally, Et3i was complexed with the anti-C2 domain antibody G99 Fab (Et3i:G99) in stoichiometric amounts in an attempt to form protein crystals.

4.4 Results

4.4.1 Crystal Structure of Et3i

The X-ray crystal structure of the human/porcine chimeric protein, “Et3i”, residues 1 - 2329 was determined to 3.2 Å resolution and refined to an R_{work} of 0.2146 and R_{free} of 0.2879 (Figure 36). Et3i was crystalized in a novel FVIII space group $P2_1$ compared to previously published FVIII models in $P4_12_12$. Molecular replacement (MR) was accomplished using prior

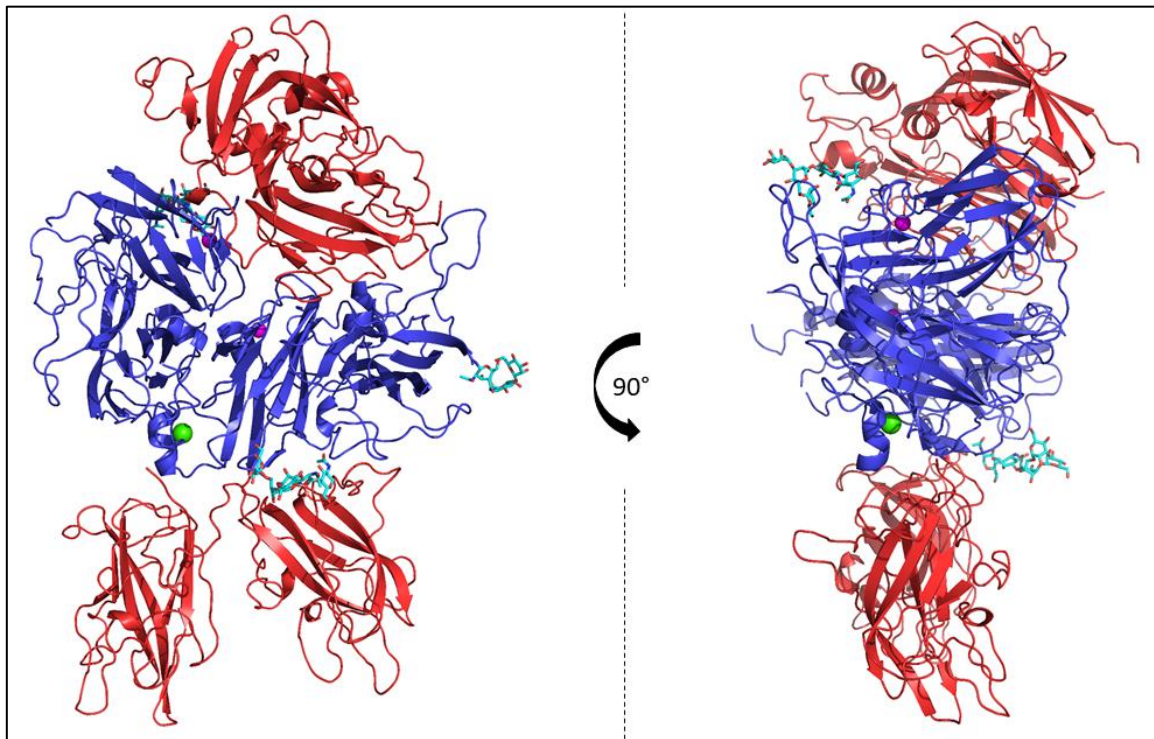


Figure 36 Structure of Et3i Molecule A. This protein chimera contains porcine A1 and A3 domains (blue), and human A2, C1 and C2 domains (red). Metal ligands, calcium (green) and copper (magenta) are shown. Asparagine linked glycan ligands (teal) were modeled at N240, N1810, and N2118.

^{xxii} (IWS(II)p.58)

hFVIII as a template (PDB: 2R7E¹⁰³). The model geometry for this FVIII construct is significantly more robust than previously published FVIII models.

Two molecules of Et3i were observed in the asymmetric unit, molecules “A” and “B” (Figure 37). Each molecule contained three metal ligands, two copper and one calcium. The improved electron density allowed for greater confidence in modeling important structural elements. First, improvement of A1 domain metal coordination site, residues 316-318 (HHH) was accomplished. Additionally, the improved electron density allowed accurate placement of asparagine-linked glycans at residues N240 (Molecule A: N-NAG₂-BMA-MAN₂; Molecule B: N-NAG₂-BMA-MAN₂), N1810 (Molecule A: N-NAG₂-BMA; Molecule B: N-NAG(FUC)-NAG-BMA-MAN₄), and N2118 (Molecule A: N-NAG₂-BMA-MAN₂; Molecule B: N-NAG₂-BMA-MAN₂).



Figure 37 Two molecules in the Et3i asymmetric unit. A significant conformational difference was observed between the C2 domain of molecule A (red), and molecule B (cyan).

Poor non-crystallographic symmetry (NCS) up to 14 Å was observed between the Molecule A and Molecule B C2 domains (Figure 38). Refinement with the Phenix MorphModel tool resolved a whole C2 domain “roll” of approximately 12 Å between the molecule A and B of the asymmetric unit (Figure 39).

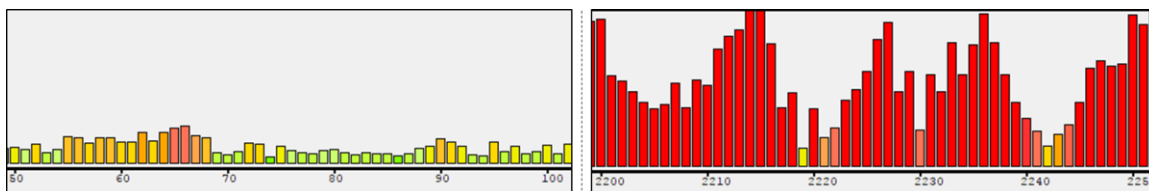


Figure 38 Spatial Comparison of Non-Crystallographic Symmetry (NCS) between Et3i Molecule A and B. The difference between Molecule A and Molecule B is reported in relative distance (Y-axis, Å) for each residue (X-axis). Well behaved data on the left (residue) ~1 Å difference. The molecule B C2 domain (right) ~11 Å NCS distances.

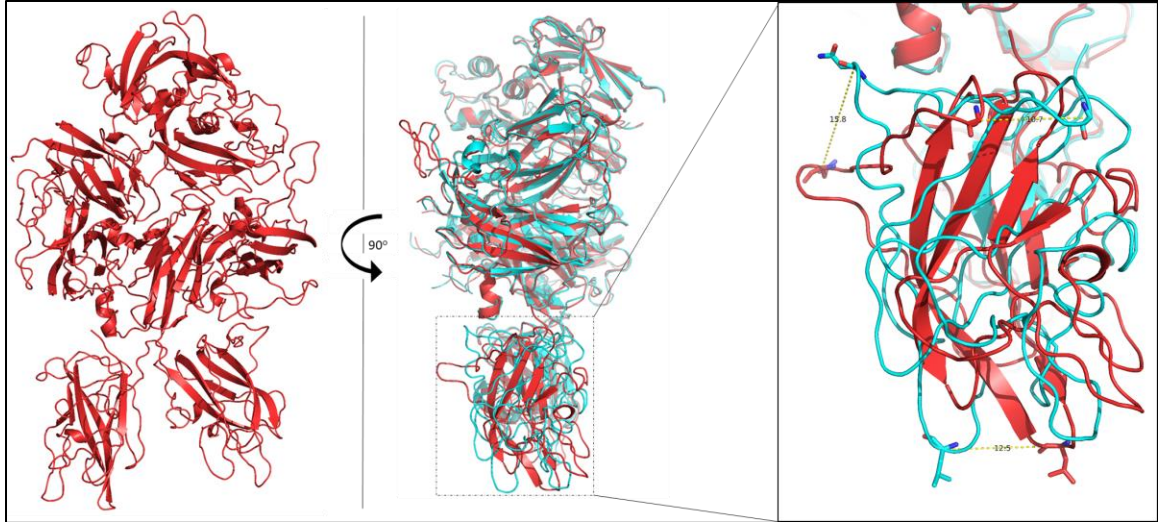


Figure 39 C2 Domain Comparison in Overlay of the Molecule A and B in Profile. The Et3i A & B molecules were aligned to each other in PyMol. With Molecule A and B overlaid, a ~ 10 Å rotation of the C2 domain was observed. Distances were measured between three arbitrary residues of the A / B molecule overlaid pair, including: L2252 (12.5 Å), G2268 (10.7 Å), and N2277 (15.8 Å).

4.4.2 Rebuilding the hFVIII structure with ET3i Model

Based on the observation that the newly solved ET3i model could be refined against the data sets for either previous hFVIII (2R7E or 3CDZ) structure factors and significantly improve the R_{free} and R_{work} , rebuilding the entire hFVIII structure based on the Et3i model was undertaken. Using the completed Et3i model as a template, an improved hFVIII model was constructed. This model contains the improved architecture of the Et3i molecule in hFVIII derived electron density data set in comparison to previously published FVIII models (PDB:2R7E¹⁰³, 3CDZ¹⁰⁴). The Et3i residues in the A1 and A3 domains were mutated to the human FVIII sequence *in silico* with WinCoot. When the new hFVIII model was refined against previous hFVIII data, the rebuilt model of hFVIII attained increased model accuracy with an improved R_{free} of 0.2749 compared to previous R_{free} 0.347 (2R7E¹⁰³).

4.4.3 Attempted Improved Crystallization of Et3i, Et3i:G99, and PNGaseF

Improvements to the 2014 crystal of Et3i were attempted, including a variety of trays and optimizations with a new prep of Et3i from Expression Therapeutics (6/5/2017, 0.8473 mg/mL)

and anti-C2 domain G99 antibody Fabs. While small and well defined Et3i crystals were readily obtained, the trials but did not yield crystals of sufficient size or quality to diffract X-rays.

PNGaseF was employed to deglycosylate asparagine-linked glycans from Et3i, by cleaving the innermost asparagine and N-acetylglucosamine bond.^{xxiii} Cleavage of Et3i was successful, but the protein remained recalcitrant to crystallization (Figure 40). The three asparagine-linked glycan sites modeled in Et3i were at N240 (A1 domain), N1810 (A3 domain), and N2118 (C1 domain).

The FVIII Heavy Chain (A1-A2) contains the N240 glycan site, while the FVIII Light Chain (A3-C1-C2) contains N1810 and N2118.

Deglycosylated Et3i was complexed with Fabs of G99 in stoichiometric amounts, but crystals of sufficient size to diffract X-rays were not formed (Figure 41). Trays of glycosylated Et3i:G99 complex formed crystals, but none diffracted X-rays sufficiently to calculate an electron density map.^{xxiv}

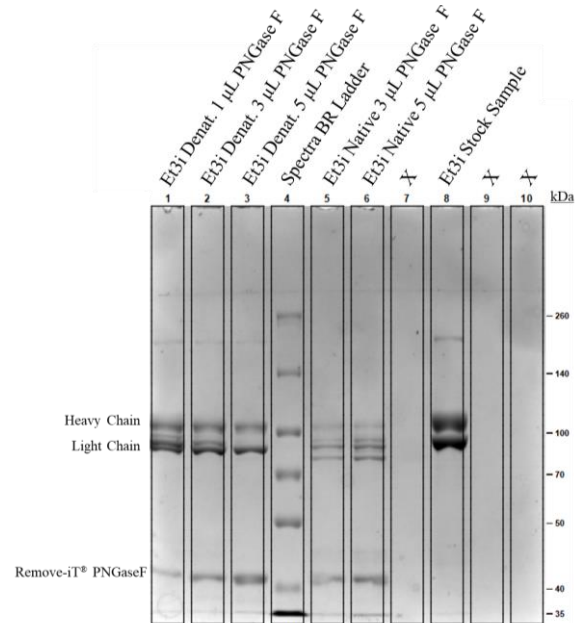


Figure 40 Deglycosylation of Et3i by PNGase F. The reaction was completed under denaturing (lanes 1-3) and native (lanes 5-6) conditions and visualized with a 7.5% acrylamide SDS-PAGE gel. (8.8.2017 IWS(II)p.56)

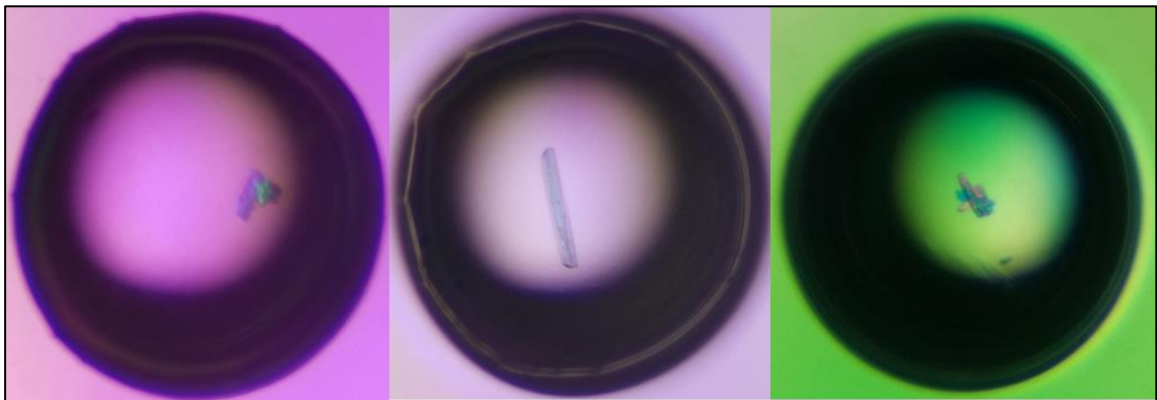


Figure 41 Morphologies of Deglycosylated Et3i Crystals. These crystals were exposed to X-rays and diffracted in a manner indicative of a biological molecule, but the resolution of data was not an improvement over already established 2014 Et3i data. (12.18.2017 IWS(II) p.147)

^{xxiii} (IWS (II)p.56,126)

^{xxiv} (IWS(II)p.144)

4.5 Discussion

4.5.1 Improvements of Et3i Model Compared to Previously Published FVIII models

This is the highest resolution structure of B-domain deleted (BDD) FVIII to date. The improved resolution of 3.2 Å compared to previously published models at 3.7 Å or 3.98 Å (2R7E¹⁰³ and 3CDZ¹⁰⁴, respectively) allowed for more confidence in structural modeling and distribution of surface electrostatic charge (Figure 42, Figure 43). The correction of two amino acid register errors in the A2 domain at residues Q645 and S654 resulted in significant reassignment of the solvent accessible residues and surface charge of the A2 domain (Figure 44). Additionally, the metal chelation sites were improved at H316-H318 (Figure 45). Overall, a more robust model geometry, significantly lower Ramachandran and rotamer outliers, and lower R_{free} have been achieved in this model.

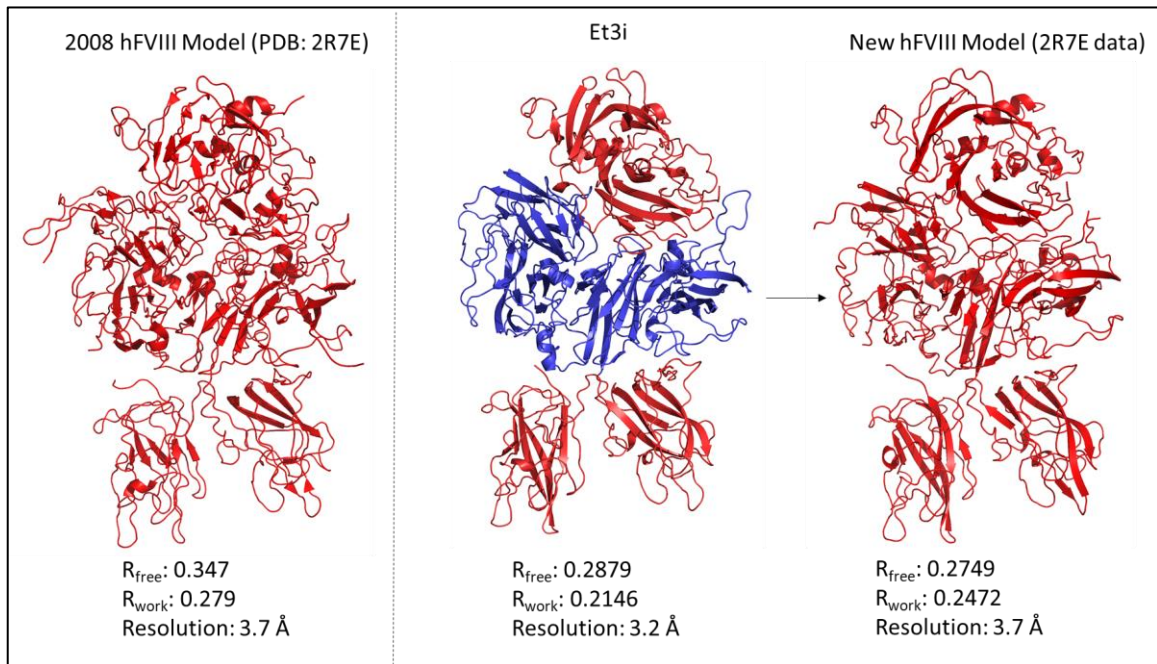


Figure 42 **Comparison of Et3i and Improved hFVIII to Previous Model.** Amino acid register corrections were primarily performed in the A2 domain. A significant improvement in the apparent secondary structure for Et3i and new hFVIII models was observed compared to previous FVIII structures.

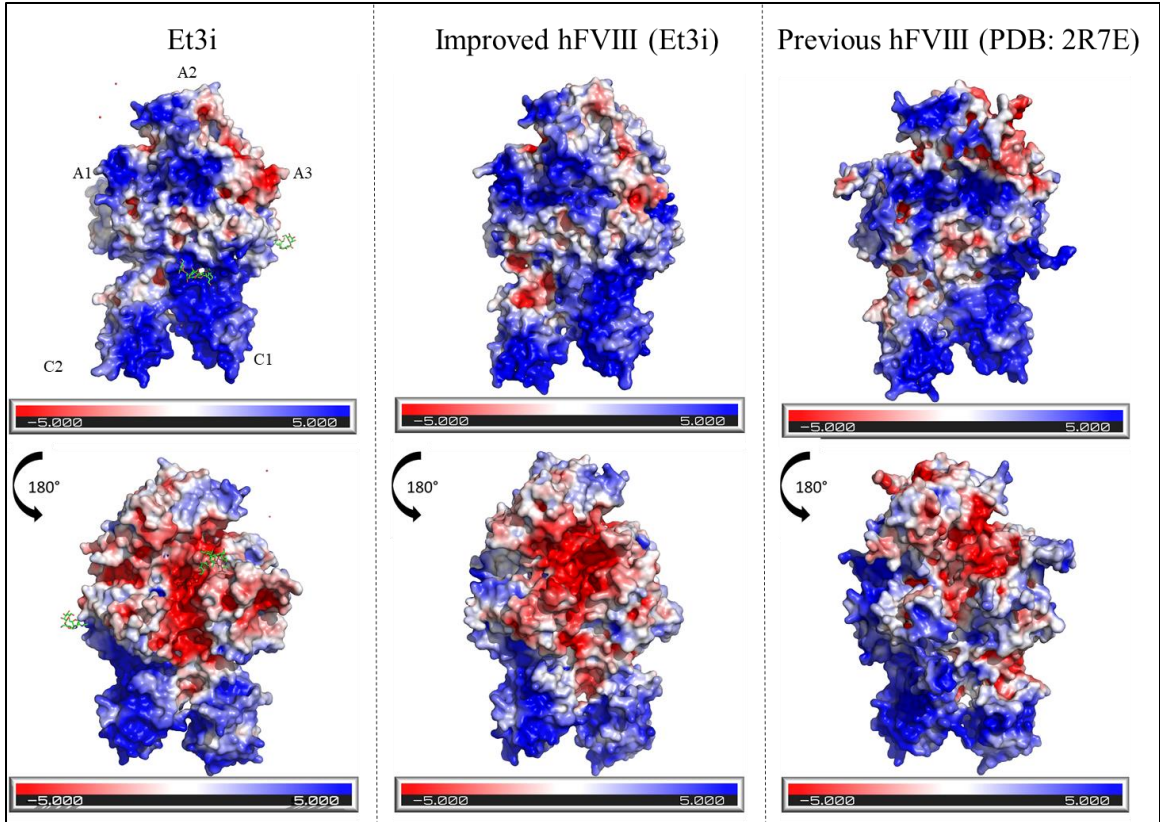


Figure 43 Comparison of Surface Electrostatics between Et3i and hFVIII Models. Surface charge calculations were accomplished using PDB2PQR and visualized with APBS software (blue = positive charge, red = negative charge). A significant electrostatic difference was observed in the FVIII A2 domain

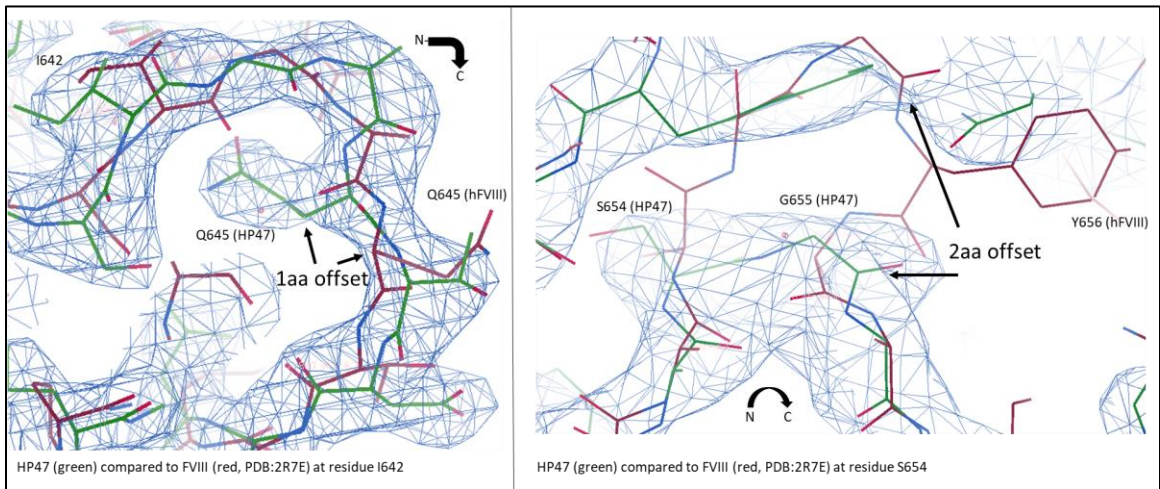


Figure 44 A2 Domain Amino Acid Register Improvement. The enhanced resolution of the Et3i crystal in comparison to previous hFVII models corrected an amino acid register error which propagated for 55 residues in the A2 domain.

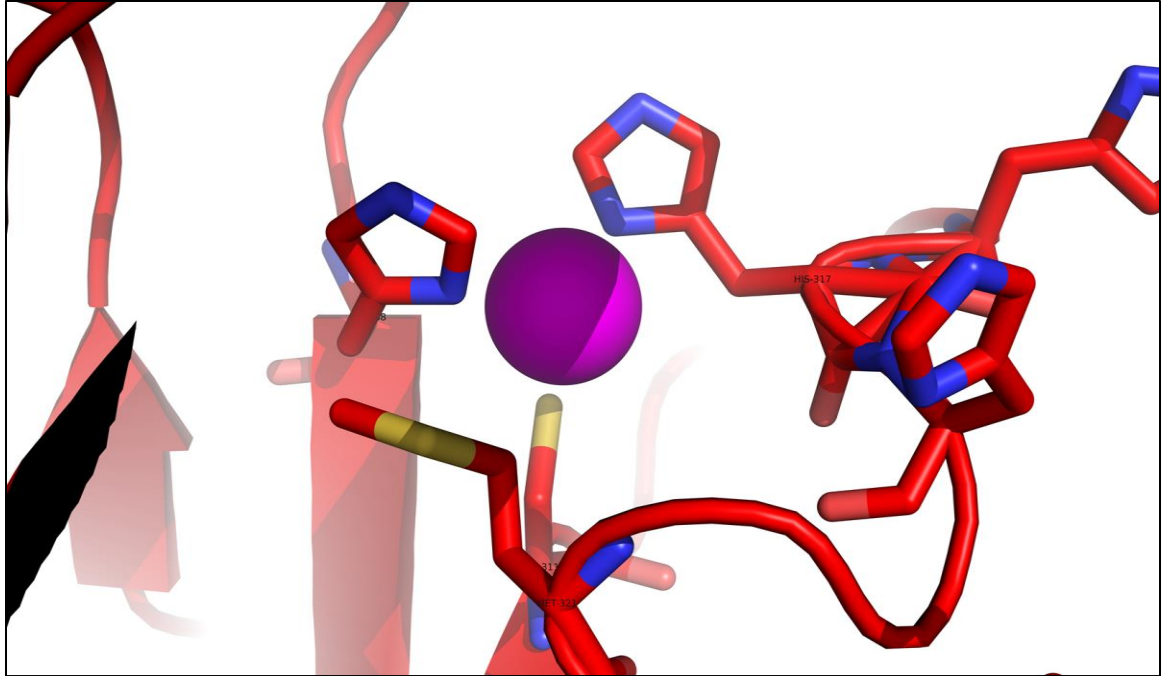


Figure 45 *Cu binding site in ET3i. His317, Met321, Cys 311, and His268 appear to coordinate Cu2402. Ile313 appears to provide steric support to the metal binding site.*

4.5.2 Conformational Change of Et3i C2 Domains

The conformational movement of the C2 domain between the Et3i molecule A and B is the first observed in FVIII models. The C2 domain, in conjunction with the C1 domain, plays a major role in binding phosphatidylserine (PS) rich surfaces of activated platelets localized to the site of vascular injury. Previously, only small conformational movement within the C2 domains of FVIII and FV had been reported (Figure 46).²⁶ In FVIII, a β -hairpin loop containing residues M2199 and F2200 displayed a 5 Å movement. In FV, a β -hairpin turn (W2063, W2064) of the C2 domain undergoes a 12 Å motion from a “closed” to “open” position. This motion is hypothesized to

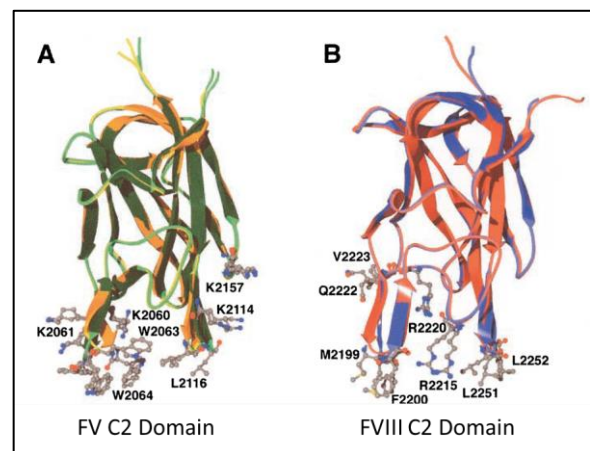


Figure 46 *Previously Published C2 Domain Conformation Shifts. Previous conformations of the C2 domain involved restrained movement of distal β -hairpin loops. (Spiegel and Stoddard, 2002)*

play a role in binding PS-rich platelet surfaces and the conformational shift relies on FV's unique flexibility granted by the steric freedom of residue G2065. In comparison, at residue 2065 FVIII contains alanine instead of glycine and is not thought to be sterically capable of a similar movement.

Instead of β -hairpin loops, the conformations observed between the Et3i C2 denoted whole C2 domain rotation within the cup interface of the adjacent C1-A1 domains. While this movement could simply be a result of the low interdomain interactions of the C2 pocket as described,¹⁰⁴ this whole domain shift could allow for more advantageous platelet surface interactions.

Context for the whole C2 domain shift can be provided by consideration of published literature. In 2013, Walter et al. communicated the molecular structure of hFVIII C2 domain in complex with two anti-C2 domain antibodies 3E6 and G99 (PDB: 4KI5⁹⁶) (Figure 47).

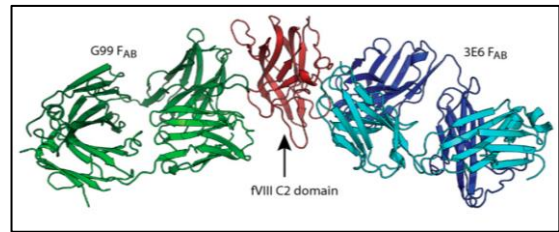


Figure 47 Molecular Depiction of hFVIII C2 Domain in Complex with 3E6 and G99 antibody Fabs. (Walter et al., 2013)

and G99 (PDB: 4KI5⁹⁶) (Figure 47). In 2015, Brison et al. communicated that 3E6 antibody abrogated C2 binding to PS-rich lipid surfaces. From this, an updated model for residues involved in PS binding was proposed, including C2 domain residues R2215, K2183, and F2200 (Figure 48).⁹⁸ Based upon this new PS binding model, the C2 domain's 3E6 epitope can be interpreted as analogous to a PS-rich surface plane of an activated platelet where FVIIIa binds during hemostasis.

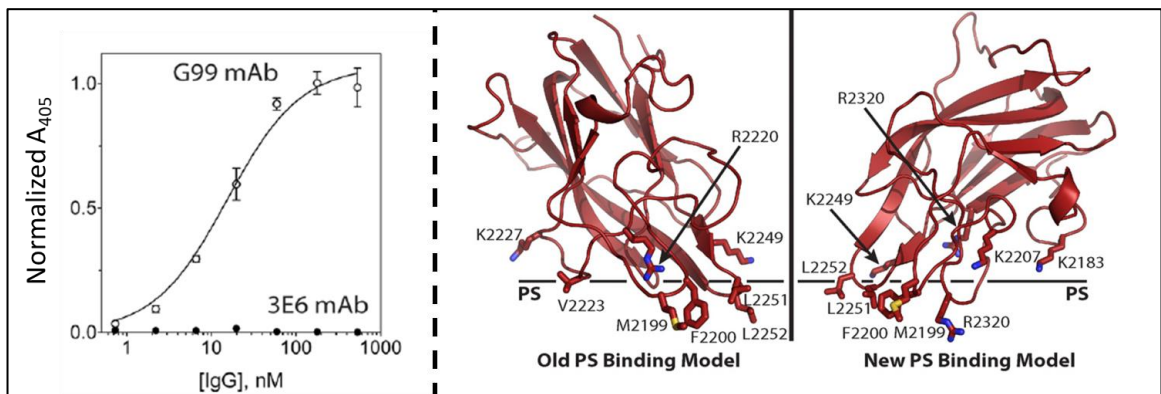


Figure 48 Brison et al. 3E6 Antibody Abrogates PS Binding and New PS Binding Model. (LEFT) The nullification of A₄₀₅ indicating C2 phosphatidylserine lipid binding was assessed by ELISA. (RIGHT) Brison et al. proposed a new model implicating 3E6 epitope C2 residues as necessary for lipid binding (Brison et al., 2015)

A superposition of the Et3i Molecule A and Molecule B into the Walter et al. anti-C2 ternary antibody structure highlights the effect the whole domain C2 conformational shift has on the relative distance of the C1 domain from the analogous 3E6 binding epitope (Figure 49). Based on this hypothesis, the observed conformations of the C2 domain could contribute advantageous flexibility of the FVIII molecule to bind to PS-rich surfaces.

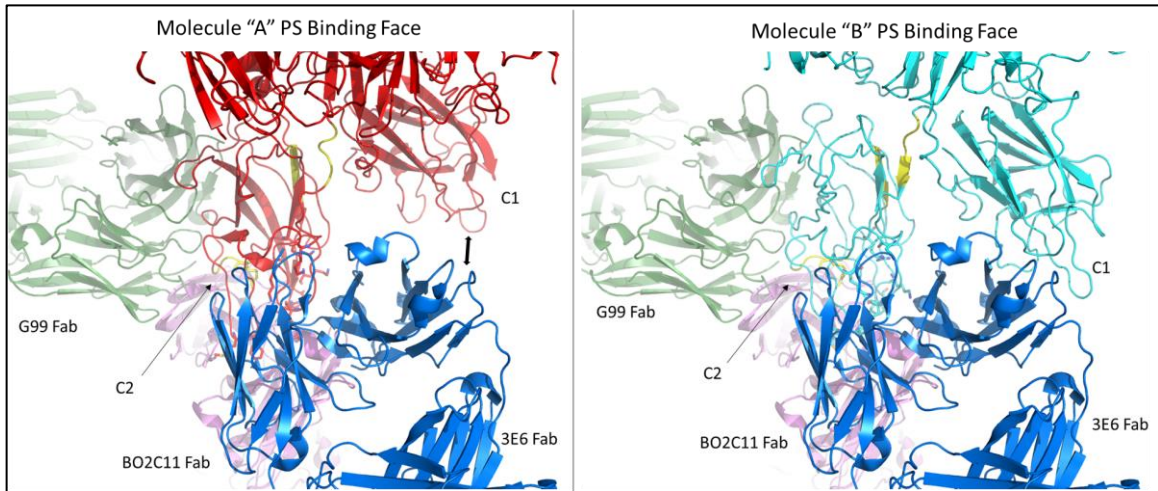


Figure 49 C2 Domain Conformation Shift in Context with 3E6. The Et3i A and B molecules are shown superimposed into the previously published anti-C2 ternary complex (Walter et al., 2013, PDB:4KI5). In the B molecule, the PS-binding C1 domain of FVIII is brought closer to the 3E6 binding face of C2.

4.5.3 Crystallization of Et3i

It was attempted to repeat the conditions that successfully yielded the Et3i crystals from 2014, but these attempts and further optimizations were not successful in creating a crystal that diffracted better than what has already been obtained. Although the model of Et3i has been refined, the structure of Et3i in complex with inhibitory antibodies such as G99 is of substantial interest. Therefore, improvements to Et3i crystal conditions remain a high priority. Crystal trays of Et3i and G99 were attempted but yielded only weakly diffracting crystals.

To remove dynamic carbohydrate ligands, Et3i was treated with PNGase F. Treatment to remove glycans from Et3i with PNGase F was apparent under denaturing conditions, but less conclusive in native conditions. Further optimization and investigation of the native condition Et3i

is warranted before use in crystal trials. For future crystallization attempts, including those of Et3i:G99, additional preparatory steps are likely warranted, including size exclusion chromatography of the protein complexes, and additional crystallization conditions and methods.

Conclusion

Isolated C1 Domain of FVIII in Complex with Inhibitory Antibodies

Noteworthy progress has been made towards the production and purification of the FVIII C1 domain from a bacterial vector. Additionally, anti-C1 Fabs were successfully produced on-site from murine hybridomas. Initial crystallographic screening of C1:Fab complexes have yet to yield protein crystals capable of X-ray diffraction, but the morphology of microcrystals and phase separation observed in hanging-drop vapor diffusion trials is promising.

While opportunities exist to enhance the yield and purity of our recombinant or mammalian culturing procedures, the project has arrived at a point where the optimization of crystallographic conditions for the C1:Fab complex is of priority. From the project's current position, a protein crystal and subsequent molecular model could feasibly be obtained in short order.

This project established the ability for the Spiegel lab to perform mammalian cell culturing in-house at Western Washington University. This capacity opens new avenues for future research with more complex FVIII structural targets, including current preliminary work with a complete porcine sequence FVIII, "POL1212" (a gift from the Lollar lab, Emory University).

In the near term for hemophiliacs, prophylactic infusions of replacement FVIII will remain the therapeutic mainstay. However, for those ~30% of patients who develop an inhibitor, the ITI procedure is expensive, reversible and not an ideal long-term solution. Ultimately, knowledge of the immunogenic epitopes for FVIII is of principle importance. Continued X-ray crystallographic studies of FVIII in complex with inhibitory antibodies could create a comprehensive topographic map of immunogenicity. This information could direct development of engineered FVIII proteins with reduced inhibitor response. In the not-too-distant future, engineered low-immunogenicity FVIII constructs could be implemented in human gene therapy, effectively curing this devastating disease that has afflicted humankind throughout history.

Structure Determination of Et3i and Improvements to the human FVIII model

As a protein candidate for ITI campaigns, the human/porcine chimeric FVIII construct “Et3i” has demonstrated augmented expression and activity *in vivo* relative to wildtype hFVIII. At 3.2 Å, the Et3i structure is the highest resolution model of FVIII to date. The improved model delivers an increased validity of molecular geometry and reassigns the amino acid register of ~70 residues in the A2 domain. As a result, the surface electrostatics of the protein are substantially updated and may hold clues to the future elucidation of molecular interactions.

Assessment of the two Et3i molecules observed in the crystallographic asymmetric unit revealed a conformational change between the C2 domains. This novel whole-domain movement could have substantial physiological implications in the context of FVIII binding phosphatidylserine-rich activated platelet surfaces.

The Et3i model’s porcine A1 and A3 domains were mutated *in silico* to the human sequence to generate a superior human FVIII (hFVIII) model. The novel Et3i-derived hFVIII model demonstrated improved model accuracy when compared to prior hFVIII structural data. Both the Et3i and enhanced hFVIII models will provide a more sophisticated molecular foundation from which to understand FVIII’s activity in hemostasis. Furthermore, continued attempts to crystallize Et3i with anti-C1 or anti-C2 antibodies could further expound the specific FVIII residues that mitigate the immunogenic response, docking to activated platelet surfaces, or binding to von Willebrand Factor.

Bibliography

- (1) Rosner, F. Hemophilia in the Talmud and Rabbinic Writings. *Annals of Internal Medicine* **1969**, 70 (4), 833.
- (2) Major, R. H. A History of Medicine. In *A History of Medicine*; Charles C. Thomas, 1954; Vol. 1, p 252.
- (3) Potts, D. M.; Potts, W. T. W. *Queen Victoria's Gene: Haemophilia and the Royal Family*, Pbk. ed.; Sutton Pub: Stroud, 1999.
- (4) Otto, J. C. An Account of an Hemorrhagic Disposition Existing in Certain Families: *Clinical Orthopaedics and Related Research* **1996**, 328, 4–6.
- (5) Nasse, C. F. Von Einer Erblichen Neigung Zu Todtlichen Blutungen. *Arch. Med. Erfahr* **1820**, 1, 385.
- (6) Müller, J.; Baly, W.; Bell, J. *Elements of Physiology*; Philidelphia: Lea and Blanchard, 1843.
- (7) Lane, S. HÆMORRHAGIC DIATHESIS. *The Lancet* **1840**, 35 (896), 185–188.
- (8) Schmidt, A. Neue Untersuchungen über die Faserstoffgerinnung. *Pflüger, Archiv für die Gesamte Physiologie des Menschen und der Thiere* **1872**, 6 (1), 413–538.
- (9) Arthus, M.; Pagès, C. Nouvelle Theorie Chimique de La Coagulation Du Sang. *Arch Physiol Norm Pathol* **1890**, 5, 739–746.
- (10) Pekelharing, C. Untersuchung Über Das Fibrinferment. *Internat Beitr Zschr Wissensch Med (Festschr Rudolf Virchow)* **1891**, 1, 433–456.
- (11) Stormorken, H. The Discovery of Factor V: A Tricky Clotting Factor. *Journal of Thrombosis and Haemostasis* **2003**, 1 (2), 206–213.
- (12) Wright, A. E. On a Method of Determining the Condition of Blood Coagulability for Clinical and Experimental Purposes, and on the Effect of the Administration of Calcium Salts in Haemophilia and Actual or Threatened Haemorrhage: [Preliminary Communication]. *BMJ* **1893**, 2 (1700), 223–225.
- (13) Hammarsten, O. Beiträge Zur Kenntnis Der Fibrinbildung. **1899**, 28, 98–114.
- (14) Morawitz, P. Die Chemie der Blutgerinnung. *Ergebnisse der Physiologie* **1905**, 4 (1), 307–422.
- (15) Patek, A. J.; Taylor, F. H. L. HEMOPHILIA. II. SOME PROPERTIES OF A SUBSTANCE OBTAINED FROM NORMAL HUMAN PLASMA EFFECTIVE IN ACCELERATING THE COAGULATION OF HEMOPHILIC BLOOD. *Journal of Clinical Investigation* **1937**, 16 (1), 113–124.
- (16) Owren, P. PARAHÆMOPHILIA. *The Lancet* **1947**, 249 (6449), 446–448.
- (17) Laki, K.; Lorand, L. On the Solubility of Fibrin Clots. *Science* **1948**, 108 (2802), 280–280.
- (18) Koller, F.; Loeliger, A.; Duckert, F. Experiments on a New Clotting Factor (Factor VII). *Acta Haematologica* **1951**, 6 (1), 1–18.
- (19) Christmas Disease A Condition Previously Mistaken For Haemophilia Author(s): Rosemary Biggs, A. S. Douglas, R. G. MacFarlane, J. V. Dacie, W. R. Pitney, C. Merskey and J. R. O'Brien. *The British Medical Journal* **1952**, 2 (4799), 1378–1382.
- (20) Rosenthal, R. L.; Dreskin, O. H.; Rosenthal, N. New Hemophilia-like Disease Caused by Deficiency of a Third Plasma Thromboplastin Factor. *Proc. Soc. Exp. Biol. Med.* **1953**, 82 (1), 171–174.
- (21) Ratnoff, O. D.; Colopy, J. E. A FAMILIAL HEMORRHAGIC TRAIT ASSOCIATED WITH A DEFICIENCY OF A CLOT-PROMOTING FRACTION OF PLASMA 1. *Journal of Clinical Investigation* **1955**, 34 (4), 602–613.

- (22) Graham, J. B.; Barrow, E. M.; Hougie, C. Stuart Clotting Defect. II. Genetic Aspects of a 'New' Hemorrhagic State. *Journal of Clinical Investigation* **1957**, *36* (3), 497–503.
- (23) Telfer, T. P.; Denson, K. W.; Wright, D. R. A 'New' Coagulation Defect. *British Journal of Haematology* **1956**, *2* (3), 308–316.
- (24) MacFarlane, R. G. An Enzyme Cascade in the Blood Clotting Mechanism, and Its Function as a Biochemical Amplifier. *Nature* **1964**, *202*, 498–499.
- (25) Davie, E. W.; Ratnoff, O. D. Waterfall Sequence for Intrinsic Blood Clotting. *Science* **1964**, *145* (3638), 1310–1312.
- (26) Spiegel, P. C.; Stoddard, B. L. Optimization of Factor VIII Replacement Therapy: Can Structural Studies Help in Evading Antibody Inhibitors? *British journal of haematology* **2002**, *119* (2), 310–322.
- (27) Hoffman, M.; Monroe III, D. M. A Cell-Based Model of Hemostasis. *Thrombosis and haemostasis* **2001**, *85* (06), 958–965.
- (28) Dallman, P. R.; Pool, J. G. Treatment of Hemophilia with Factor VIII Concentrates. *New England Journal of Medicine* **1968**, *278* (4), 199–202.
- (29) Pool, J. G.; Hershgold, E. J.; Pappenhagen, A. R. High-Potency Antihemophilic Factor Concentrate Prepared from Cryoglobulin Precipitate. *Nature* **1964**, *203* (4942), 312–312.
- (30) Pool, J. G. Cryoprecipitated Factor VIII Concentrate. In *Thrombosis et diathesis haemorrhagica. Supplementum.*
- (31) Manco-Johnson, M. J.; Abshire, T. C.; Shapiro, A. D.; Riske, B.; Hacker, M. R.; Kilcoyne, R.; Ingram, J. D.; Manco-Johnson, M. L.; Funk, S.; Jacobson, L.; et al. Prophylaxis versus Episodic Treatment to Prevent Joint Disease in Boys with Severe Hemophilia. *New England Journal of Medicine* **2007**, *357* (6), 535–544.
- (32) Oldenburg, J.; Pavlova, A. Genetic Risk Factors for Inhibitors to Factors VIII and IX. *Haemophilia* **2006**, *12* (s6), 15–22.
- (33) Allain, J.-P.; Frommel, D. Antibodies to Factor VIII. V. Patterns of Immune Response to Factor VIII in Hemophilia A. *Blood* **1976**, *47* (6), 973–982.
- (34) Hall, A. G.; Tilby, M. J. Mechanisms of Action of, and Modes of Resistance to, Alkylating Agents Used in the Treatment of Haematological Malignancies. *Blood reviews* **1992**, *6* (3), 163–173.
- (35) Brackmann, H. H.; Gormsen, J. Massive Factor-VIII Infusion in Haemophiliac with Factor-VIII Inhibitor, High Responder. *The Lancet* **1977**, *310* (8044), 933.
- (36) Astermark, J. Immune Tolerance Induction in Patients with Hemophilia A. *Thrombosis Research* **2011**, *127*, S6–S9.
- (37) White, G. C. Hemophilia: An Amazing 35-Year Journey from the Depths of HIV to the Threshold of Cure. *Trans. Am. Clin. Climatol. Assoc.* **2010**, *121*, 61–73; discussion 74–75.
- (38) Russell, L. The Inadequate Reponse of the FDA to the Crisis of AIDS in the Blood Supply.Pdf. Harvard Law School 1995.
- (39) McDougal, J. S.; Martin, L. S.; Cort, S. P.; Mozen, M.; Heldebrant, C. M.; Evatt, B. L. Thermal Inactivation of the Acquired Immunodeficiency Syndrome Virus, Human T Lymphotropic Virus-III/Lymphadenopathy-Associated Virus, with Special Reference to Antihemophilic Factor. *J. Clin. Invest.* **1985**, *76* (2), 875–877.
- (40) Evatt, B. L. The Tragic History of AIDS in the Hemophilia Population, 1982-1984. *Journal of Thrombosis and Haemostasis* **2006**, *4* (11), 2295–2301.
- (41) Gitschier, J.; Wood, W. I.; Goralka, T. M.; Wion, K. L.; Chen, E. Y.; Eaton, D. H.; Vehar, G. A.; Capon, D. J.; Lawn, R. M. Characterization of the Human Factor VIII Gene. *Nature* **1984**, *312*, 326–330.
- (42) Levinson, B.; Kenwick, S.; Lakich, D.; Hammonds, G.; Gitschier, J. A Transcribed Gene in an Intron of the Human Factor VIII Gene. *Genomics* **1990**, *7* (1), 1–11.

- (43) Levinson, B.; Kenwrick, S.; Gamel, P.; Fisher, K.; Gitschier, J. Evidence for a Third Transcript from the Human Factor VIII Gene. *Genomics* **1992**, *14* (3), 585–589.
- (44) Sauna, Z. E.; Lozier, J. N.; Kasper, C. K.; Yanover, C.; Nichols, T.; Howard, T. E. The Intron-22-Inverted F8 Locus Permits Factor VIII Synthesis: Explanation for Low Inhibitor Risk and a Role for Pharmacogenomics. *Blood* **2015**, *125* (2), 223–228.
- (45) Mann, S. A. *Broken Blood: A Reflection of Loss and Hope in the Hemophilia Community*; CreateSpace: San Bernadino, CA, 2015.
- (46) van der Flier, A.; Liu, Z.; Tan, S.; Chen, K.; Drager, D.; Liu, T.; Patarroyo-White, S.; Jiang, H.; Light, D. R. FcRn Rescues Recombinant Factor VIII Fc Fusion Protein from a VWF Independent FVIII Clearance Pathway in Mouse Hepatocytes. *PloS one* **2015**, *10* (4).
- (47) Butenas, S.; Parhami-Seren, B.; Undas, A.; Fass, D. N.; Mann, K. G. The “Normal” Factor VIII Concentration in Plasma. *Thrombosis Research* **2010**, *126* (2), 119–123.
- (48) Shiltagh, N.; Kirkpatrick, J.; Cabrita, L. D.; McKinnon, T. A. J.; Thalassinos, K.; Tuddenham, E. G. D.; Hansen, D. F. Solution Structure of the Major Factor VIII Binding Region on von Willebrand Factor. *Blood* **2014**, *123* (26), 4143–4151.
- (49) Terraube, V.; O’Donnell, J. S.; Jenkins, P. V. Factor VIII and von Willebrand Factor Interaction: Biological, Clinical and Therapeutic Importance. *Haemophilia* **2010**, *16* (1), 3–13.
- (50) Lollar, P.; Parker, C. G. Subunit Structure of Thrombin-Activated Porcine Factor VIII. *Biochemistry* **1989**, *28* (2), 666–674.
- (51) Turner, N. A.; Moake, J. L. Factor VIII Is Synthesized in Human Endothelial Cells, Packaged in Weibel-Palade Bodies and Secreted Bound to ULVWF Strings. *PLOS ONE* **2015**, *10* (10), e0140740.
- (52) Parmenter, C. D. J.; Cane, M. C.; Zhang, R.; Stoilova-McPhie, S. Cryo-Electron Microscopy of Coagulation Factor VIII Bound to Lipid Nanotubes. *Biochemical and Biophysical Research Communications* **2008**, *366* (2), 288–293.
- (53) Radtke, K.-P.; Griffin, J. H.; Riceberg, J.; Gale, A. J. Disulfide Bond-Stabilized Factor VIII Has Prolonged Factor VIIIa Activity and Improved Potency in Whole Blood Clotting Assays. *Journal of Thrombosis and Haemostasis* **5**.
- (54) Grewal, P. K. The Ashwell–Morell Receptor. *Methods in Enzymology*; Elsevier, 2010; Vol. 479, pp 223–241.
- (55) Yang, W. H.; Aziz, P. V.; Heithoff, D. M.; Mahan, M. J.; Smith, J. W.; Marth, J. D. An Intrinsic Mechanism of Secreted Protein Aging and Turnover. *Proceedings of the National Academy of Sciences* **2015**, *112* (44), 13657–13662.
- (56) Denis, C. V.; Lenting, P. J. VWF Clearance: It’s Glycosylated. *Blood* **2018**, *131* (8), 842–843.
- (57) Ward, S. E. W.; O’Sullivan, J. M.; Drakeford, C.; Aguila, S.; Jondle, C. N.; Sharma, J.; Fallon, P. G.; Brophy, T. M.; Preston, R. J. S.; Smyth, P.; et al. A Novel Role for the Macrophage Galactose-Type Lectin Receptor in Mediating von Willebrand Factor Clearance. *Blood* **2018**, *131*, 911–916.
- (58) Wood, W. I.; Capon, D. J.; Simonsen, C. C.; Eaton, D. L.; Gitschier, J.; Keyt, B.; Seeburg, P. H.; Smith, D. H.; Hollingshead, P.; Wion, K. L.; et al. Expression of Active Human Factor VIII from Recombinant DNA Clones. *Nature* **1984**, *312* (5992), 330–337.
- (59) Franchini, M.; Lippi, G. The Use of Desmopressin in Acquired Haemophilia A: A Systematic Review. *Blood Transfus* **2011**, *9* (4), 377–382.
- (60) Alkjaersig, N.; Fletcher, A. P.; Sherry, S. Xi-Aminocaproic Acid: An Inhibitor of Plasminogen Activation. *J. Biol. Chem.* **1959**, *234* (4), 832–837.
- (61) Lenting, P. J.; Muczynski, V.; Aymé, G.; Denis, C. V.; Christophe, O. D. Von Willebrand Factor Interaction with FVIII. *Blood*; 2016; Vol. 128, p SCI-8.

- (62) Doering, C. B.; Healey, J. F.; Parker, E. T.; Barrow, R. T.; Lollar, P. High Level Expression of Recombinant Porcine Coagulation Factor VIII. *Journal of Biological Chemistry* **2002**, 277 (41), 38345–38349.
- (63) Doering, C. B.; Healey, J. F.; Parker, E. T.; Barrow, R. T.; Lollar, P. Identification of Porcine Coagulation Factor VIII Domains Responsible for High Level Expression via Enhanced Secretion. *Journal of Biological Chemistry* **2004**, 279 (8), 6546–6552.
- (64) Doering, C. B.; Denning, G.; Dooriss, K.; Gangadharan, B.; Johnston, J. M.; Kerstann, K. W.; McCarty, D. A.; Spencer, H. T. Directed Engineering of a High-Expression Chimeric Transgene as a Strategy for Gene Therapy of Hemophilia A. *Molecular Therapy* **2009**, 17 (7), 1145–1154.
- (65) Zakas, P. M.; Vanijcharoenkarn, K.; Markovitz, R. C.; Meeks, S. L.; Doering, C. B. Expanding the Ortholog Approach for Hemophilia Treatment Complicated by Factor VIII Inhibitors. *Journal of Thrombosis and Haemostasis* **2015**, 13 (1), 72–81.
- (66) Reding, M. T.; Ng, H. J.; Poulsen, L. H.; Eyster, M. E.; Pabinger, I.; Shin, H.-J.; Walsch, R.; Lederman, M.; Wang, M.; Hardtke, M.; et al. Safety and Efficacy of BAY 94-9027, a Prolonged-Half-Life Factor VIII. *Journal of Thrombosis and Haemostasis* **2017**, 15 (3), 411–419.
- (67) Mei, B.; Pan, C.; Jiang, H.; Tjandra, H.; Strauss, J.; Chen, Y.; Liu, T.; Zhang, X.; Severs, J.; Newgren, J.; et al. Rational Design of a Fully Active, Long-Acting PEGylated Factor VIII for Hemophilia A Treatment. *Blood* **2010**, 116 (2), 270–279.
- (68) Konkle, B. A.; Stasyshyn, O.; Chowdary, P.; Bevan, D. H.; Mant, T.; Shima, M.; Engl, W.; Dyck-Jones, J.; Fuerlinger, M.; Patrone, L.; et al. Pegylated, Full-Length, Recombinant Factor VIII for Prophylactic and on-Demand Treatment of Severe Hemophilia A. *Blood* **2015**, 126 (9), 1078–1085.
- (69) ISRAEL, E. J.; WILSKER, D. F.; HAYES, K. C.; SCHOENFELD, D.; Combined, N. E. Simister. Increased Clearance of IgG in Mice That Lack FB2-Microglobulin: Possible Protective Role of FcRn. **1996**, 6.
- (70) Dumont, J. A.; Liu, T.; Low, S. C.; Zhang, X.; Kamphaus, G.; Sakorafas, P.; Fraley, C.; Drager, D.; Reidy, T.; McCue, J.; et al. Prolonged Activity of a Recombinant Factor VIII-Fc Fusion Protein in Hemophilia A Mice and Dogs. *Blood* **2012**, 119 (13), 3024–3030.
- (71) Gale, A. J.; Radtke, K.-P.; Cunningham, M. A.; Chamberlain, D.; Pellequer, J.-L.; Griffin, J. H. Intrinsic Stability and Functional Properties of Disulfide Bond-Stabilized Coagulation Factor VIIIa Variants. *Journal of Thrombosis and Haemostasis* **2006**, 4 (6), 1315–1322.
- (72) Healey, J. F.; Lubin, I. M.; Lollar, P. The CDNA and Derived Amino Acid Sequence of Porcine Factor VIII. *Blood* **1996**, 88 (11), 4209–4214.
- (73) Hay, C. R.; Lozier, J. N.; Lee, C. A.; Lafan, M.; Tradati, H.; Santagostino, E.; Ciavarella, N.; Schiavoni, M.; Fukui, H.; Yoshioka, A. Porcine Factor VIII Therapy in Patients with Congenital Hemophilia and Inhibitors: Efficacy, Patient Selection, and Side Effects. *Semin. Hematol.* **1994**, 31 (2 Suppl 4), 20–25.
- (74) Kruse-Jarres, R.; St-Louis, J.; Greist, A.; Shapiro, A.; Smith, H.; Chowdary, P.; Drebes, A.; Gomperts, E.; Bourgeois, C.; Mo, M.; et al. Efficacy and Safety of OBI-1, an Antihemophilic Factor VIII (Recombinant), Porcine Sequence, in Subjects with Acquired Hemophilia A. *Haemophilia* **2015**, 21 (2), 162–170.
- (75) Uchida, N.; Sambe, T.; Yoneyama, K.; Fukazawa, N.; Kawanishi, T.; Kobayashi, S.; Shima, M. A First-in-Human Phase 1 Study of ACE910, a Novel Factor VIII-Mimetic Bispecific Antibody, in Healthy Subjects. *Blood* **2016**, 127 (13), 1633–1641.
- (76) *Roche's Emicizumab Showed Positive Results in Phase III Studies (HAVEN 1 and HAVEN 2) in Haemophilia A with Inhibitors*; Basel, Switzerland; p 6/26/2017.

- (77) Konkle, B. A.; Ebbesen, L. S.; Erhardtson, E.; Bianco, R. P.; Lissitchkov, T.; Rusen, L.; Serban, M. A. Randomized, Prospective Clinical Trial of Recombinant Factor VIIa for Secondary Prophylaxis in Hemophilia Patients with Inhibitors: Factor VIIa Prophylaxis in Hemophilia. *Journal of Thrombosis and Haemostasis* **2007**, *5* (9), 1904–1913.
- (78) Antunes, S. V.; Tangada, S.; Stasyshyn, O.; Mamonov, V.; Phillips, J.; Guzman-Becerra, N.; Grigorian, A.; Ewenstein, B.; Wong, W.-Y. Randomized Comparison of Prophylaxis and On-Demand Regimens with FEIBA NF in the Treatment of Haemophilia A and B with Inhibitors. *Haemophilia* **2014**, *20* (1), 65–72.
- (79) Waters, E. K.; Sigh, J.; Friedrich, U.; Hilden, I.; Sørensen, B. B. Concizumab, an Anti-Tissue Factor Pathway Inhibitor Antibody, Induces Increased Thrombin Generation in Plasma from Haemophilia Patients and Healthy Subjects Measured by the Thrombin Generation Assay. *Haemophilia* **2017**, *23* (5), 769–776.
- (80) Murphy, S. L.; High, K. A. Gene Therapy for Haemophilia. *British Journal of Haematology* **2008**, *140* (5), 479–487.
- (81) Pierce, G. F.; Lillicrap, D.; Pipe, S. W.; Vandendriessche, T. Gene Therapy, Bioengineered Clotting Factors and Novel Technologies for Hemophilia Treatment. *Journal of Thrombosis and Haemostasis* **2007**, *5* (5), 901–906.
- (82) Kepler, J. *The Six-Cornered Snowflake*; Oxford University Press: Oxford, 2014.
- (83) Rosenow, U. F. Notes on the Legacy of Rontgen Rays.Pdf. *Medical Physics* **1995**, *22* (11), 1855–1867.
- (84) Friedrich, W.; Knipping, P.; von Laue, M. Interferenz-Erscheinungen Bei Röntgenstrahlen. *Sitzungsberichte der Mathematisch-Physikalischen Classe der Königlich-Bayerischen Akademie der Wissenschaften zu München*. **1912**, 303.
- (85) Drenth, J. *Principles of Protein X-Ray Crystallography*, 2nd ed.; Springer advanced texts in chemistry; Springer: New York, 1999.
- (86) Bragg, W. H.; Bragg, W. L. The Reflection of X-Rays by Crystals. In *Source Book in Chemistry, 1900–1950*; Leicester, H. M., Ed.; Harvard University Press: Cambridge, MA and London, England, 1968.
- (87) Kendrew, J. C.; Bodo, G.; Dintzis, H. M.; Parrish, R. G.; Wyckoff, H.; Phillips, D. C. A Three-Dimensional Model of the Myoglobin Molecule Obtained by x-Ray Analysis. *Nature* **1958**, *181* (4610), 662–666.
- (88) Perutz, M. F.; Rossmann, M. G.; Cullis, A. F.; Muirhead, H.; Will, G.; North, A. C. T. Structure of Hæmoglobin: A Three-Dimensional Fourier Synthesis at 5.5-Å. Resolution, Obtained by X-Ray Analysis. *Nature* **1960**, *185* (4711), 416–422.
- (89) *Protein Crystallization: Techniques, Strategies, and Tips: A Laboratory Manual*; Bergfors, T. M., Ed.; IUL biotechnology series; International University Line: La Jolla, Calif, 1999.
- (90) Wukovitz, S. W.; Yeates, T. O. Why Protein Crystals Favour Some Space-Groups over Others. *Nat. Struct. Biol.* **1995**, *2* (12), 1062–1067.
- (91) Blundell, T. L.; Johnson, L. N. *Protein Crystallography*; Molecular biology; Academic Press: New York, 1976.
- (92) Emsley, P.; Cowtan, K. *Coot : Model-Building Tools for Molecular Graphics. Acta Crystallographica Section D Biological Crystallography* **2004**, *60* (12), 2126–2132.
- (93) Emsley, P.; Lohkamp, B.; Scott, W. G.; Cowtan, K. Features and Development of *Coot*. *Acta Crystallographica Section D Biological Crystallography* **2010**, *66* (4), 486–501.
- (94) Adams, P. D.; Afonine, P. V.; Bunkóczi, G.; Chen, V. B.; Davis, I. W.; Echols, N.; Headd, J. J.; Hung, L.-W.; Kapral, G. J.; Grosse-Kunstleve, R. W.; et al. *PHENIX : A Comprehensive Python-Based System for Macromolecular Structure Solution*; 2012; pp 539–547.
- (95) Ramachandran, G.; Ramakrishnan, C.; Sasisekharan, V. Stereochemistry of Polypeptide Chain Configurations. *Journal of Molecular Biology* **1963**, *7* (1), 95.

- (96) Walter, J. D.; Werther, R. A.; Brison, C. M.; Cragerud, R. K.; Healey, J. F.; Meeks, S. L.; Lollar, P.; Spiegel, P. C. Structure of the Factor VIII C2 Domain in a Ternary Complex with 2 Inhibitor Antibodies Reveals Classical and Nonclassical Epitopes. *Blood* **2013**, *122* (26), 4270–4278.
- (97) Walter, J. D.; Werther, R. A.; Polozova, M. S.; Pohlman, J.; Healey, J. F.; Meeks, S. L.; Lollar, P.; Spiegel, P. C. Characterization and Solution Structure of the Factor VIII C2 Domain in a Ternary Complex with Classical and Non-Classical Inhibitor Antibodies. *Journal of Biological Chemistry* **2013**, *288* (14), 9905–9914.
- (98) Brison, C. M.; Mullen, S. M.; Wuerth, M. E.; Podolsky, K.; Cook, M.; Herman, J. A.; Walter, J. D.; Meeks, S. L.; Spiegel, P. C. The 1.7 \AA X-Ray Crystal Structure of the Porcine Factor VIII C2 Domain and Binding Analysis to Anti-Human C2 Domain Antibodies and Phospholipid Surfaces. *PloS one* **2015**, *10* (3), e0122447.
- (99) Batsuli, G.; Healey, J.; Parker, E.; Baldwin, W. H.; Cox, C.; Nguyen, B.; Lollar, P.; Meeks, S. L. *Anti-C1 Domain Antibodies Are Pathogenic in a Murine Tail Snip Model Despite Low Inhibitor Titers*; Am Soc Hematology, 2015.
- (100) Markovitz, R. C.; Healey, J. F.; Parker, E. T.; Meeks, S. L.; Lollar, P. The Diversity of the Immune Response to the A2 Domain of Human Factor VIII. *Blood* **2013**, *121* (14), 2785–2795.
- (101) Batsuli, G.; Deng, W.; Healey, J. F.; Parker, E. T.; Baldwin, W. H.; Cox, C.; Nguyen, B.; Kahle, J.; Konigs, C.; Li, R.; et al. High-Affinity, Noninhibitory Pathogenic C1 Domain Antibodies Are Present in Patients with Hemophilia A and Inhibitors. *Blood* **2016**, *128* (16), 2055–2067.
- (102) Earnshaw, S. R.; Graham, C. N.; McDade, C. L.; Spears, J. B.; Kessler, C. M. Factor VIII Alloantibody Inhibitors: Cost Analysis of Immune Tolerance Induction vs. Prophylaxis and on-Demand with Bypass Treatment. *Haemophilia* **2015**, *21* (3), 310–319.
- (103) Shen, B. W.; Spiegel, P. C.; Chang, C.-H.; Huh, J.-W.; Lee, J.-S.; Kim, J.; Kim, Y.-H.; Stoddard, B. L. The Tertiary Structure and Domain Organization of Coagulation Factor VIII. *Blood* **2007**, *111* (3), 1240–1247.
- (104) Ngo, J. C. K.; Huang, M.; Roth, D. A.; Furie, B. C.; Furie, B. Crystal Structure of Human Factor VIII: Implications for the Formation of the Factor IXa-Factor VIIIa Complex. *Structure* **2008**, *16* (4), 597–606.
- (105) Moriarty, N. W.; Grosse-Kunstleve, R. W.; Adams, P. D. *Electronic Ligand Builder and Optimization Workbench (ELBOW)*: A Tool for Ligand Coordinate and Restraint Generation. *Acta Crystallographica Section D Biological Crystallography* **2009**, *65* (10), 1074–1080.
- (106) Terwilliger, T. C.; Read, R. J.; Adams, P. D.; Brunger, A. T.; Afonine, P. V.; Grosse-Kunstleve, R. W.; Hung, L.-W. Improved Crystallographic Models through Iterated Local Density-Guided Model Deformation and Reciprocal-Space Refinement. *Acta Crystallographica Section D Biological Crystallography* **2012**, *68* (7), 861–870.
- (107) Terwilliger, T. C. Using Prime-and-Switch Phasing to Reduce Model Bias in Molecular Replacement. *Acta Crystallographica Section D Biological Crystallography* **2004**, *60* (12), 2144–2149.
- (108) Terwilliger, T. C.; Grosse-Kunstleve, R. W.; Afonine, P. V.; Moriarty, N. W.; Adams, P. D.; Read, R. J.; Zwart, P. H.; Hung, L.-W. Iterative-Build OMIT Maps: Map Improvement by Iterative Model Building and Refinement without Model Bias. *Acta Crystallographica Section D Biological Crystallography* **2008**, *64* (5), 515–524.

Appendix A

C1 IMAC Cation Optimization Purification Chromatograms

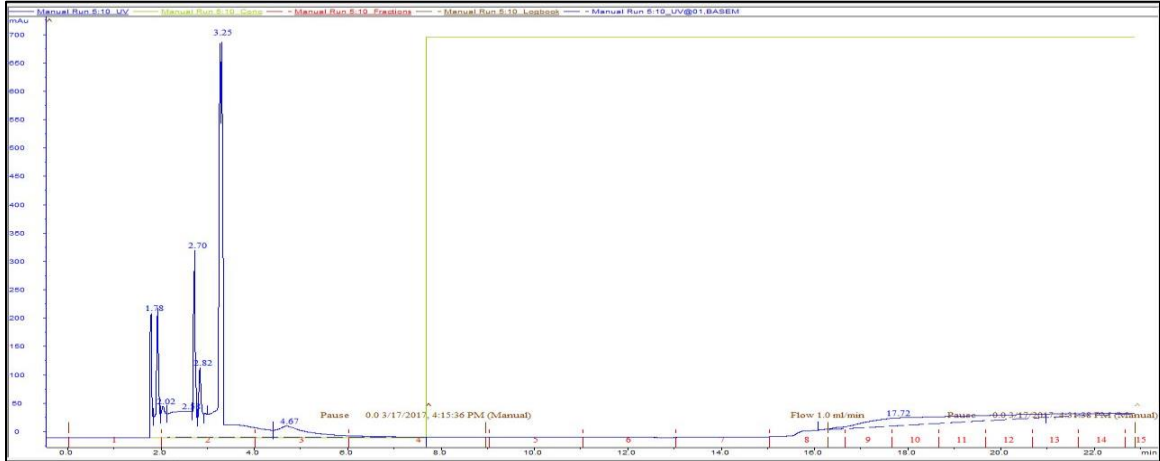


Figure 50 *CI fusion Co(II) IMAC purification*. The UV absorbance (blue) detected protein in the flow through, but following the elution step (green vertical band), no substantial protein peak eluted. (3.17.2017 IWS(I)p.138)

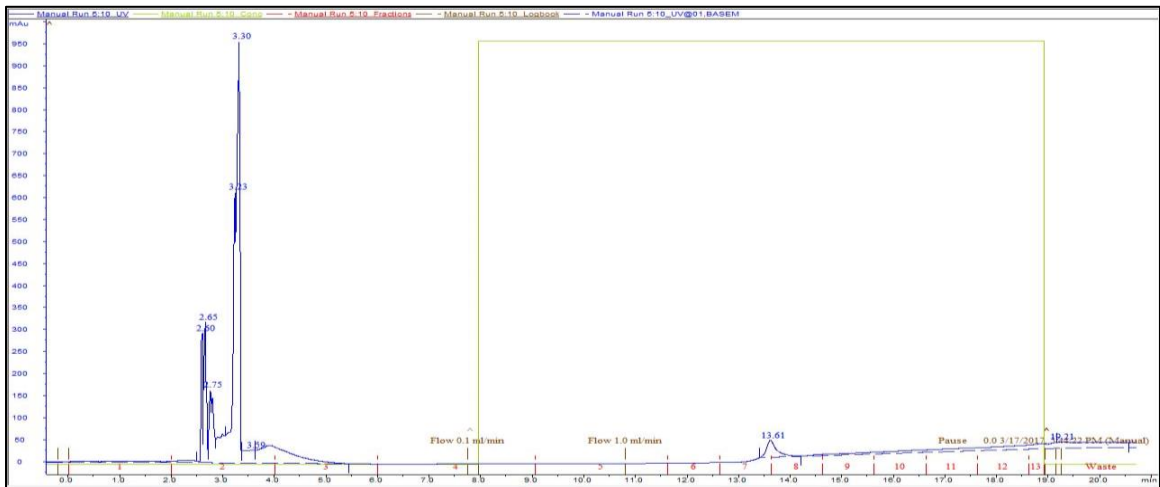


Figure 51 *CI fusion Cu(II) IMAC purification*. The UV absorbance (blue) detected protein in the flow through, but following the elution step (green vertical band), only a small protein peak eluted. This peak was not resolved on an SDS-PAGE gel. (3.17.2017 IWS(I)p.138)

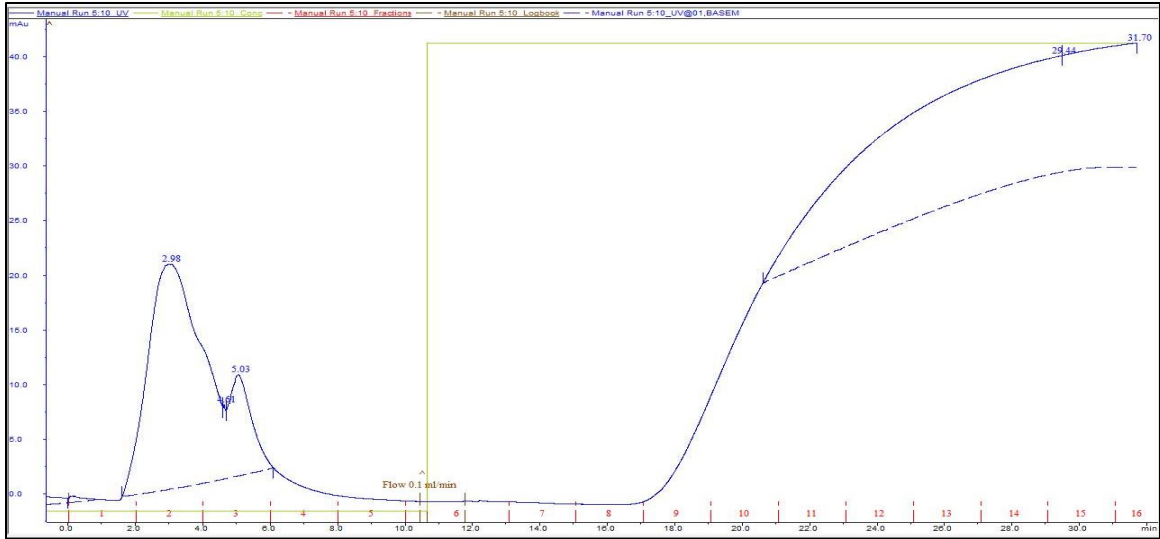


Figure 52 *CI fusion Fe(III) IMAC purification*. The UV absorbance (blue) detected protein in the flowthrough, but following the elution step (green vertical band), an unexpected large UV signal was detected. (3.17.2017 IWS(I)p.138)

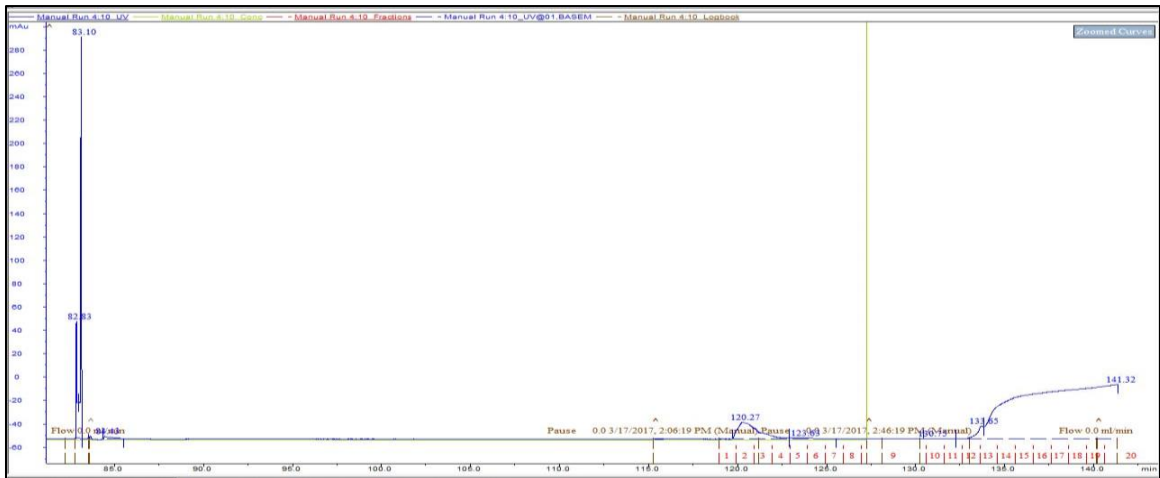


Figure 53 *CI fusion Ni(II) IMAC purification*. The UV absorbance (blue) detected protein in the flowthrough, but following the elution step (green vertical band), no substantial protein peak was detected. (3.17.2017 IWS(I)p.138)

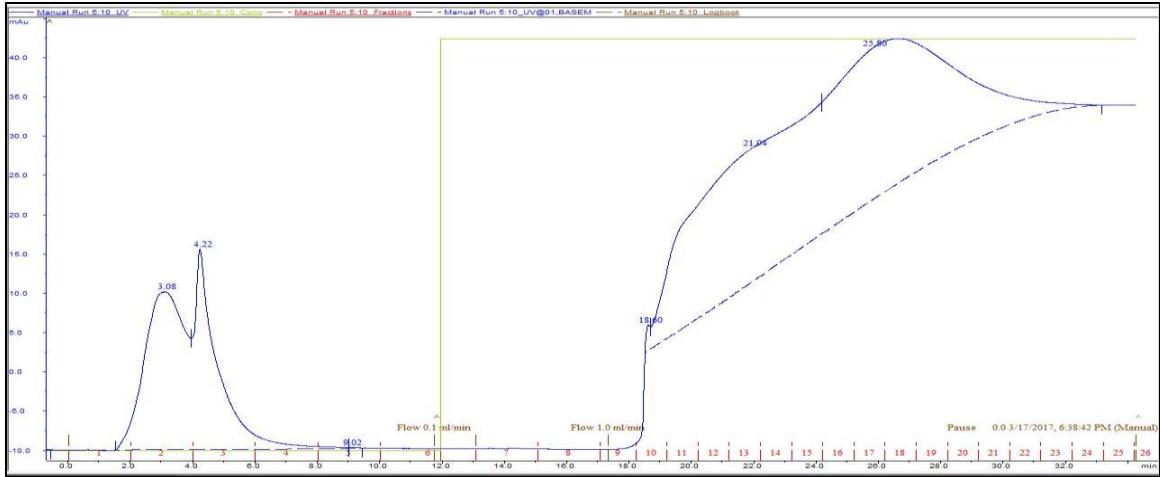


Figure 54 *CI fusion Zn(II) IMAC purification*. The UV absorbance (blue) detected protein in the flowthrough, but following the elution step (green vertical band), a large UV signal was detected. (3.17.2017 IWS(I)p.138)

Appendix B

Bi-layer Interferometry of C1 and anti-C1 Mabs

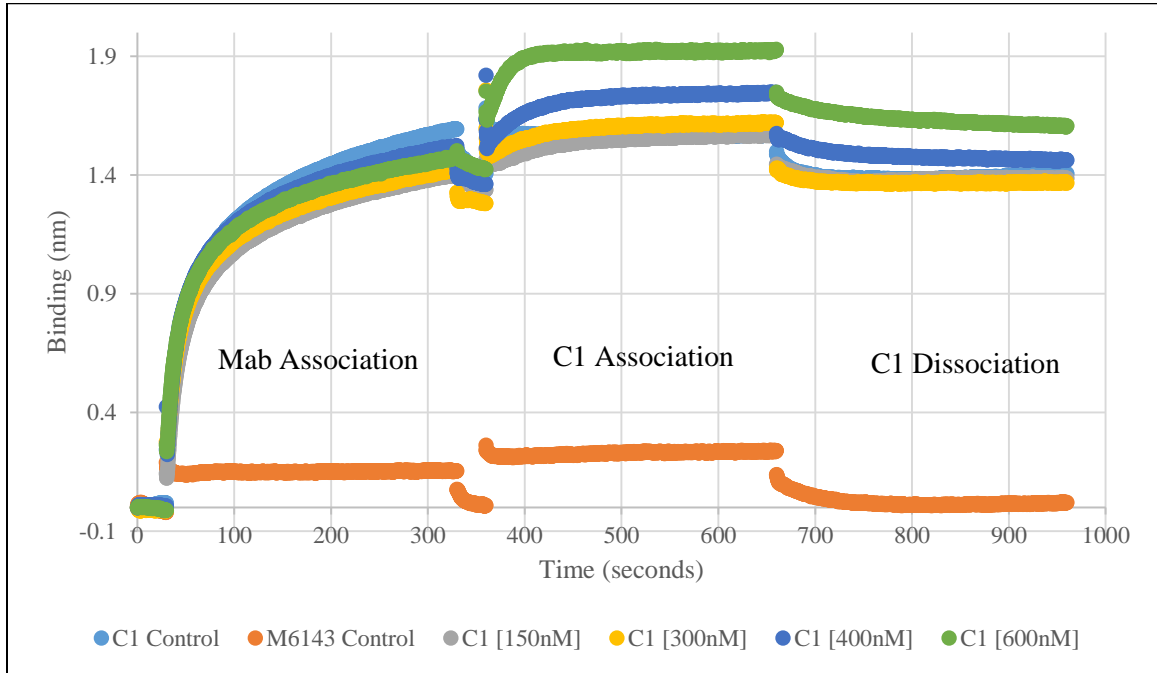


Figure 55 *Bi-layer Interferometry (BLI) C1 Titration & "Group A" Mab M6143 [300 nM].*

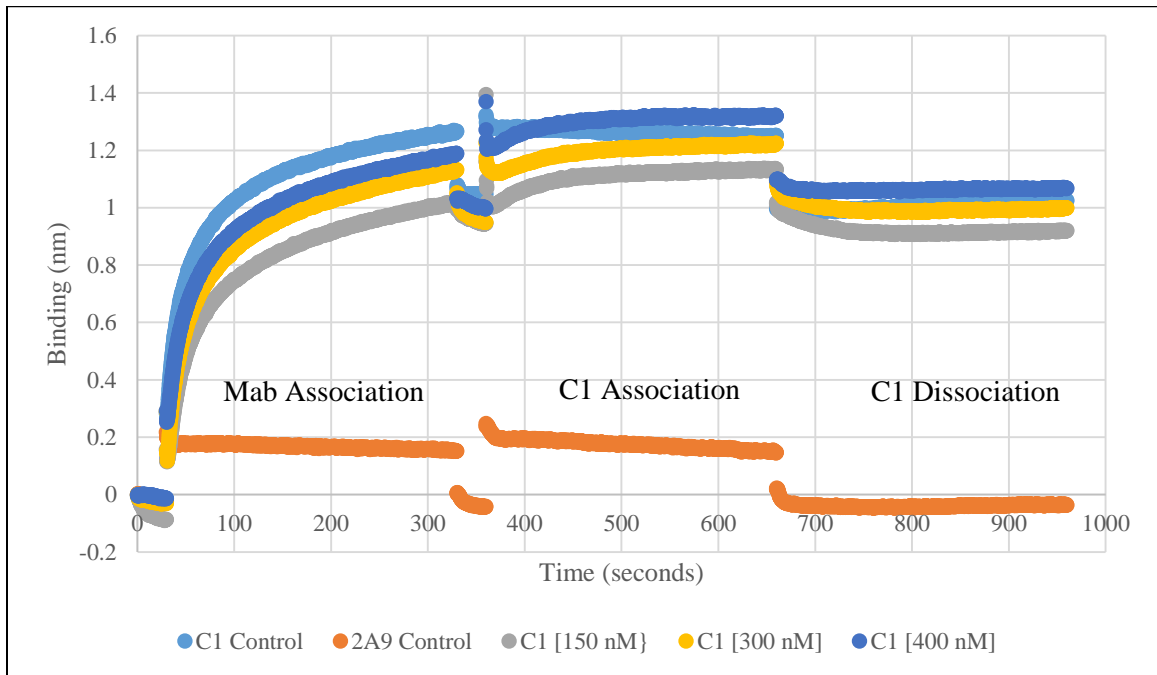


Figure 56 *BLI Titration of C1 & "Group A" Mab 2A9 [300 nM]. The 2A9 [600 nM] condition was poorly behaved and is omitted from this figure.*

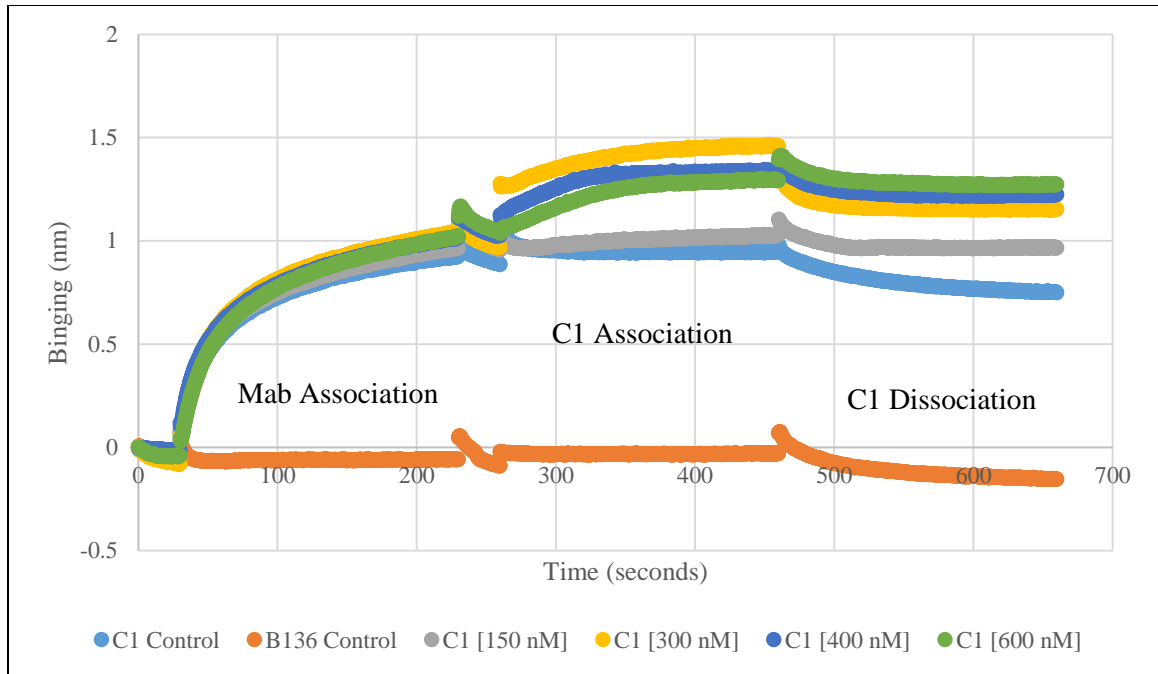


Figure 57 BLI Titration of C1 & "Group B" Mab B136 [300 nM].